Antimicrobial nano-ninjas as chaperones of gemcitabine for pancreatic cancer

Rachel Louise Foulkes

MPhil in Pharmacy

December 2019

Keele University

Abstract

Pancreatic cancer is well known for its extremely high death rate, with the current treatments purely used to extend and better the quality of the patient's life instead of providing a “cure”. Because of this, novel drug delivery methods are being looked into. Initially, hybrid nanoparticles (HNPs) comprised of iron and silver were synthesised and characterised using dynamic light scattering (DLS), transmission electron microscopy (TEM) and inductively coupled plasma optical emissions spectroscopy (ICP-OES). The heating ability of these nanoparticles was tested using the surface plasmon resonance properties which silver is well known for, with the only issue found being the spread of heat when dispersed in agar. As well as this, the HNPs were tested for their ability to kill gram-negative bacteria, both with and without the modified gemcitabine, with no statistically significant differences in their effects. A novel targeting agent was successfully attached to the surface of the HNPs but was unsuccessful in targeting the pancreatic cancer cell lines BxPC-3 and PANC-1. Modified gemcitabine, as used in previous studies within this research group, was successfully loaded onto the surface of HNPs, as proven by HPLC. The drug release was not consistent with previous reports and the cytotoxicity results were also found to be inconclusive overall.

Overall, the HNPs synthesised here could potentially be used as a dual treatment for pancreatic cancer tumours, but further work is necessary in order to allow them to be used in a clinical setting.

Acknowledgements

Initially, and most importantly, I would like to thank my incredible supervisor, Dr Clare Hoskins for taking me on as a master's student within her research group and for her endless patience and support throughout the year. Thanks also go to her and her research group for providing me with both gold hybrid nanoparticles and the modified gemcitabine required for me to complete this work.

Thank you to Rebecca Harrison for allowing me to test my samples in her microbiology lab and for her expertise in all things bacterial. Thanks to Dr Gavin Miller and his research group for allowing me to use equipment in his laboratory when required and for synthesising the targeting linker and to Dr Jóhannes Reynisson for providing the molecular modelling information for this linker. Thank you to Karen Walker for training me in the preparation and visualisation of TEM samples.

I owe a great deal to our brilliant laboratory technician, Mark Arrowsmith, who has, on several occasions, run my ICP samples when I have had a very busy lab day, is always willing to answer my stupid questions, and made sure that my hand didn't fall off in the Great *Aqua Regia* debacle of 2019. Special thanks also go to Mel for teaching me the mythical ways of statistical analysis and HPLC, as well as always being around when I need any support or advice, and to Liam for his incredible motivational speeches and for always making time for breakfast.

I would also like to thank my incredible friends and family, who have played an integral part in the completion of this thesis, except for participating in the laboratory work or the write-up. Special mentions go to my wonderful lunch companions Lydia, Aatikah, Jess, Haleema, Pratters, and Harvey, who are always there when I need them and never fail to make me laugh.

Common Abbreviations

˚C	Degrees Celsius
µg	Microgram
µL	Microlitre
5FU	5-fluorouracil
(T)	Heated sample
AG	Gemcitabine plus nab-paclitaxel
AgHNPs	Silver hybrid nanoparticles
AgNPs	Silver nanoparticles
AuHNPs	Gold hybrid nanoparticles
AMF	Alternating magnetic frequency
ANOVA	Analysis of Variance
DLS	Dynamic Light Scattering
EUCAST	European Committee on Antimicrobial Susceptibility Testing
FTIR	Fourier transform infrared
h	Hour(s)
HPLC	High-performance liquid chromatography
IC_{50}	Half maximal inhibitory concentration
ICP-OES	Inductively coupled plasma optical emissions spectroscopy
IONPs	Iron oxide nanoparticles
L-GEM	Modified gemcitabine (Figure X)
MRI	Magnetic resonance imaging
MIC	Minimum inhibitory concentration
Nimo	Nimotuzumab
Nimo-gem	Nimotuzumab plus gemcitabine
PAXG	Gemcitabine plus nab-paclitaxel plus cisplatin and capecitabine
PBS	Phosphate-buffered saline
PDAC	Pancreatic ductal adenocarcinoma
PDI	polydispersity index
PEI	poly(ethyleneimine)
PFS	Progression-free survival
PSMA	Prostate specific membrane antigen
SD	Standard deviation
SPIONs	Superparamagnetic iron oxide nanoparticles
TEM	Transmission electron microscopy

Contents

1.0 Introduction

1.1 Cancer

1.11 Pancreatic cancer

Cancer remains a global problem, with increasing incidence being attributed to a variety of factors including the ever-increasing ageing population and the many risk factors that have been correlated to cancer (Bray *et al.*, 2018). Although there has been a great deal of progress when it comes to the treatment of the majority of cancers, some types of cancer have been somewhat left behind in regard to improvements in survival rates and treatment options.

Pancreatic cancer is often diagnosed in people within the age range of 40-80 (Siegel, Miller and Jemal, 2018), with an expected 5-year survival in the United Kingdom and the United States of less than 10% (Siegel, Miller and Jemal, 2018; Office for National Statistics, 2019). On a global scale, this translates to pancreatic cancer being, for both men and women, the 7th leading cause of cancer-related death, with as many deaths as there are new cases of pancreatic cancer (Bray *et al.*, 2018). Several risk factors for pancreatic cancer have been identified, including obesity (Larsson, Orsini and Wolk, 2007; Jiao *et al.*, 2010), smoking (Zou *et al.*, 2014), heavy alcohol consumption (Michaud *et al.*, 2010; Tramacere *et al.*, 2010), long-term diabetes (Ben *et al.*, 2011; Starup-Linde *et al.*, 2013), and hereditary factors (Permuth-Way and Egan, 2009; Jacobs *et al.*, 2010). The involvement of genetic factors in pancreatic cancer was determined when it was discovered that tumour tissues, metastasised tissues, and the intratumoral environment were determined to be heterogenic (Yachida *et al.*, 2010; Burrell *et al.*, 2013).

More than 90% of patients diagnosed with pancreatic cancer have pancreatic ductal adenocarcinoma (PDAC), where cancer develops from exocrine pancreatic cells (Hidalgo *et al.*, 2015). As well as being the most prevalent form of pancreatic cancer, PDAC also has a

high mortality, with a 6% 5-year survival rate (Ying *et al.*, 2016). By 2030, PDAC is expected to be the second greatest cause of cancer-related death in the US (Rahib *et al.*, 2014). PDAC is clearly identifiable by the presence of precursor lesions, with these being well documented within the literature (Matthaei *et al.*, 2011; Wu *et al.*, 2011; Macgregor-Das and Iacobuzio-Donahue, 2013). These lesions are categorised into three different grades based on the levels of abnormal cell growth, known as dysplasia, within tissues, with 1 being low levels of dysplasia and 3 high levels of dysplasia (Hruban *et al.*, 2001).

Survival rates of pancreatic cancer are very poor, with several different reasons attributed to this.

One of the main contributors is the absence of early warning signs that can be noted in some other forms of cancer, increasing the difficulty of early diagnosis (Kleeff *et al.*, 2016). This is clearly reflected in the fact that locally advanced and metastatic pancreatic cancer, stages 3 and 4 respectively, are the most commonly diagnosed stages of pancreatic cancer (Chiaravalli *et al.*, 2017). Metastasis is often seen in patients with pancreatic cancer, with the most common sites of spread being the liver, peritoneum, and lungs (Chiaravalli *et al.*, 2017) and 90% of patients presenting with metastasis after death (Nguyen and Massagué, 2007). There are, however, several methods that can be used for the diagnosis of pancreatic cancer available, including magnetic resonance imaging (MRI), biopsy and fine-needle aspiration (Lee and Lee, 2014).

Other contributing factors towards poor pancreatic cancer survival rates include a lack of biomarkers (Chand *et al.*, 2016), progression of metastasis in the early stages of the disease (Saung and Zheng, 2017), a poor immune response and tumours hijacking the immune system (Kleeff *et al.*, 2016), and current chemotherapeutics facing resistance (Chand *et al.*, 2016).

1.12 Current pancreatic cancer therapies

Several different therapies have been utilised against pancreatic tumours with little effect. Commonly used chemotherapy agents and radiotherapy face the ever-increasing issue

of resistance, whereas new treatments face issues including slow development and approval (Garrido-Laguna and Hidalgo, 2015). The main therapeutic used as a treatment for pancreatic cancer is gemcitabine (2',2'-difluorodeoxycytidine), which can be used for the treatment of other cancers, including lung and breast cancers (Geller *et al.*, 2017). However, gemcitabine merely prolongs the lives of patients, providing no real "cure" (Burris *et al.*, 1997) and now faces resistance, like other traditional chemotherapeutic agents. Gemcitabine itself, seen in Figure 1, has an interesting mechanism of action. Gemcitabine is initially phosphorylated within cells by two known enzymes, initially by deoxycytidine kinase and secondly by pyrimidine nucleoside monophosphate kinase (Heinemann et al., 1988; Hatiz et al., 1998; Van Rompay et al., 1999), to form the gemcitabine diphosphate. There are several ways in which these phosphorylated gemcitabine moieties work, including inhibition of DNA synthesis (Huang *et al*., 1991), inhibition of enzymes (Heinemann *et al.*, 1992), and apoptosis induction *via* caspase signalling (Ferreira *et al.*, 2000).

Gemcitabine has been used as a baseline of sorts when trialling new treatments for pancreatic cancer, with this drug being used either as a comparison to a potential new treatment for pancreatic cancer or used in conjunction with other cancer therapeutics in order to enhance the anticancer effects.

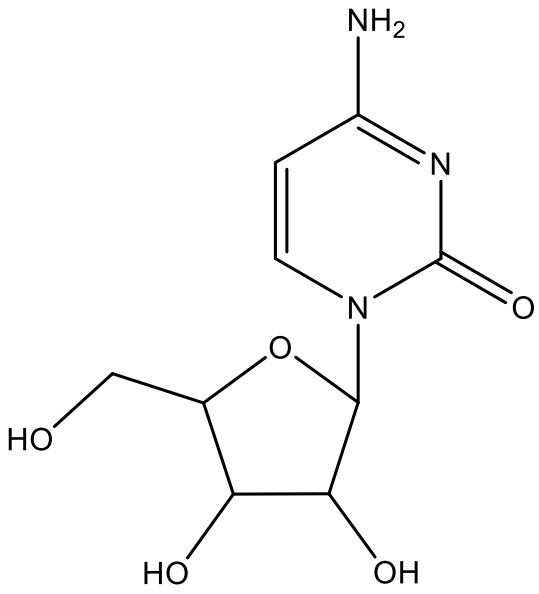

Figure 1: The structure of gemcitabine

Reni and co-workers treated patients with advanced pancreatic cancer with gemcitabine in combination with cisplatin, epirubicin, and fluorouracil (5FU) (Reni *et al.*, 2005). 60% of patients were found to have a progression-free survival (PFS) of 4 months when taking the combination treatment in comparison to 28% for gemcitabine alone. As well as this, there was a 2-year overall survival of 11.5% for patients on the combination treatment, compared to a 2.1% 2-year survival when taking gemcitabine alone. Generally, the quality of life of patients taking the combination treatment was better than those on gemcitabine alone or those undergoing no treatment (Reni *et al.*, 2006). This study is flawed in the short length of time that the patients were monitored after treatment, using a 2-year overall survival instead of determining a median overall survival, as seen in a plethora of other research, making it less comparable. As well as this, establishing an average PFS is also useful in determining the effects of the drug, or drug combination, on halting the progression of cancer.

Erlotinib has previously been combined with gemcitabine and used as a treatment for patients with pancreatic cancer that was either unresectable, locally advanced, or metastatic (Moore *et al.*, 2007). There was a median overall survival of 6.24 months for the gemcitabine and erlotinib compared to 5.91 months for gemcitabine alone, with a PFS of 3.75 months and 3.55 months respectively. There were more side effects reported for the combination treatment than for gemcitabine alone, but these were mainly mild to moderate. Interstitial lung disease-like syndromes were seen to occur more frequently in patients undertaking the combination treatment, which was explained as being due to an additive effect of the drugs.

Gemcitabine and capecitabine have also been combined as a treatment for patients with advanced pancreatic cancer to give a slightly improved overall survival, with patients on the combination treatment having a median survival of 7.1 months and gemcitabine alone 6.2 months (Cunningham *et al.*, 2009). The PFS of each treatment was found to be 5.3 months and 3.8 months respectively. The incidence of grade 3 (severe) and grade 4 (potentially life-threatening) side effects decreased other than hand-foot syndrome, which increased by 4%,

and neutropenia, which increased by 13%. A large-scale study also compared the combination of gemcitabine and capecitabine against gemcitabine alone in over 700 patients who had previously received surgical resection treatments for pancreatic cancer tumours (Neoptolemos *et al.,* 2017). There was found to be a median overall survival of 28 months for the combination treatment compared to 25.5 months for the group taking gemcitabine alone. The relapse-free survival of patients was also seen to differ between the treatments, with the median values being 13.9 months and 13.1 months respectively. The grade 3 and 4 side effects neutropenia (38 *versus* 24%), hand-foot syndrome (7% *versus* 0%) and diarrhoea (6% *versus* 2%) were all more common in patients taking the combination treatment than those on gemcitabine alone, but otherwise the side effects were generally low for each treatment pathway. 6 patients died during the treatment due to an adverse event, 5 from the gemcitabine treatment arm and 1 from the combination treatment. Of the five patients on gemcitabine, one person died from a cardiac disorder, one from multi-organ failure and three from benign, malignant, and unspecified neoplasms. The patient on the gemcitabine plus capecitabine therapy died from infection or infestations. This combination treatment is currently used in the UK as a pancreatic cancer therapy (NHS England Specialised Services Clinical Reference Group for Chemotherapy, 2018).

Patients with metastatic pancreatic adenocarcinoma were treated with gemcitabine and nab-paclitaxel (Abraxane®) (von Hoff *et al.,* 2013). There was a 1.8-month greater survival when using Abraxane® than when on gemcitabine alone, which is reflected in the median PFS for each treatment, with these being 5.5 and 3.7 months for Abraxane® and gemcitabine respectfully. One of the issues with this combination was an increase in grade 3 and 4 side effects, including neuropathy (16% increase), neutropenia (11% increase) and fatigue (10% increase).

A similar study tested gemcitabine-nab-paclitaxel combined with cisplatin and capecitabine (PAXG) to nab-paclitaxel-gemcitabine (AG) for patients with locally advanced

or borderline resectable pancreatic adenocarcinoma (Reni *et al.*, 2018). The median PFS of patients on the PAXG treatment was 12.5 months compared to 9.9 months for those on the AG treatment. The median survival of patients in both treatment arms were very similar, with the median survival of PAXG patients being 20.7 months compared to 19.1 months for AG patients. However, there were fewer grade 3 and 4 side effects reported in the PAXG arm, other than cholangitis (1% increase) and neutropenia (15% increase).

FOLFIRINOX, a treatment that combines 5FU, folinic acid, irinotecan, and oxaliplatin, has also been suggested as a treatment for pancreatic cancer (Conroy *et al.*, 2011). Conroy *et al.* compared FOLFIRINOX to gemcitabine in a study for patients with metastatic pancreatic cancer (Conroy *et al.*, 2011). Patients in the FOLFIRINOX arm had an overall survival and PFS of 11.1 months and 6.4 months respectively, with both of these values greater than those of patients in the gemcitabine arm, who had an overall survival of 6.8 months and a PFS of 3.3 months. However, the FOLFIRINOX treatment did not work for 60-70% of patients and came with worsening of grade 3 and 4 side effects. Side effects that were seen to worsen included thrombocytopenia, neutropenia and sensory neuropathy, with no statistics on the degree to which the side effects were worsened present in the research and indicating high toxicity to healthy cells. In a separate paper, the same researchers further explored the effects of the FOLFIRINOX treatment *versus* gemcitabine on the same patient population (Gourgou-Bourgade *et al.*, 2013). It was determined that patient quality of life was not significantly different between the two pathways. The only major difference was that patients in the FOLFIRINOX arm of the study had diarrhoea during the first two months of treatment.

Ducreux *et al.* administered oxaliplatin alongside 5FU to patients with advanced pancreatic cancer, which gave a greater overall survival than each agent individually, with the overall survival of patients being 9 months for the combination treatment in comparison to 3.4 months and 2.4 months for oxaliplatin and 5FU respectively (Ducreux *et al.*, 2004). The

median time to progression for each of these treatments were 4.2 months, 2.0 months, and 1.5 months respectively. Although some patients presented with grade 3-4 side effects, including neutropenia, nausea, vomiting, and stomatitis, there were deaths related to toxicity.

Another study by Wang-Gillam *et al.* utilised nanoliposomal irinotecan with 5FU and folinic acid, which was also found to extend survival in patients with PDAC who had previously been receiving some form of gemcitabine therapy (Wang-Gillam *et al.*, 2016). There was a median survival of 6.1 months for patients using nanoliposomal irinotecan with 5FU and folinic acid compared to 4.2 months when using 5FU and folinic acid alone. There was found to be a median PFS of 3.1 months using the nanoliposomal treatment and 1.5 months for 5FU and folinic acid. There were also some grade 3-4 side effects, including neutropenia, vomiting, and fatigue, but this did not appear to majorly impact the quality of life of patients.

Another treatment for pancreatic cancer is nimotuzumab (nimo). Strumberg and colleagues used nimo initially as a monotherapy for 54 patients, finding a median PFS of 6.7 weeks and a median overall survival of 18.1 weeks (Strumberg *et al.*, 2012). Of these patients, only 3 were found to exhibit grade 3 side effects, where one suffered a haemorrhage but went on to have a full recovery, one had a gastrointestinal obstruction and the other deep vein thrombosis. Other side effects were exhibited but these were grade 1 and 2 so were far more manageable.

Later studies went on to use nimo alongside gemcitabine (nimo-gem). Su *et al.* tested nimo-gem on 18 patients, finding a median PFS of 3.71 months, a median overall survival of 9.29 months, and a 1-year survival of 38.9% (Su *et al.*, 2014). 6 of the patients in this study experienced a grade 3 side effect, with no grade 4 side effects reported. One patient was seen to exhibit grade 3 neutropenia and 5 patients grade 3 nausea/vomiting. A gemcitabine monotherapy was not used in this case, so it is hard to determine a synergistic effect between nimo and gem than in other studies. Schultheis and co-workers tested nimo-gem against

gemcitabine co-administered with a placebo, with 192 patients were split equally into each treatment group (Schultheis *et al.,* 2017). The median overall survival for patients taking nimo-gem was found to be 2.6 months longer than for gemcitabine alone (8.6 *versus* 6.0 months respectively) and the median PFS was 1.7 months longer than using gemcitabine alone (5.1 months *versus* 3.4 months). Grade 1 and 2 side effects were common in both treatment groups and the number of patients experiencing at least one serious adverse event were similar for the nimo-gem and gemcitabine groups (65.6% and 58.1% respectively). There was also found to be no statistically significant difference in the quality of life found between the two groups.

Even though the studies presented have been able to increase the survival time of patients with pancreatic cancer, there are currently no studies that are able to provide a definitive "cure". Many of the drugs currently used for pancreatic cancer are used to extend and improve the quality of life of patients, but often to no avail with quite severe side effects. These side effects occur because the current delivery system is not targeted towards cancerous tissues and therefore can affect other tissues and organs. It would be possible to bypass these side effects using a drug delivery system, with a targeted system being especially useful. In fact, the only option that may provide a cure for patients with pancreatic cancer is surgical resection, but this is only viable for approximately 15% of patients who must be in the early stages of disease progression (Stathis and Moore, 2010), then must subsequently undergo chemotherapy (Conroy *et al.*, 2016). In the majority of cases, this is still unsuccessful, with a poor 5-year survival rate and 80% chance of relapse even with surgical resection and chemotherapy (Neoptolemos *et al.*, 2004; Ducreux *et al.*, 2015).

1.13 Pancreatic tumours, the tumour microenvironment, and resistance to chemotherapeutics

Several different aspects of tumours and their microenvironment are causing the current issues with perfusion of chemotherapeutics into tumours, with this being the most pressing issues we face in treating cancer.

A clear example of issues with the perfusion of drugs into solid tumours was seen in the study by Tannock and colleagues using MGH-U1 human bladder cancer cells and EMT-6 mouse mammary cells to develop multicellular layers for their permeation into solid tumours, including paclitaxel, etoposide, vinblastine, cisplatin, and gemcitabine, with etoposide having the greatest and vinblastine the worst permeation (Tannock *et al.*, 2002). The poor perfusion of drugs into tumours becomes more obvious when considering the greater intercapillary distance and poor blood flow present in tumours.

The tumour microenvironment contains a plethora of components that increase the difficulty of drug penetration into solid tumours (Topalian *et al.*, 2012; Klemm and Joyce, 2015), as well as several features of the tumour microenvironment being implicated in cancer initiation, progression and metastasis (Hwang *et al.*, 2008).

Dermal fibroblasts have also been seen to confer resistance, as when co-cultured with pancreatic and colorectal cell lines, resistance to gemcitabine was seen to increase (Straussman *et al.*, 2012).

Cancer stem cells have also been identified in pancreatic tissues (Hermann *et al.*, 2007; Li *et al.*, 2007). Li *et al.* noticed in human pancreatic adenocarcinoma the existence of cancer stem cells (Li *et al.*, 2007). Cells expressing the markers CD44, CD24 and ESA were seen to differentiate or self-renew in NOD/SCID mice when human pancreatic adenocarcinomas were injected intraperitoneally. These cells were also seen to have a much greater tumorigenic potential than cells that were non-tumorigenic. Similarly, Hermann *et al.* found evidence for the existence of cancer stem cells in pancreatic cancer (Hermann *et al.*,

2007). It was noted that pancreatic cancer cells that expressed the CD133 marker had high tumorigenicity than those that did not express the marker, causing an orthotopic tumour to form in athymic mice.

Tumour-associated macrophages have been heavily implicated in tumour progression, typically recruited by various cytokines, including vascular endothelial growth factor and chemokines (Mantovani and Sica, 2010). As well as this, they are able to generate pro-angiogenic factors, including vascular endothelial growth factor and COX-2-derived prostaglandin E2, and can decrease tumoricidal activity (Mantovani *et al.*, 2008). tumour-associated macrophages have also been known to produce Sema4D (Sierra *et al.*, 2008) and Gas6 (Loges *et al.*, 2010), which promote angiogenesis and proliferation of cancer cells respectively. Components of the extra-cellular matrix of tumour cells (Kim *et al.*, 2009b) and products from tumour cells, including CSF-1 and IL-10 (Hagemann *et al.*, 2006) are known to enhance the pro-tumour abilities of tumour-associated macrophages.

Cancer-associated fibroblasts are able to stimulate angiogenesis and mediate inflammation by employing macrophages (Erez *et al.*, 2010). As well as this, cancer-associated fibroblasts can promote tumour growth *via* extracellular matrix remodelling and angiogenesis, with a gene signature recognised within these fibroblasts being able to promote inflammation. Finally, it was shown that carcinoma cells were able to "educate" normal dermal fibroblasts to express proinflammatory genes.

Chronic inflammation is another source of tumour progression. B cell activation has been seen to initiate chronic inflammation, leading to epithelial carcinogenesis in an HPV16 mouse model (de Visser, Korets and Coussens, 2005).

Several proteoglycans have been seen to play a role in cancer biology. Heparan sulphate proteoglycans have pro-angiogenic activity (Iozzo, 2001), glypicans and syndecans cause the promotion and inhibition of the initiation and progression of cancer (Filmus and Selleck, 2001; Sanderson and Yang, 2008), and small leucine-rich proteoglycans block

receptor tyrosine kinase activity (Iozzo and Schaefer, 2010).

Repetitions in the MYC oncogene have allowed this gene to initiate and propagate tumour formation (Grippo and Sandgren, 2012; Lin *et al*, 2013). MYC expression has been seen to increase within precursor tumours and lesions (Mazur *et al.*, 2010; Witkiewicz *et al.*, 2015), with Notch2 implicated as a MYC modulator in PDAC in numerous cell lines (Mazur *et al.*, 2010).

There are several components of tumours in PDAC that are associated with enhancing tumour progression and resistance to chemotherapeutics, including stroma and dense desmoplastic infiltration, frequently found in solid tumours (Hwang *et al.*, 2008). Human pancreatic stellate cells have also been seen to increase colony formation, tumour proliferation and invasion (Hwang *et al.*, 2008). 80% of the tumour mass in PDAC is stroma (Erkan *et al.*, 2012), with the suggestion that pancreatic stellate cells are responsible for this (Apte *et al.*, 2004). Pancreatic stellate cells make up 4% of the pancreas (Apte *et al.*, 1998), with the relationship between activated pancreatic stellate cells and collagen expression being used as an index for stroma activation, frequently used for patients with PDAC to determine their prognosis, with lower values meaning relatively good prognosis for the patient (Erkan *et al.*, 2008). Pancreatic stellate cells have also been implicated in the facilitation of local tumour growth and metastasis using both *in vivo* and *in vitro* models (Xu *et al.*, 2010).

Several factors within tumours can increase resistance to different anticancer agents, increasing the difficulty of treating pancreatic cancer.

1.2 Bacteria

1.21 The role of intratumoural bacteria in anti-cancer therapies

Intratumoral bacteria is the most recently implicated cause of resistance for anticancer therapies. As tumour tissues are hypoxic and necrotic, they provide the perfect environment for bacterial growth (Zu and Wang, 2014). These conditions can be explained by the speed of

growth of tumour tissues and poor vascularisation, leading to a poor supply of oxygen (St Jean, Zhang and Forbes, 2008). Tumour tissues have a much lower oxygen pressure than their non-cancerous counterparts, with the normal range being 20-100 mmHg and the range within cancer tumours being 0-20 mmHg (Dewhirst, Cao, and Moeller, 2008). These intratumoral bacteria have been implicated specifically in gemcitabine resistance.

A study completed by Lehouritis and co-workers looked into the impact of bacteria on anticancer drugs, one of which being gemcitabine (Lehouritis *et al.,* 2015). CT26 tumours injected with *Escherichia coli* subsequently injected with gemcitabine showed a larger tumour volume than the bacteria-free counterpart. As well as this, the overall survival of the mice was poorer for those injected with *Escherichia coli,* with these mice living on average 11 days less than their control counterparts.

Straussman *et al.* also completed a study looking into the components of the tumour microenvironment that mediate resistance (Straussman *et al.,* 2012). When filtering their fibroblast-conditioned medium, they noticed that resistance to gemcitabine no longer occurred, indicating something else that was present could cause resistance. Further studies went on to determine that the cancer cell lines co-cultured with human dermal fibroblasts contained *Mycoplasma* DNA, with a large proportion of the bacterial DNA belonging specifically to *Mycoplasma hyorhinis* (Geller *et al.,* 2017). Within a mouse model, *Mycoplasma hyorhinis* was seen to enter tumour cells, causing resistance by the deamination of gemcitabine to 2’2-difluorodeoxyuridine. Further, gemcitabine resistance was tested for in 27 different bacterial species, with 13 of these able to inhibit gemcitabine’s function in preventing the human colorectal carcinoma cell line RKO. Human PDAC tissues were specifically tested for bacteria, especially important when considering gemcitabine is the main line of treatment. A much greater proportion of PDAC tissues were found to contain bacteria than the control counterparts, with 76% of the PDAC tissues and 15% of normal pancreatic tissues containing bacteria. Based on the rDNA, the most commonly found class bacteria

within the cancerous tissues was Gammaproteobacteria, with most of these belonging to the families *Pseudomonadaceae* and *Enterobacteriaceae*. When co-culturing the bacteria found to be present in PDAC tissues with both human colon carcinoma cell lines RKO and HCT116, it was found that 93% of these were gemcitabine resistant.

To counteract this, antibiotics could be co-administered with anti-cancer drugs. This was investigated within the research of Geller *et al.*, who determined that antibiotic administration alongside gemcitabine improved the efficacy of the anti-cancer drug using a colon carcinoma mouse model (Geller *et al.*, 2017).

However, resistance to antibiotics is constantly getting worse, with some bacteria even becoming resistant to multiple antibiotic agents as a consequence of our misuse of these valuable drugs over the past 20 years or so.

1.22 The effect of antibacterial resistance on pancreatic cancer treatment

Pancreatic cancer tissues have been shown to contain bacteria, with a large proportion of these (51.7%) attributed to the class Gammaproteobacteria (Geller *et al.*, 2017). Of these, the majority were found to belong to the *Pseudomonadaceae* and *Enterobacteriaceae* bacterial families. Some bacteria categorised into these families have been associated with resistance to at least one or more antibiotic. Examples of these include *Escherichia coli*, *Salmonella* species, and *Pseudomonas aeruginosa*. It has been hypothesised by these researchers that the bacteria present in pancreatic tissue are able to migrate from the duodenum, where the pancreatic duct opens, as bacteria are well known to reside within this area (Ou *et al*., 2009; Nistal *et al*., 2012). Supporting evidence to this hypothesis was seen from patient samples, as instrumentation of the pancreatic duct was associated with considerably more bacteria in patient tumours in comparison to patients who had not undergone such procedures (Geller *et al*., 2017). Other routes, such as bacteria entering

through the vasculature into pancreatic cancer tumours, are theoretically possible but at the time of writing, there was no evidence to support this.

Because of this, there is a clear need to co-administer an antibacterial agent alongside pancreatic cancer treatments in order for gemcitabine to retain its efficacy. It would be possible to co-administer current antibiotics alongside this treatment, but there are several issues with this. Resistance to antibiotics is rising, with several bacteria now resistant to one or more type of antibiotic, including *Escherichia coli* (Picozzi *et al.*, 2014), *Klebsiella pneumoniae* (Ruiz de Alegría *et al.*, 2011; Sarojamma and Ramakrishna, 2011) and methicillin-resistant *Staphylococcus aureus* (Kaur and Chate, 2015). As well as this, lack of education surrounding the use of antibiotics has led some of the populous to believe that antibiotics could be used for several ailments, including the common cold which is a virus. Finally, there are no antibiotics currently on the market that could cater to the many different types of bacteria present within tumour tissues. This is because antibiotics rely on several different mechanisms to kill bacteria that do not work for all species.

The mechanisms by which these bacteria are resistant to antibiotics differ, with these either being intrinsic or acquired. There are several mechanisms by which either of these can occur.

Intrinsic resistance is the resistance that bacteria have naturally. One of the most common types of intrinsic resistance is overexpression of efflux pumps, allowing bacteria to remove antibiotics from within the cells. Examples of this include *Staphylococcus aureus* (Kosmidis *et al.*, 2012), *Pseudomonas aeruginosa* (Pumbwe and Piddock, 2000) and *Enterobacteriaceae* (Everett *et al.*, 1996). Another key that can have an impact on whether antibiotics can successfully penetrate bacteria is the ultrastructure of bacteria. A key example of this is the antibiotic vancomycin, as this is unable to cross the membrane of gram-negative bacteria but can cross the membrane of gram-positive bacteria (Nikaido, 1976). This is due to differences in the cell walls of gram-negative and gram-positive bacteria, with gram-negative

bacteria having an extra outer membrane within their cell walls.

Acquired resistance is where bacteria either mutate or obtain genes from other bacteria that confer resistance. Methicillin-resistant *Staphylococcus aureus* (MRSA) is an important example of where gene transfer can cause further antibiotic resistance (Ito *et al.*, 2013). Acquisition of the Staphylococcal Cassette Chromosome *mec* changes methicillin-susceptible *Staphylococcus aureus* to methicillin-resistant *Staphylococcus aureus,* therefore increasing the resistance of *Staphylococcus aureus* to a greater range of antibiotics. A key example of where gene mutations have led to antibiotic resistance is the development of extended-spectrum β-lactamases, which are present in several bacteria including *Escherichia coli* (Picozzi *et al.*, 2014). These enzymes are able to hydrolyse certain antibiotics, including aztreonam and cephalosporins, rendering them inactive (Picozzi *et al.*, 2013).

The obvious issues with administering general antibiotics outweigh any benefits of administering them alongside current chemotherapeutics. Other materials with antibacterial, or even antimicrobial, properties may be more appropriate and would provide a more broad-spectrum antibacterial effect.

1.3 Nanoparticles

1.31 Iron oxide nanoparticles for cancer therapy

Iron oxide nanoparticles (IONPs) have multiple biomedical uses, including their use as MRI contrast agents (Estelrich, Sánchez-Martín, and Busquets, 2015) and drug delivery agents (Jain *et al.*, 2005; Petri-Fink *et al*., 2005; Hu, Neoh and Kang, 2006).

IONP-based delivery systems for hydrophobic drugs have been explored by Jain and co-workers (Jain *et al*., 2005). Formulations of oleic acid-pluronic-coated IONPs were generated and then loaded these with doxorubicin. Alike other studies, there was no effect on the magnetic properties of the IONPs after adding the additional layers. The formulations generated were successful, with cellular uptake and dose-dependent cytotoxicity demonstrated

against both the PC-3 prostate cancer cell line and the MCF-7 breast cancer cell line.

Other studies have developed superparamagnetic IONPs (SPIONs) with polyvinyl acetate attached, then further functionalised these with amino, carboxy, or thiol groups in a study by Petri-Fink *et al*. (Petri-Fink *et al*., 2005). Here, the work aimed to determine if any of the nanoparticles, functionalised or non-functionalised, could interact with the human melanoma cell lines Me191, Me237, Me275, and Me300. It was ascertained that the amino-SPIONs had preferential uptake in two of the cell lines, Me237 and Me275, entering the cells rather than solely binding to the surface of the cells. The other nanoparticle formulations were not seen to interact with any of the cell lines. Cytotoxicity of the amino-SPIONs was tested on Me237 and Me275, with a higher polymer concentration being able to induce a cytotoxic effect.

Hu, Neoh, and Kang loaded tamoxifen onto magnetite-PLLA composites in order to provide a potential targeted treatment for oestrogen receptor-positive breast cancer, due to the treatment alone being known to cause endometrial cancer (Hu, Neoh and Kang, 2006). Varying concentrations of the composites, from 50 to 500 mg mL^{-1}, were used and tested these against the MCF-7 breast cancer cell line at 37°C. Overall, it was found that the viability of the cells decreased from 76 to 23% over 4 days, with increasing concentrations of the composites causing increased damage.

Khan and co-workers looked into the effects of bare IONPs on the human lung adenocarcinoma cell line A549 and the human lung epithelial cell line IMR-90 (Khan *et al*., 2012). IONPs were found to cause necrotic cell death in the cancerous cell line alone *via* the production of reactive oxygen species and autophagy, which did not occur in the normal human cell line.

Kumar *et al*. looked into the use of quercetin alongside dextran-coated IONPs and quercetin-coated IONPs (Kumar *et al*., 2014). Quercetin itself is very versatile, with anti-cancer effects exhibited on colon, lung and ovarian cancer cell lines, as well as having anti-

inflammatory, anti-oxidant and anti-viral properties (Kumar *et al*., 2014). In this study, the MCF-7 breast cancer cell line was used to test the combinations and individual components. There was good biocompatibility with the magnetite carrier, with cell viability of 78-90%, using a maximum concentration of 100 μg mL^{-1} over 24 h. There was a dose-dependent effect seen when using the quercetin-loaded IONPs, with a low cell viability of 25%, lower than that of quercetin alone. The release of quercetin was also found to be pH-dependent, with greater quantities released in acidic conditions than basic.

Alarifi and co-workers aimed to assess the toxicity and genotoxicity of IONPs in the human breast cancer cell line MCF-7, and the mechanisms by which these occur (Alarifi *et al*., 2014). IONPs exhibited both a cytotoxic and genotoxic effect on this cell line, with apoptosis being deemed the primary cause of cell death, acting in both a time-dependent and dose-dependent manner.

A study by Wu *et al*. looked into polydopamine coated SPIONs as potential cancer theranostic agents (Wu *et al*., 2015). These were tested on the mouse fibroblast cell line (HT3T3), human hepatocellular cell line (HepG2) and human cervical cancer (HeLa) cell lines, as well as testing cytotoxicity on these cell lines and NIH3T3 (mice fibroblast). Overall, cytotoxicity was low when using the nanoparticles alone, with the highest concentration of nanoparticles (0.5 mM) unable to reduce cell viability below 80%. Cytotoxicity was affected when using the combination of laser irradiation, an external magnetic field, and the nanoparticles, with no greater than 20% cell viability in the two cancerous cell lines.

Rao *et al*. created SPIONs loaded with epirubicin that are pH-sensitive, with the aim of these being able to selectively release epirubicin into tumour tissue or cancerous cells (Rao *et al*., 2015). SPIONs were found to have good biocompatibility on both a normal skin model (HaCaT) and a model based on melanoma cells (WM266), with antitumour activity also seen with the drug-loaded SPIONs.

Peixoto *et al*. tested free rhodium (II) citrate, rhodium (II) citrate loaded maghemite

nanoparticles, and citrate loaded maghemite nanoparticles, with these tested on breast cancer tumours xenografted onto Balb/c mice (Peixoto *et al*., 2015). It was found that both the rhodium (II) citrate and citrate-loaded maghemite nanoparticles were able to significantly reduce tumour area, with significant toxicity seen.

Mu *et al*. developed IONPs to carry gemcitabine, chlorotoxin and hyaluronic acid in order to try and effectively bypass the blood-brain barrier for the treatment of glioblastoma (Mu *et al*., 2016). Initially, the loaded IONPs were tested on two types of glioblastoma multiform cells: SF-763 and U-118. From the results obtained, the conjugated gemcitabine was seen to be as good at causing a decrease in cell viability as free gemcitabine. A mouse model was also used to find out that this combination successfully crossed the blood-brain barrier.

Ali *et al*. made IONPs coated with dextran and then conjugated onto this erlotinib, as it has been known to be selective for epidermal growth factor receptor that is found in many cancer types (Ali *et al*., 2016). The system was designed to release the drug at pH 5 in order to ensure release solely into intracellular late endosomes. The cytotoxic effects of this combination were confirmed both *in vitro* and *in vivo*, both using the human lung adenocarcinoma cell line CL1-5-F4, where the *in vivo* study was completed on a tumour xenografted onto BALB/c mice. It was also noted that the IONP-dextran combination without the drug was unable to cause any cytotoxic damage to the cells.

Zanganeh *et al*. looked into the use of a type of IONPs called ferumoxytol as a potential treatment of cancer (Zanganeh *et al*., 2016). Initially, it was determined that these nanoparticles had no direct effect on cancer cells alone but were able to cause macrophage polarization towards M1 macrophages. In several models, including the *in vivo* small lung cancer cell liver metastases mouse model and female FVB/N mice with MMTV-PyMT-derived cancer cells injected into the mammary fat pads, it was demonstrated that there was a significant reduction in tumour growth. This was deemed to be caused by the polarisation

effect ferumoxytol has on macrophages, as an *in vitro* test determined these had no cytotoxic effect on several cell lines, including the cancerous cell lines MMTV-PYMT (mouse model of breast cancer), MDA-MB-468 (human mammary gland), HT1080 (human fibrosarcoma) and non-cancerous cell lines RAW264.7 (macrophages), ATCC (human dermal fibroblast), PCS-201-012 (human dermal fibroblast), and HUVECS (human umbilical vein endothelial cells).

Popescu *et al*. tested gemcitabine-functionalised IONPs and free gemcitabine on BT474 (breast cancer carcinoma), HepG2 (human liver cancer) and MG-63 (osteocarcinoma) cell lines (Popescu *et al*., 2017). The BT474 and HepG2 cell lines showed greater resistance to both free and conjugated gemcitabine than the MG-63 cell line, with this resistance seen in other studies (Matsumoto *et al*., 2008; Wu *et al*., 2014). There was greater cytotoxicity in both BT474 and HepG2 when using the IONPs as a carrier of gemcitabine than gemcitabine alone and slower release of gemcitabine. The MG-63 cells were reported to be highly sensitive to gemcitabine, with free gemcitabine having a more noticeable cytotoxic effect but the nanoconjugate being as equally cytotoxic over 72 h. In each case, both free gemcitabine and conjugated gemcitabine were able to cause morphological changes in each of the cell lines.

1.32 Silver nanoparticles for cancer therapy

Generally, nanoparticles have several properties that make them useful in imaging, drug delivery, and creating cancer biomarker profiles of cancerous tumours (Lim, Gurung and Hande, 2017). Silver nanoparticles (AgNPs) have several applications for cancer, have been associated with anticancer properties and have used against several cancer types including leukaemia (Guo *et al*., 2013), breast cancer (Franco-Molina *et al.*, 2010), lung carcinoma (Foldbjerg *et al*., 2011), hepatocellular carcinoma (Kim *et al.*, 2009a) and glioblastoma (Lim, Gurung and Hande, 2017).

There are different methods by which AgNPs act in an anti-cancer manner.

Gou *et al*. determined that AgNPs produce reactive oxygen species, reducing the viability of the cells, causing DNA damage and inducing apoptosis (Guo *et al*., 2013). This

confirmed results from Lim *et al*. and Ahamed, AlSalhi and Siddiqui (Ahamed, AlSalhi and Siddiqui, 2010; Lim *et al*., 2012).

Lim, Gurung, and Hande determined that AgNPs have antineoplastic activity and appear to act in a similar manner to many current chemotherapeutics and have been seen to cause cytoskeletal deformities (Lim, Gurung and Hande, 2017). Another study by Sriram *et al*. looked into the effects of AgNPs against Dalton's lymphoma (Sriram *et al.,* 2010). It was confirmed that there was a significant decrease in tumour volume of 5 mL compared to a control in Swiss albino mice, with the average tumour volumes being 7.3 mL and 2.3 mL respectively. AgNPs administered *via* intraperitoneal injection were able to extend the lifespan of the mice to 32 days compared to the control, with an average life span of 18 days.

Several studies have utilised AgNPs, often in conjunction with other anti-cancer agents, to produce some anti-cancer effects on cancer cell lines.

AgNPs have been biogenically synthesised using phloroglucinol in a study by Kumar *et al*., in which these AgNPs were tested against the breast cancer cell line MCF-7 and were described as having impressive cytotoxicity (Kumar *et al*., 2018). Using phloroglucinol alone was seen to have a greater cytotoxic effect than the phloroglucinol synthesised AgNPs. However, there were no tests to determine any cytotoxic effects of phloroglucinol on healthy cells. However, the phloroglucinol AgNPs did show good cytotoxicity and would probably be less toxic to the surrounding healthy cells.

Guo *et al*. created PVP-coated AgNPs and found that they caused damage in leukaemia cell lines MB4, HEL, HL-60, THP-1, DAMI and SHI-1 cells, with less damage seen to occur in healthy cells (Guo *et al*., 2013). AgNPs were seen to cause the most damage to THP-1 cells and the least damage to the SHI-1 cells. It was also determined that there was no difference in the anticancer activities of the sizes AgNPs of 3 and 11 nm due to the insignificant difference between their hydrodynamic diameters. There was also evidence for apoptosis, mitochondrial damage, reactive oxygen species formation, and DNA damage.

Jeyaraj *et al*. generated biogenic AgNPs which showed cytotoxicity towards breast cancer MCF-7 cancer cell lines, where an increase in AgNPs concentration gave an improved effect (Jeyaraj *et al.*, 2013). Along with this, there was clear evidence of apoptosis in the form of apoptotic bodies, supporting the Guo *et al*. study. The MCF-7 cells showed visible signs of damage, mainly in the form of shape changes, including shrinkage and coiling, when treated with AgNPs compared to the controls.

DNA-dependent protein kinases have been used alongside AgNPs, modifying their anticancer ability against glioblastoma (U257) and breast cancer (MCF-7 and MDA-MB-231) cells (Lim, Gurung, and Hande, 2017). It was found that after 48 h, the shape of the cancerous cells had altered, compared to their control counterparts, alike other studies. Further, their report found that AgNPs were able to reduce cancer proliferation, cause cell death, a reduction in the expression of c-Myc and caused DNA damage.

Biogenic AgNPs have also been used alongside Galactomannan, which enhanced their anticancer abilities against human A549 lung adenocarcinoma cells, HCT116 colorectal carcinoma cells and HepG2 hepatocellular carcinoma cell lines, compared against a control of 3T3-L1 mouse fibroblast cell lines, displaying a lower level of toxicity towards normal cells (Padinjarathil *et al.*, 2018).

In a study by Zhang and Xiao, AgNPs combined with low-intensity ultrasound were tested against healthy human BEAS-2B bronchial epithelial cells and human A549 lung adenocarcinoma cells (Zhang and Xiao, 2018). This led to a massive decrease in cell viability in the cancer cell line compared to the healthy cell line, in which there was minimal damage.

Yuan, Peng, and Gurunathan utilised AgNPs with gemcitabine to determine if their combined effect had any enhanced anticancer effects against ovarian cancer cells (Yuan, Peng and Gurunathan, 2017). AgNPs and gemcitabine were initially tested individually, determining that a concentration of 25 nM of gemcitabine produced a cytotoxic effect. There was an also an increase in cytotoxicity in AgNPs seen at 25 mM, both after a 24 h incubation

period. The combination of AgNPs and gemcitabine was able to cause a much more efficient decrease in cell viability compared to the two alone. The results also showed that a lower concentration of AgNPs alongside gemcitabine was able to cause the death of cancer cells.

Overall, AgNPs are known to have a strong anti-cancer ability against several different types of cancer and varying cell lines, which is enhanced by using other anti-cancer agents alongside them. Although there is clearly a plethora of research into the use of AgNP for cancer therapy, research into the use of AgNPs for pancreatic cancer is very limited, with only two examples available at the time of writing.

Zielinska and co-workers tested the anticancer ability of two differently sized AgNPs, 2.6 nm and 18nm, on the human pancreatic cancer PANC-1 and non-cancerous telomerase immortalised hTERT cell lines (Zielinska *et al.*, 2018). AgNPs were seen to have a much stronger cytotoxic effect against the PANC-1 cell lines than the hTERT, with the smaller nanoparticles outperforming the 18 nm nanoparticles, giving a 16 times stronger cytotoxic effect. The effects of AgNPs were compared to the use of gemcitabine alone, showing that AgNPs were better at decreasing PANC-1 cell viability. The AgNPs were found to act in different methods, including inducing apoptosis, necrosis, causing ultrastructure changes to cause cell death in PANC-1 cells, and preventing cell proliferation, and were also seen to cause an increase in the levels of nitric oxide present in the cells, with 2.6 nm AgNPs producing the greater amount.

Similarly, Barcińska *et al.* essentially confirmed several findings in the Zielisnka *et al.* study, with reactive oxygen species production and nitric oxide found in PANC-1 cell lines at higher concentrations than those in hTERT (Barcińska *et al.*, 2018). Nitric oxide concentrations in this study were also found to be much higher than in Zielinska *et al.* for the PANC-1 cells, as well as determining the production of reactive oxygen species was found to be twice as high in the PANC-1 cell lines than the hTERT cell lines. Finally, the cell cycle

was found to be significantly impacted, with changes to the ultrastructure of mitochondria also evident.

1.33 The antimicrobial properties of silver nanoparticles

Several materials could be utilised alongside gemcitabine to kill intratumoral bacteria, including silver. Silver has been used for its antibacterial properties since ancient times, with these properties investigated for multiple applications, including wound dressings and films (Holt and Bard, 2005).

Silver ions have several modes of action by which they can inhibit bacteria, such as affecting DNA replication (Marini *et al*., 2007), interfering with the permeability of bacterial membranes and respiratory chain enzyme inhibition (Lok *et al*., 2007). As well as this, the distribution of silver differs, with 40% only surface binding and 60% entering the bacteria (Holt and Bard, 2005). A recent suggestion by Marini *et al.* noted AgNPs releasing silver ions, alike the mode of action of silver nitrate (Marini *et al*., 2007) and have also been seen to exhibit antibacterial action *via* entering bacteria by means of binding and passing through the cell wall (Shrivastava *et al*., 2007).

As well as exhibiting an antibacterial effect, AgNPs have also been seen to affect fungi, viruses, and protozoa.

Multiple studies have looked into this, with AgNPs having effects on different viruses, including influenza virus (Papp *et al*., 2010), HIV-1 (Elechiguerra *et al.,* 2005; Lara *et al.*, 2010), and hepatitis B (Lu *et al*., 2008). Pathogenic plant fungi, including *Botrytis cinereal, Alternaria alternata, and Fusarium oxysporum*, have been shown to be affected by AgNPs even at low concentrations *in vivo* (Kim *et al*., 2012a). AgNPs have also been seen to decrease the viability of *Cryptosporidium parvum* oocytes, a type of protozoan egg that is relatively unaffected by chlorination and are a leading cause of water-related diseases (Cameron *et al.,* 2016).

The antimicrobial activity of AgNPs is heavily affected by their properties, including their size, surface charge, drug-carrying ability, and biocompatibility.

Both Morones *et al.* and Martinéz-Castañón *et al*. have shown that smaller AgNPs have a greater bactericidal effect (Morones *et al*., 2005; Martínez-Castañón *et al*., 2008). Brown and co-workers found that using AgNPs to carry the antibiotic ampicillin drastically improved its efficacy (Brown *et al*., 2012). The surface charge and the stability of AgNPs can also be determined, allowing insight into if the synthesis has occurred successfully and to evade agglomeration (Petica *et al*., 2008). A final key property that AgNPs need to have is biocompatibility, with toxicity to surrounding tissues needing to be at a minimal level.

Several studies have looked into utilising the antibacterial properties of AgNPs against several types of bacteria.

Shrivastava *et al.* tested AgNPs antibacterial effects on *Staphylococcus aureus* (ATCC 25923), *Escherichia coli* (ATCC 25922), multi-drug resistant *Salmonella typhus* strain and ampicillin-resistant *Escherichia coli* (Shrivastava *et al*., 2007). High concentrations of AgNPs, 25 $\mu g\ mL^{-1}$, were able to inhibit the growth of all bacterial strains.

Morones and co-workers tested the effects of AgNPs on the gram-negative bacterial strains *Salmonella typhus, Escherichia coli, Pseudomonas aeruginosa* and *Vibrio cholerae,* with no information about where these bacteria came from (Morones *et al*., 2005). At concentrations higher than 75 $\mu g\ mL^{-1}$, none of the bacteria tested showed significant growth, but below this concentration, there were differences in the resistance, with *Escherichia coli* and *Salmonella typhus* being less resistant than *Pseudomonas aeruginosa* and *Vibrio cholerae*.

An investigation of the effects of size on AgNPs antibacterial effect was undertaken by Martinéz-Castañón *et al.* by synthesising nanoparticles of 7, 29 and 89 nm (Martínez-Castañón *et al*., 2008). Initial observations determined that the 89 nm nanoparticles had a slightly altered shape and were found to have the poorest effect on the bacteria *Escherichia*

coli (ATCC 25922) and *Staphylococcus aureus* (ATCC 25923). The smallest of the AgNPs exhibited the greatest antibacterial effect on both bacteria.

Although AgNPs clearly have an antimicrobial effect, multiple studies have looked into combining AgNPs with current antibacterial agents.

Biogenically synthesised AgNPs have been tested alongside antibiotics against four bacterial strains; *Escherichia coli*, *Salmonella typhi*, *Staphylococcus aureus* and *Micrococcus luteus*, all of which were obtained from the Culture Collection Centre but the specific strains used were not listed (Fayaz *et al.*, 2010). The antibacterial effect of the antibiotics was increased when used with the AgNPs, with a greater effect on *Escherichia coli* and *Salmonella typhi*, both gram-negative, than *Staphylococcus aureus* and *Micrococcus luteus*, both gram-positive, an effect of their differently structured cell walls.

Efforts have also been made into the combination of antimicrobial agents in order to improve their effects, with a large number of studies utilising AgNPs.

Polymeric colloids coated with AgNPs were developed by Chen and co-workers and tested against *Escherichia coli* (DH5-Alpha) for their antibacterial properties (Chen *et al.*, 2014). Bacterial growth was found to be completely inhibited. The antibacterial effects were also seen to be size and dose-dependent, with the lowest dosage range of 1 to 10 $\mu g\ mL^{-1}$ having minimal impact and the 500 $\mu g\ mL^{-1}$ being able to completely prevent bacterial growth.

Silver ion release had been tested in a variety of different silver forms in a study by Shankar, Wang, and Rhim (Shankar, Wang and Rhim, 2016). Here, AgNPs were added into alginate-based composite films in order to maintain a steady release of silver ions, then tested these on *Escherichia coli* (ATCC 43895) and *Listeria monocytogenes* (ATCC 15313). These citrate-reduced AgNPs were able to exert a significant antibacterial effect, with a greater impact on *Escherichia coli* (gram-negative) than *Listeria monocytogenes* (gram-positive). In the same study, laser-ablated AgNPs were also found to have a poorer effect than the AgNPs

alone.

Acharya *et al.*, in a similar study to that of Shankar, Wang, and Rhim, developed nano-formulations of AgNPs and alginate or gelatine (Acharya *et al.*, 2017). Gram-negative strains of bacteria were again found to be more susceptible to the effects of these nano-formulations than gram-positive bacteria, with testing completed on various species including *Staphylococcus aureus, Salmonella typhi*, *Escherichia coli* and *Pseudomonas aeruginosa*, all of which were characterised by the Microbial Type Cell Culture (MTCC).

AgNP-containing poly(methyl methacrylate) nanofibers were synthesised by Kong and Jang to allow for an antibacterial effect over a prolonged period, alike that in Shankar, Wang and Rhim (Kong and Jang, 2008). These nanofibers were tested on the bacteria *Escherichia coli* (ATCC 8739) and *Staphylococcus aureus* (ATCC 6538), for which these nanofibers had superior antibacterial properties to both silver sulfadiazine and silver nitrate.

Most of the studies utilised various bacteria to test AgNPs. There was a clear difference in their effects on gram-positive and gram-negative bacteria, with gram-positive bacteria not succumbing to the effects of AgNPs so easily. However, there was still clear cellular damage and cell death detected in gram-positive bacteria.

1.4. Aims and objectives

In this thesis, hybrid nanoparticles (HNPs) containing iron oxide and silver will initially be synthesised and characterised. Following this, laser irradiation will be performed on naked hybrid nanoparticles to determine their ability to heat to a temperature suitable to trigger the retro Diels-Alder mechanism for the release of the drug L-GEM using agar as a mimic for human tissues. Naked hybrid nanoparticles will also have the drug L-GEM attached to their surface, then testing of the release of the drug from the surface of these nanoparticles will be tested, as well as their cytotoxicity and uptake *in vitro*. Following this, naked hybrid nanoparticles will have a novel targeting agent attached to their surface to determine successful uptake and retention of these nanoparticles within two pancreatic cancer cell lines

in vitro. Finally, the prodrug gemcitabine, naked hybrid nanoparticles, and hybrid nanoparticles with L-GEM attached will be tested for their antibacterial activity on gram-negative bacteria.

2.0 Synthesis and characterisation of hybrid nanoparticles

2.1 Introduction

2.11 Hybrid iron oxide nanoparticle synthesis

There has been increasing interest in developing HNPs. They can be used to provide IONPs with a layer of protection against oxidation and subsequent free radical production, as well as providing them with the unique properties from both the core and shell materials used (Mandal *et al.*, 2005). The majority of HNPs reported in the literature focus on gold-coated IONPs for use as image-guided and thermally triggered drug delivery systems. As knowledge and progress in this field grows, researchers have turned to other metallic coating options for IONPs which hold their own unique and interesting properties. Of these, silver-coated IONPs have been of recent interest. This is because of the unique plasmonic properties of silver (much like gold) as well as their inherent antimicrobial action.

In a study by Mandal and co-workers, gold and silver were reduced onto the surface of IONPs using glucose, which allows for better control of shell growth due to being only a mild reducing agent, as well as being both biofriendly and nontoxic (Mandal *et al.*, 2005). The nanoparticles generated still retained their magnetic properties and had increased stability, compared to non-coated IONPs. Alike this study, Iglesias-Silva *et al.* also generated silver-coated IONPs using glucose as a reducing agent (Iglesias-Silvia *et al.*, 2007). Chin, Iyer, and Raston functionalised IONPs with dopamine, then coated these with a layer of gold nanoparticles, with a final layer of gold or silver reduced onto the surface using glucose, as seen in the aforementioned studies (Chin, Iyer and Raston, 2009).

Mahmoudi and Serpooshan created silver-coated SPIONs (Mahmoudi and

Serpooshan, 2012). SPIONs coated with carboxylated dextran had silver ions attached using ethanediylbis-(isonicotinic) then the silver reduced onto the surface using sodium borohydride in deionised water (DI).

This chapter details both the synthesis and characterisation of hybrid silver-coated IONPs which will subsequently be used an antimicrobial nano-ninja for thermally triggered delivery of gemcitabine to pancreatic cancer.

2.2 Experimental

2.21 Synthesis of iron oxide nanoparticles

Sodium hydroxide (1.02 g, 0.14 M) and potassium nitrate (1.82 g, 0.10 M) were dissolved in DI water, with nitrogen bubbled through and left to reflux for 1 h. Iron sulphate heptahydrate (3.82 g, 0.69 M) was sonicated in sulphuric acid (20 mL, 0.02 M) using an MSE Soniprep 150 Plus. This was then added dropwise to the solution under nitrogen and left for 1 h. A nitrogen balloon replaced the stream of nitrogen and the reaction was stirred for 24 h. The nanoparticles were magnetically separated, washed, and then redispersed in DI water. The size, surface charge, and polydispersity index were all measured.

2.22 Synthesis of silver nanoparticles

The procedure to generate silver nanoparticles (AgNPs) was established by Agnihotri, Mukherji, and Mukherji (Agnihotri, Mukherji and Mukherji, 2014). Briefly, sodium borohydride (7.5 mg, 1.98 mM) and trisodium citrate dihydrate (0.11 g, 3.74 mM) were dissolved in deionised water and heated to 60˚C for 0.5 h. Silver nitrate (0.0172 g, 1.01 mM) was added dropwise and the temperature was subsequently increased to 90˚C. Sodium hydroxide (0.1 M) was used to increase the pH to 10.5 and the solution was stirred until there was a noticeable colour change, where the solution went from clear to orange.

2.23 Surface modification of IONPs

2.231 $PEI_{750,000}$

IONPs were sonicated in poly(ethylenimine) (PEI) solution (molecular weight: 750,000, 100 mL, 5 mg mL^{-1}) for 2 h using an MSE Soniprep 150 Plus. The nanoparticles were magnetically separated, washed, and then redispersed in DI water, forming IONP-PEI. The size, surface charge, and polydispersity index were all recorded.

2.232 Silver nanoparticles

IONP-PEI (5 mL) was stirred in the silver seed nanoparticle solution for 2 h at room temperature. The nanoparticles were magnetically separated, washed, and then redispersed in DI water, giving IONP-PEI-AgNP. The size, surface charge, and polydispersity index were all recorded.

2.233 PEI_{2000}

IONP-PEI-AgNP (5 mL) were stirred in solution of PEI_{2000} for 2 h (molecular weight: 2000, 1 mg mL^{-1}). The nanoparticles were magnetically separated, washed, and then redispersed in DI water, giving IONP-PEI-AgNP-PEI. The size, surface charge, and polydispersity index were all recorded.

2.234 Silver coating to form HNPs

2.2341 5 layers

IONP-PEI-AgNP-PEI (5 mL) was added to sodium hydroxide (110 mL, 9.09 mM), stirred at 60˚C. Solutions of silver nitrate (58.9 mM) and hydroxylamine (0.2 M) were created.

The hydroxylamine (750 µL) and silver nitrate (500 µL) were added to the solution once every 10 min for a total of 5 times, the solution then stirred for 30 min. The final nanoparticles were washed with DI water, magnetically separated, then redispersed in DI

water, forming the IONP-PEI-AgNP-PEI-Ag (HNPs). The size, surface charge, and polydispersity index were all recorded.

2.24 Dynamic Light Scattering

The size, surface charge, and polydispersibility index of the nanoparticles at each stage of the synthesis were determined using a Malvern Zetasizer Nano ZS. Solutions were diluted in DI water and measured at 25ºC. Samples were measured in triplicate and an average value recorded.

2.25 Transmission Electron Microscopy

Copper grids (200 mesh, Agar Scientific Co, UK) were placed in chloroform, then left to air dry on filter paper. A glass slide was cleaned using Velen tissue, then quickly dipped in Formvar® solution (0.5 mg mL^{-1}), so that 75% of the slide was covered and subsequently removed, drained then dried by swirling the slide under the heat of a lamp. A razor blade was then used to score the sides of the slide and lowered onto the surface of the water in order to release the film from the glass glide. The copper grids were then placed onto areas of the Formvar that appeared the correct thickness, indicated by the colour of the film (gold or silver), shiny side up. The copper grids were then removed from the slide by gently going around the edge of the grids, then stored until samples were loaded onto them.

The samples (2 µL) were pipetted onto the grids on a strip of parafilm and numbered, left to air dry, with a cover to avoid dust contaminating the samples, then stored prior to viewing using TEM. The samples were then visualised using JEOL 100CX TEMSCAN/JEOL 1230 TEM.

2.26 ICP-OES analysis of the metal content of the hybrid nanoparticles

2.261 Preparing standard solutions

Iron (1001 ppm) and silver (1000 ppm) ICP standards were prepared in water (0.5 – 10 ppm). This stock solution was analysed at 238.204 nm for iron and 328.068 nm for silver on an Agilent Technologies 700 Series ICP-OES.

2.262 Preparing the samples and blank

Samples (400 µL) were added to 2 mL *Aqua Regia* (1:1 HCl:HNO_3), then heated to 60˚C until a colour change occurred indicating that all the particles had been digested. This solution was diluted in DI water and analysed at 238.204 nm for iron and 328.068 nm for silver. Where appropriate, the standard deviation (SD) is stated for three repeats.

2.3 Results and discussion

2.31 Synthesis of hybrid nanoparticles

There were several stages involved in the synthesis of these HNPs, with a schematic of the layering involved shown in Figure 2.

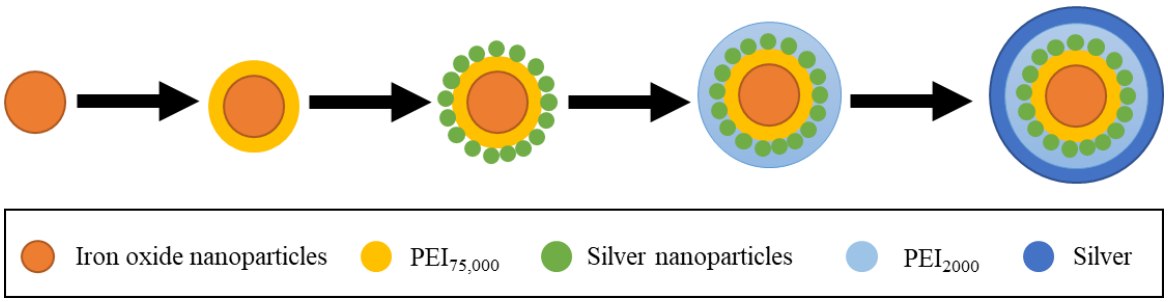

Figure 2: A schematic of the synthetic process utilised to generate the HNPs

Initially, IONPs were generated using a standard coprecipitation method. Since both iron oxide and silver have a negative surface charge, the polymer cationic PEI was used as a cushion between layers. As well as acting as a "charge buffer", these layers also help to

increase the stability of the nanoparticles in solution, especially as the magnetic nature of IONPs causes them to aggregate. Furthermore, the addition of a polymer cushion hinders any electron migration from the silver coating inward towards the IONP which can quench magnetic ability. After the initial addition of a long chain PEI, with a molecular weight of 750,000, the AgNP seeds were added. These AgNPs were specifically synthesised at a low size (<20 nm) using a method by Agnihotri, Mukherji, and Mukherji as these were required to act as anchor points for the subsequent reduction of silver to form the complete HNP coating (Agnihotri, Mukherji and Mukherji, 2014).

After this, a short-chained PEI, with a molecular weight of approximately 2000, was used to stabilise the silver seeds onto the surface and prevent any drop-off, subsequently, silver was reduced onto the surface under basic conditions, forming the complete silver shell. The silver shell will be tested for its ability to heat up when exposed to laser irradiation in later studies for applications in the triggered release of modified gemcitabine and as a potential thermally labile delivery vehicle.

2.32 Characterisation of hybrid nanoparticles

HNPs were successfully characterised using several techniques, including dynamic light scattering (DLS), transmission electron microscopy (TEM), and inductively coupled plasma optical emission spectroscopy (ICP-OES), with DLS and TEM used at each stage of the synthesis.

Zeta potential measurement was a key technique used to monitor and to determine whether each step in the synthetic pathway was successful. As IONPs, AgNP, and silver all have a negative surface charge, a cationic polymer, PEI, was added in between these layers in order to successfully combine these to form HNPs. Polymers of different lengths were used at the two separate stages, with the first long-chained PEI used for wrapping around the IONPs and the shorter chained PEI for stability. The addition of the differently charged layers allowed for the relatively successful determination of whether each synthesis stage had

worked correctly. A clear example of this comes from an early stage synthesis of the HNPs, with Figure 3 illustrating the changes in surface charge throughout the synthesis. Initially, the IONPs were found to have a positive surface charge, which was unusual, but the addition of PEI was seen to be a success due to the increase in positive charge from +20.3 mV to +48.7 mV. The addition of the silver seeds brought the surface charge down to -17.5 mV, with this returning to +17.3 mV upon the addition of the second PEI layer. Finally, the addition of the silver layer was found to have a surface charge of -8.91, indicating that the nanoparticles definitely had some silver coating. These hybrids could not be used, however, due to their low silver content, implying that HNPs were not fully coated, and their overall low iron content. Complete coating is necessary for these nanoparticles because of the reliance on sulphur-silver interactions for drug loading and the attachment of any targeting ligands.

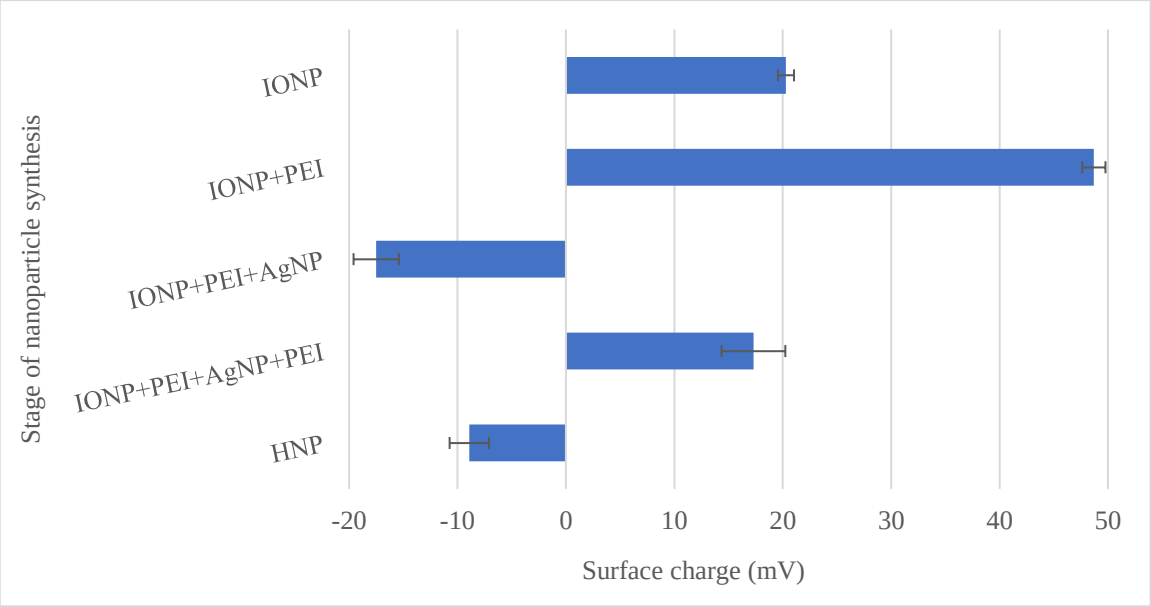

Figure 3: The change in the surface charge of the HNPs at different stages of their synthesis, from the initial "naked" IONPs to the final HNPs, where the error bars indicate the standard deviation.

Table 1 contains detailed information about one batch of HNPs synthesised. Here, the size decreases as you go through the synthesis, with the zeta potential increasing and decreasing throughout the process. Closer to the end of the synthesis, it clearly became more difficult to see a clear size decrease. For the AgNP attachment and the final silver layer, the

surface charge is positive, but these are lower positive values than those of the PEI layers and they are relatively low values of positivity.

Table 1: The size and surface charge information for a later batch of the HNPs for each stage of the synthesis. The final iron and silver concentrations were 3.27 mg mL^{-1} and 4.20 mg mL^{-1} respectively.

	Diameter (nm) ± SD	Zeta potential (mV) ± SD	PDI ± SD
IONP	1663 ± 294.3	-40 ± 0.737	0.683 ± 0.106
IONP-PEI	1090 ± 79.32	+54.5 ± 1.07	0.654 ± 0.008
IONP-PEI-AgNP	856 ± 120.3	+6.98 ± 2.09	0.448 ± 0.073
IONP-PEI-AgNP-PEI	279.4 ± 6.505	+24.7 ± 2.94	0.288 ± 0.039
HNP	271 ± 27.65	+9.55 ± 1.82	0.356 ± 0.006

As well as looking at the surface charge, other factors that were used to determine the addition of each layer were the polydispersity index (PDI) and the size of the nanoparticles. IONPs tend to initially have a much higher size and PDI than expected due to their magnetic properties. Hence, the addition of new layers tends to stabilise the nanoparticles, which is reflected in a decrease in both the size and PDI values, with PDI indicating the size uniformity of the nanoparticles. Table 1 shows a general decrease from the initial PDI of the naked IONPs to a much lower value for the final HNPs generated. Although a lot of information can be obtained about the hybrids, DLS cannot be used alone to determine the successful generation of these nanoparticles, due to several limitations with the technique, hence TEM was used to confirm the size of the nanoparticles.

The magnification power of TEM allows for the visualisation of HNPs, as well as allowing for the visualisation of each stage of the synthesis. There are, however, limitations with the technique, including not necessarily being able to tell the difference between the nanoparticle types, as seen in some of the TEM images taken in Figure 4.

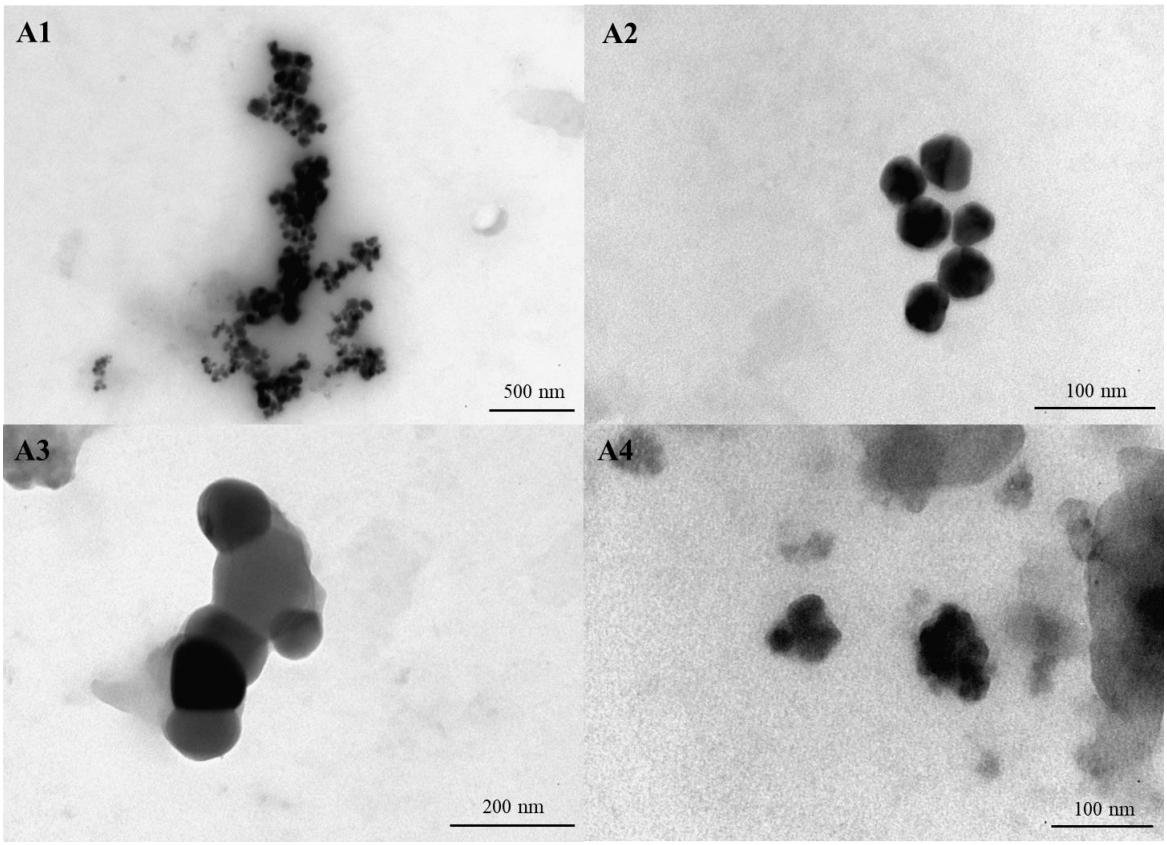

Figure 4: TEM images of HNPs at various stages of their synthesis A1) IONPs coated with $PEI_{750,000}$, A2) Silver nanoparticle seeds, A3) and A4) IONPs coated with $PEI_{750,000}$, silver nanoparticles, and PEI_{2000}.

These were synthesised early in the research, hence the sizes of the IONPs and AgNPs are probably larger than the nanoparticles used in the later stages of the synthesis, where the techniques were better executed.

TEM images taken of HNPs synthesised within another batch, can be observed in Figure 5. Here, there are changes in the morphology that make the hybrid nanoparticle synthesis more obvious. For example, in B1, the IONPs appear to be more angular than the final HNPs presented in B2, which are clearly spherical. As well as this, the IONPs alone also appear to aggregate more than the final HNPs, which is more than likely due to the magnetic forces being stronger without the extra layers. The silver nanoparticles alone also appear to aggregate, but this is a normal property of colloidal solutions.

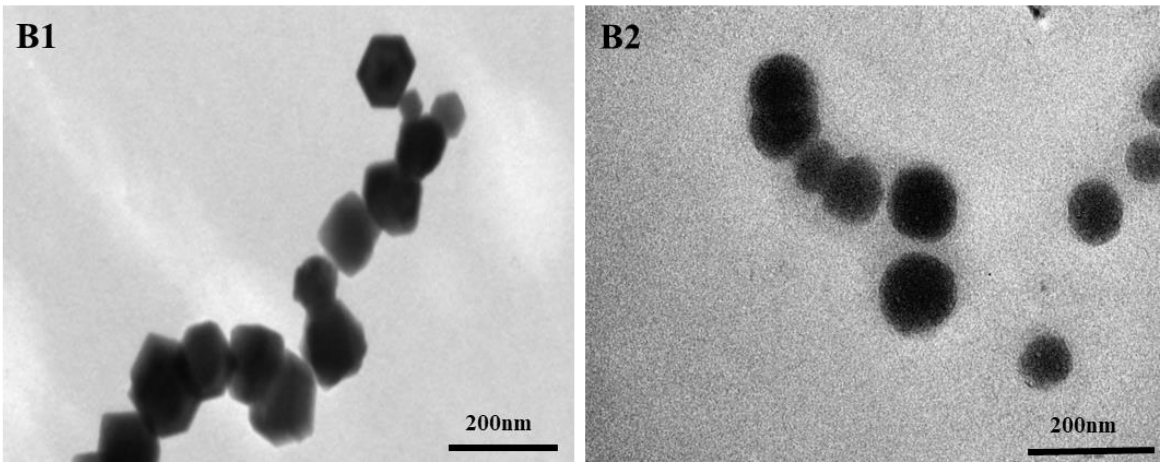

Figure 5: Synthesis of IONPs (B1) and HNPs (B2).

The concentrations and the proportions of metals that made up HNPs were determined by inductively coupled plasma optical emission spectroscopy (ICP-OES). This was particularly important for later studies, in which the addition of these metals was important, including the antibacterial testing and cell culture work. This involved the use of *Aqua Regia* to acid digest the metallic nanoparticles, as solid samples will lead to a blockage in the ICP-OES machine. Two different batches of hybrid IONPs were generated and used for later studies. The initial batch had a much lower concentration of Fe and Ag (0.65 ± 0.012 mg mL^{-1} and 0.02 ± 0.001 mg mL^{-1} respectively) than the newer batch (1.02 ± 0.01 mg mL^{-1} and 0.602 ± 0.015 mg mL^{-1} respectively). This is most likely due to initial teething areas in the synthesis and repetition of the technique, allowing for consistent improvements to be made. Further evidence of this can be seen in more recent syntheses of the HNPs, where there was found to be 3.27 mg mL^{-1} of iron and 4.20 mg mL^{-1} of silver.

Coating of the nanoparticles in silver was determined to be successful using several techniques in combination. Other studies who have generated similar materials include those by Mandal and co-workers (Mandal *et al.*, 2005), Chin, Iyer, and Raston (Chin, Ayer and Raston, 2009), and Iglesias-Silva and colleagues (Iglesias-Silva *et al.*, 2007). Within each of these studies, there was no use of a technique to determine the concentrations of each metal present on these nanoparticles. This makes it more difficult to determine if the concentrations

obtained during this work are relatively standard to other studies. All of the studies did utilise TEM in order to visualise their nanoparticles. Generally, the nanoparticles synthesised within the aforementioned research were smaller than the ones obtained in this study, where all of the papers listed used TEM to determine the size. The difference in size can be explained, as this study utilises an extra layer of polymer and silver seeds in the centre of the hybrids, which is not seen in the studies by Mandal and co-workers, Chin, Iyer and Raston, and Iglesias-Silva and colleagues.

In other studies, similarly structured HNPs have been generated but with gold used in place of silver. Hoskins *et al.* developed IONPs coated with gold seeds, a gold coating, and a gold coating with a layer of polyethylene glycol (Hoskins *et al.*, 2012). It is obvious that the concentration of iron obtained was greater than that obtained within this study, with the greatest concentration being 1.02 mg mL^{-1} and the smallest concentration of iron in the Hoskins *et al.* study being 1.86 mg mL^{-1} for the gold HNPs (AuHNPs). The concentration of gold loaded onto these nanoparticles was also much higher than for the silver hybrids developed here, with the lowest amount of gold loaded being 3.06 mg mL^{-1} for the PEGylated hybrids. This study also managed to get gold concentrations at larger values than those of the iron, which implies a much better coating ability than what was seen in this study. Barnett and co-workers looked into the loading of gold seeds and a gold layer onto different sized IONPs, in order to form AuHNPs (Barnett *et al.*, 2012). Their results differ depending on the thickness of the layers of gold added onto the IONPs, as well as the size of the IONPs themselves. Generally, the nanoparticles with gold seeds had a much lower concentration of gold than those with the shell alone, meaning that the seeded nanoparticles had a lower loading than the silver HNPs here and the coated nanoparticles generally had a higher loading than the silver HNPs.

Curtis *et al.* completed ICP-OES analysis on their samples, determining that the concentrations of iron and gold were 2.6553 ± 0.155 mg mL^{-1} and 0.6827 ±

0.0043 mg mL^{-1} respectively (Curtis *et al.*, 2015). This does, however, imply that there was greater coating with the silver hybrids than with the gold hybrids when comparing the loading of each metal per 1 mg mL^{-1} of iron. This study is most similar to the work here, as they contain both gold seeds and a final gold layer, hence is the easiest to compare to in that respect. However, it is difficult to truly understand the success of loading silver onto the iron oxide, as there are few studies that layer silver in the same manner that is shown here.

A potential method that could be used in order to try and make the synthesis of these HNPs more replicable is microfluidics. Microfluidics allows for the use of smaller quantities of reagents and samples, decreasing costs (Whitesides, 2006). This would allow for greater control of the size of the nanoparticles, whether these be IONPs, AgNPs or the overall final product, and would greatly improve the reproducibility. As well as this, using microfluidics may allow for better control of the thickness of the silver shell. Microfluidics has previously been used to make liposomes for biomedical purposes (Guimarães Sá Correia *et al.*, 2016).

2.4 Conclusion

Here, HNPs composed of silver and iron oxide were successfully synthesised, with confirmation of this involving the use of three analytical techniques; TEM, DLS, and ICP-OES. The ability of these particles to act as ‘nano-heaters’ for thermally releasing drug delivery vehicles will be explored in Chapter 3.

3.0 Investigation into the plasmonic properties of hybrid nanoparticles

3.1 Introduction

HNPs have been synthesised for various applications, with one of the more recent uses for these being heat triggered drug delivery agents. This is due to their unique plasmonic properties. These properties arise from “surface plasmons”, collective oscillations which occur due to the interaction between the free electrons in silver nanoparticles and light (Mie, 1908; Xia and Halas, 2005). This causes peaks to become visible in extinction spectra when excited by a specific wavelength of light, known as the resonance frequency. This phenomenon has been widely studied and has led to the development of several different applications, such as biosensing (Haes and Van Duyne, 2002; Mock *et al.*, 2002; McFarland and Van Duyne, 2003), characterisation of films (Johnston *et al.*, 1995; Granqvist *et al.*, 2013), binding kinetics (Tassa *et al.*, 2010), and drug release kinetics (Korhonen *et al.*, 2015).

Hoskins and co-workers developed gold-coated IONPs as thermally triggered drug delivery systems (Hoskins *et al.*, 2012). These nanoparticles were tested for toxicity on pancreatic cancer cell lines *in vitro* and *in vivo*, having no significant effect on the viability of these cells (Malekigorji *et al.*, 2017; Oluwasanmi *et al.*, 2017). Further testing determined that time and concentration had a clear effect on the heating ability of these nanoparticles when exposed to laser irradiation, with the highest concentration having the best heating ability, based on the concentration of iron (Curtis *et al.*, 2015; Oluwasanmi *et al.*, 2016).

Curtis *et al.* tested the heat dissipation of hybrid gold IONPs (Curtis *et al.*, 2015). Different concentrations of HNPs were dispersed in 2% agar phantom, exposed to laser irradiation for 60 sec, with the temperature monitored using an infrared camera. Within this study, there was found to be no statistically significant difference in the heating ability of the

highest concentrations of nanoparticles (50 µg mL^{-1} and 500 µg mL^{-1}), with each showing a temperature increase of 25˚C and 30˚C respectively over the 60 sec irradiation cycle. As well as this, heat dissipation was seen as wide as 6 mm from the irradiation point at the 60 sec time point, which led to the conclusion that this may have implications in the use of this technology in cancer therapeutics.

In this chapter, the HNPs synthesised within Chapter 2 will be analysed using UV-visible spectroscopy in order to determine an appropriate laser wavelength for irradiation. From here, both the heating profile of the HNPs and the associated heat dissipation will be determined during laser irradiation.

3.2 Methods

3.21 Preparation of nanoparticles

Hybrid gold nanoparticles were prepared by Dr Clare Hoskins using a previously established method (Hoskins *et al.,* 2012).

All other nanoparticle preparations are described in Chapter 2 (sections 2.21 to 2.23).

3.22 UV-Visible spectroscopy

Diluted samples of IONPs, IONP-PEI-AgNP, AgNPs, AgHNPs and AuHNPs were generated and run on a Varian CARY 50 Bio UV-visible spectrophotometer. The samples were scanned between 200-800 nm on the Varian UV Scan Application using a Hellma® Analytics High Precision Cell (HQQ 310H, 10 mm path length). Repeats were not run.

3.23 Laser irradiation of the hybrid nanoparticles

This procedure was adapted from Curtis *et al*. (Curtis *et al.*, 2015). A 2% agar phantom was added into 35 mm Petri dishes. HNPs of 0 µg mL^{-1}, 25 µg mL^{-1} and 50 µg mL^{-1}, were dispersed within the phantom. These were then subjected to laser irradiation at 1064 nm for around 60 sec using a MAL-LASER-YB5 Q-switched Nd:YAG Laser Treatment System

(WeiFang MingLiang Electronics Company Ltd., China) pulsed with a laser spot diameter of 3 mm (10 ns, 6 Hz). Temperature changes within the bulk agar were recorded using an Optris PI640 Thermal Imaging Camera (Optris, Germany). Samples were measured in triplicate and compared to a control sample of agar alone. The thermal changes within the beam culmination point and the heat dissipation away from this point were measured and reported. Optris PI Connect software was used to record the data (Optris, Germany). Samples were measured in triplicate and compared to a control sample of agar alone

3.24 Statistical analysis

Any graphs generated were created on Microsoft Excel, with the mean value reported and error bars indicating the SD.

Statistical tests were run on the IBM SPSS Statistics 24 software, with the statistical test or tests run stated in the results and discussion.

3.3 Results and discussion

UV-visible spectroscopy was utilised to determine the surface plasmon resonance of silver and from this the wavelength that the laser should be used at. The spectra of IONPs, IONP-PEI-AgNP, AgNPs, AgHNPs and AuHNPs can be seen in Figure 6. AuHNPs were generated by Dr Clare Hoskins, as per the method stated in Barnett *et al.* (Barnet *et al.*, 2012).

There are clear peaks for the IONPs (586.94 nm), AgNPs (404.96 nm), AuHNPs (616.99 nm) and HNPs (638.00 nm). For the IONP-PEI-AgNPs, the peak was not as clear as those of the other nanoparticles, which may be due to not having the full coating of silver. The peak positions give an indication of the success of IONP coating with silver, as the IONP peak has clearly shifted in the AgHNP sample. The same can be said when looking at the difference in the peak positions of the AgNPs and the AgHNPs. These shifts are also indicative of a change in the size of the nanoparticles, as the final hybrids will be larger than both the IONPs and AgNPs. As well as this, the dip in the spectrum of AgHNPs at around 300

nm can also be seen in the UV-visible spectrum of AgNPs, which can also be used to determine the presence of silver on the surface of the final HNPs.

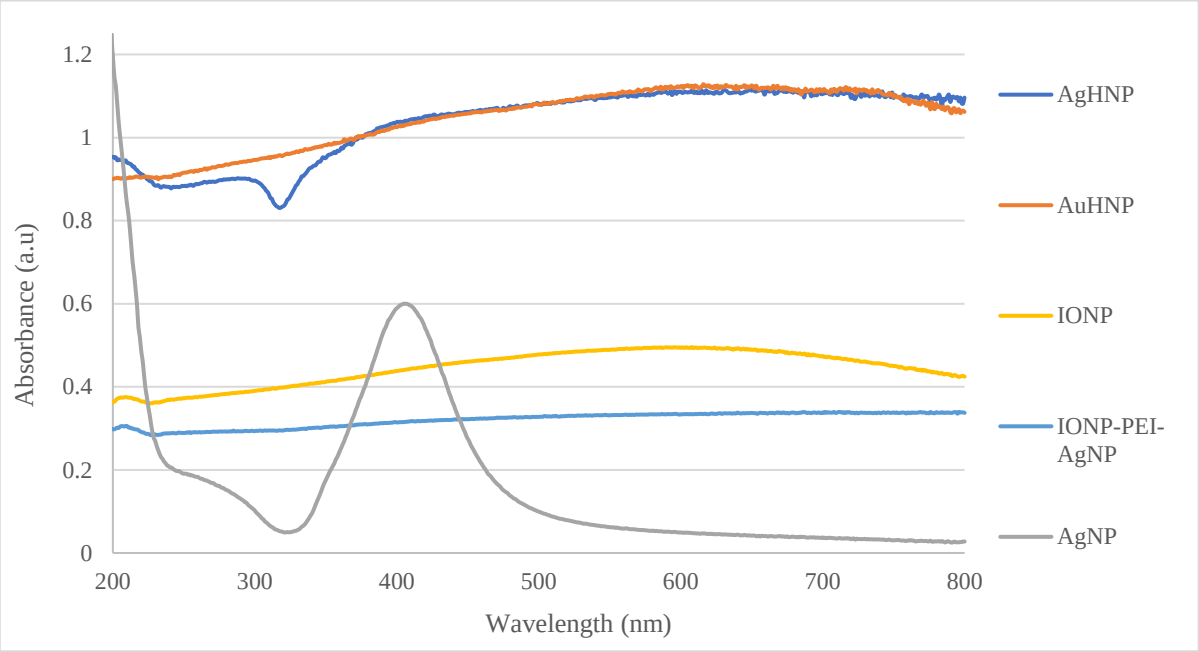

Figure 6: The UV-vis spectra silver HNPs (AgHNPs), AuHNPs, IONPs, IONPs coated with PEI and AgNPs, and AgNPs alone.

Previous studies using AuHNP were irradiated at 1064 nm, allowing these HNPs to produce heat quickly. In order to determine whether the same method could be applied to the AgHNPs, it was clear that UV-vis should also be run on the AuHNPs to compare their surface plasmon resonances. When looking at the spectra, it can be seen that the two samples greatly overlap, with the only clear differences seen around 300 nm where there is a dip in the spectra of the AgHNPs that matches the one seen around that area in the AgNPs. The AgHNPs do appear to plateau more than the AuHNPs, but there does not appear to be any other major differences between the two. This overlap implies that the surface plasmon resonances for these hybrids should be the same, hence the 1064 nm laser could be used for the AgHNPs. Hoskins and co-workers previously used UV-visible spectroscopy to determine an appropriate wavelength for laser irradiation of AuHNPs (Hoskins *et al*., 2012). The peaks for the IONPs and gold nanoparticles were seen to be further to the left of the spectrum than that of the AuHNPs, indicating successful coating of the IONPs by gold. The shift in the peak seen in the

Hoskins *et al.* study matches what was seen within the within this work, except using silver instead of gold.

In order to determine if HNPs generated here were able to successfully heat up inside biological tissues, HNPs were dispersed in 2% agar phantoms, with irradiation using a wavelength of 1064 nm for 60 sec. Agar has been used in several studies as a mimic for biological tissues (Aranda-Lara, Torres-Garcia, and Oros-Pantoja, 2014; Dabbagh *et al.*, 2014; Curtis *et al.*, 2015) hence would be able to provide accurate information about the heating ability of these hybrids within the tumour environment. The wavelength 1064 nm has been proven to be safe for human skin, as this wavelength is commonly used for tattoo removal, skin rejuvenation (Tanaka, Matsuo, and Yuzuriha, 2011) and mole removal (Kim *et al.*, 2012b). An infrared camera was used in order to provide accurate information about the temperature change of the agar over time and the dissipation of the heat across the agar, with these measurements taken at the laser culmination point. The data showed that there was a difference in the heating abilities of both the 25 µg mL^{-1} and 50 µg mL^{-1} nanoparticles when looking at the average temperature over time (Figure 7) and when looking at the average temperature change over time (Figure 8).

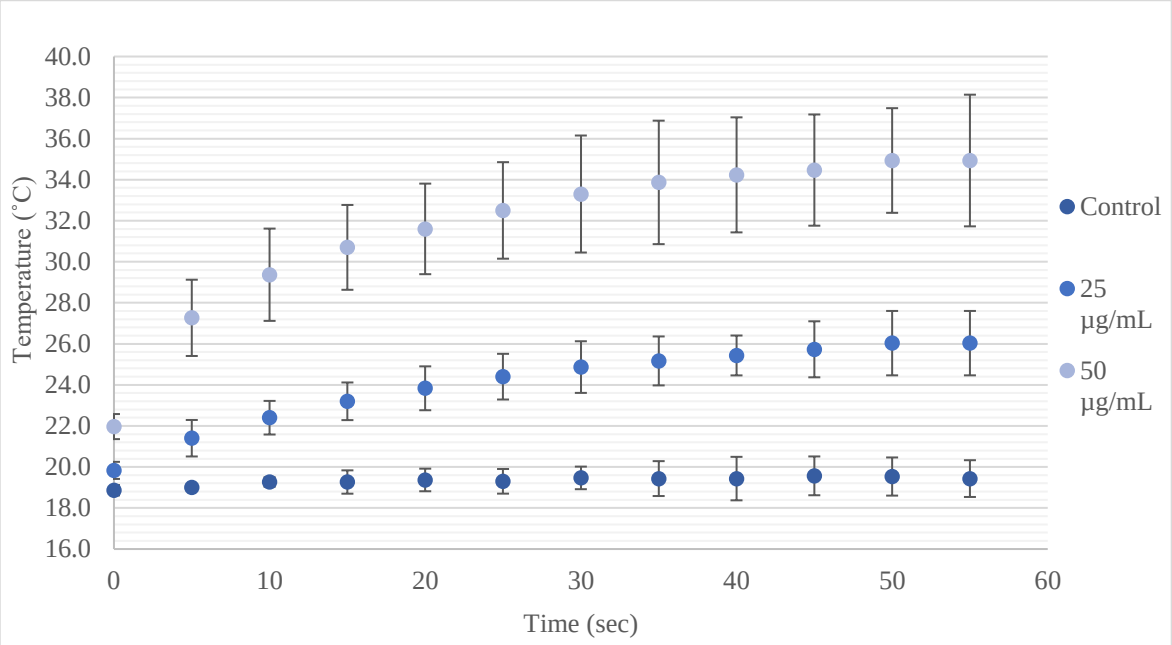

Figure 7: The average temperature at different time intervals for different concentrations of HNPs.

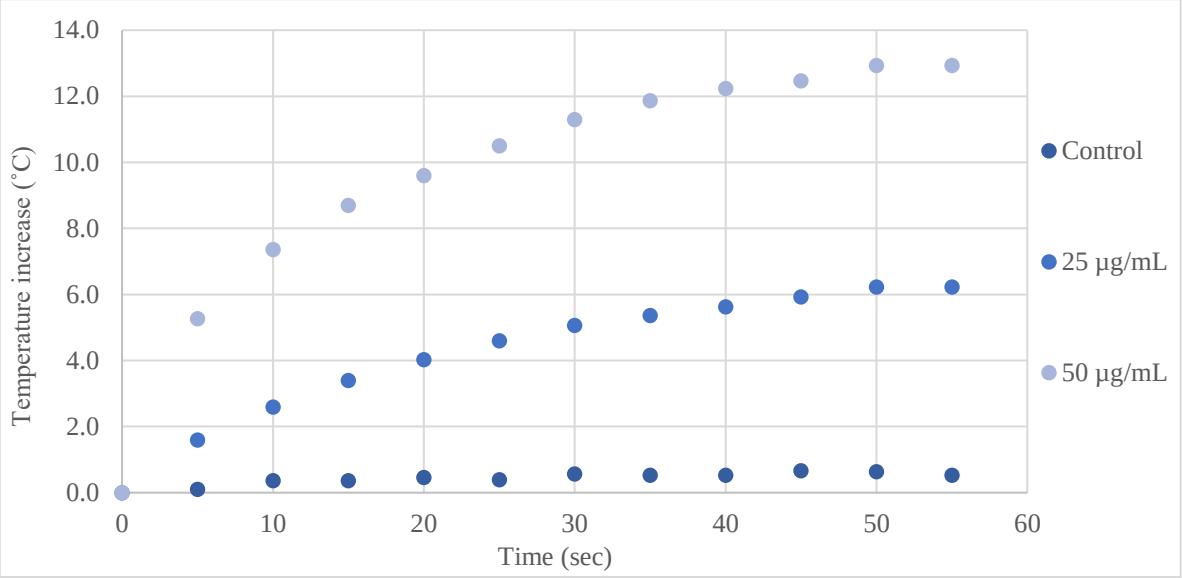

Figure 8: The average change in temperature over time for hybrid nanoparticle concentrations, 25 µg mL^{-1} and 50 µg mL^{-1}, alongside a control, when exposed to laser irradiation at 1064 nm.

When exposed to laser irradiation, the control heated to a maximum temperature of 19.6˚C, with a no real increase in temperature over the period. The nanoparticles with an iron concentration of 25 µg mL^{-1} showed a steady increase over the time period, with the maximum temperature reaching 26.0˚C. The nanoparticles with an iron concentration of 50 µg mL^{-1} showed a relatively fast increase over the time period, with the maximum temperature reaching 34.9˚C. The maximum increase in temperature was found to be 0.7˚C, 6.2˚C and 12.9˚C for the control, 25 µg mL^{-1} and 50 µg mL^{-1} respectively.

A two-way ANOVA was used to analyse the data for the temperature change over time when using HNPs of different concentrations. This was in order to deduce whether the time, concentration, and an interaction between the two had a statistically significant impact on the temperature. As the data was found to both deviate from normality using Shapiro-Wilk ($p<0.05$) and had inequality of variances based on Levene's test ($p<0.05$), data transformations were attempted on the data. After completing a $\log_{10}$ data transform, the equality of variances based on Levene's test was found to be above the threshold ($p>0.05$), but the data still deviated from normality. Because ANOVA's are relatively robust against deviations from normality, and there were minimal deviations within the data acquired, the

two-way ANOVA was continued, with a significance level of $p = 0.01$ to compensate for the error in normality. The results of this determined that there was a statistically significant interaction between time and concentration of HNPs ($p<0.01$) and that the data for the concentration and time were both individually statistically significantly different. Pairwise comparisons were then completed in order to determine at which time and concentration there was a statistically significant difference.

Initially, the mean differences between the concentrations were looked at over time with the mean differences between the time points for each concentration looked at subsequently.

At the initial time point (0 sec), there was a statistically significant difference between the 0 μg $mL^{-1}$and 50 μg mL^{-1} samples ($p<0.01$). There was no statistically significant difference between the 0 μg $mL^{-1}$and 25 μg mL^{-1}. As well as this, there was also no statistically significant difference between 25 μg mL^{-1} and 50 μg mL^{-1} samples. The same results can be seen for both the 5 sec and 10 sec time intervals. After this, there are statistically significant differences between all of the concentrations at each of the time points, indicating that over time, there is better heating when using the nanoparticles than without the nanoparticles and that the higher concentration nanoparticles were better able to heat than the lower concentration after 10 sec.

There was deemed to be no statistically significant difference between any of the time points for the control ($p>0.01$). For the 25 μg mL^{-1}, there was no statistically significant difference between the time points 0, 5, 10, and 15 sec. The 5 sec time point was also not statistically significantly different from the 20 sec time point. The 10 and 15 sec time points were both not statistically significantly different to all of the remaining time points (20, 25, 30, 35, 40, 45, 50 and 55 sec). All of the remaining time points were found to only be statistically significantly different to the 0 sec time point except for 45, 50 and 55 sec, which were all also statistically significantly different from 5 sec. For 50 μg mL^{-1}, 0 sec was

statistically significantly different to all other time points ($p<0.01$). 5 sec was found to be statistically significantly different to 30, 35, 40, 45, 50 and 55 sec. The 10, 15, 20 and 25 sec time points were all found to only be statistically significantly different from 0 sec. 30, 35, 40, 45, 50 and 55 were all only found to be statistically significantly different to the 0 and 5 sec time points.

These data seem to give an indication that time has a very weak effect on the temperature produced by HNPs and that the concentration of HNPs is the main reason for the difference in temperature produced. The starting temperature for the 50 μg mL^{-1} HNPs was statistically significantly different from the control and 25 μg mL^{-1} sample, being higher than both other samples by 3.1˚C and 2.2˚C respectively. The average start temperature did increase for all of the samples, and it can be very difficult to control the temperature of the room. As well as this, the temperature was still relatively ambient and initial start temperature did not appear to have a significant effect on the results when looking at the overall temperature increase, comparing each sample to its own starting temperature (Figure 8).

As well as determining the heating capacity of these nanoparticles, the spread of the heat was also investigated (Figures 9 and 10). Heat dissipation is an important factor in the use of thermally triggered drug delivery or, indeed, thermal ablation therapies. In both of these applications, it is desirable to produce localised heat in order to exert the desired effect only within the irradiation site whilst protecting the surrounding healthy tissues.

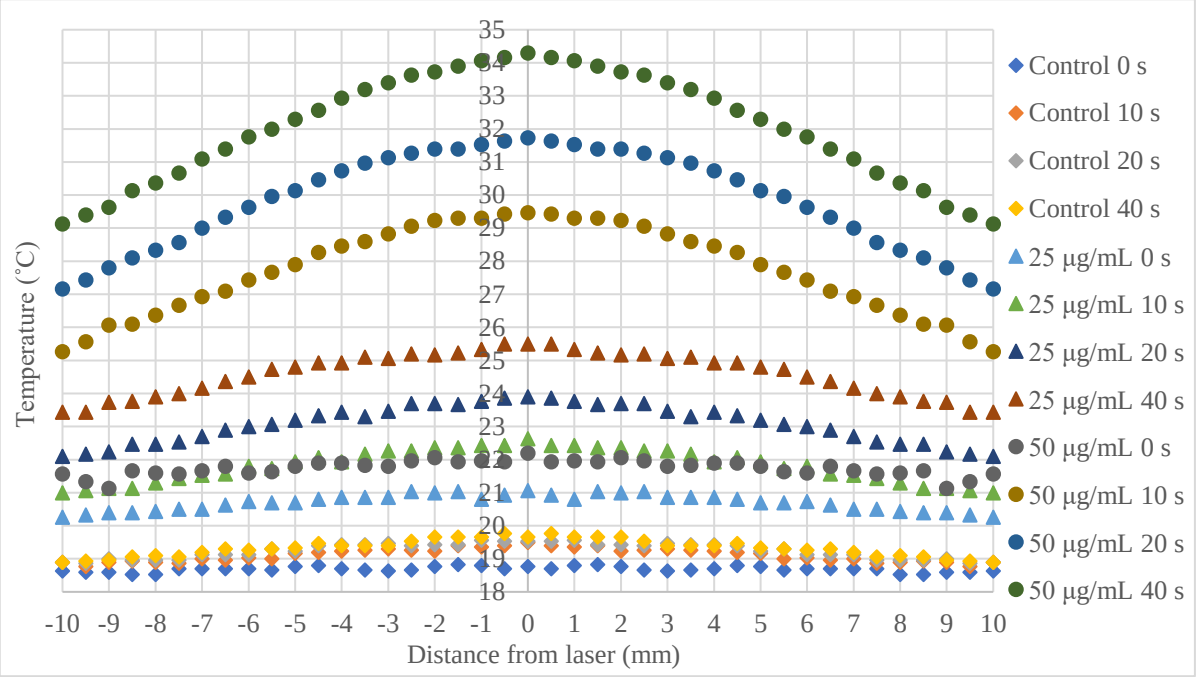

Figure 9: The heat dissipation when firing laser light (1064 nm), where the diamonds represent the control, the triangles the 25 µg mL^{-1} HNPs and the circles 50 µg mL^{-1} HNPs. The time intervals indicate the temperature during nanoparticle irradiation.

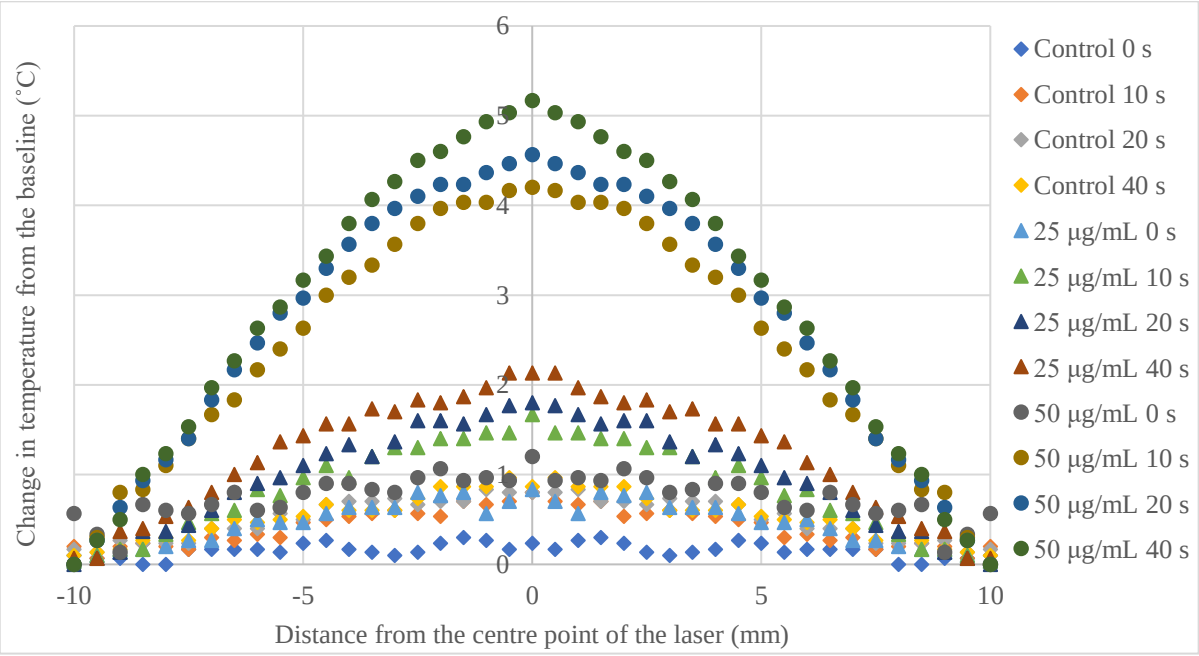

Figure 10: The change in temperature from the starting temperature of the agar when firing laser light (1064 nm), where the diamonds represent the control, the triangles the 25 µg mL^{-1} HNPs and the circles 50 µg mL^{-1} HNPs. The time intervals indicate the temperature during nanoparticle irradiation.

The heat dissipation from the laser culmination point was measured at four different time intervals; 0 sec, 10 sec, 20 sec and 40 sec with the spread of the temperature measured using the thermal imaging software provided in order to obtain accurate information of the temperature across the agar. Figures 8 and 9 show the data collected, with Figure 8 representing the average temperature of the agar across the 10 mm distance, and Figure 9 the average temperature increase across the same distance.

From the data (Figures 8 and 9), it is easy to see that the data for the control at each of the time points did not differ greatly from one another. For the 25 μg mL^{-1} hybrids, there is an increase in the temperature spread at each time point, but these do not seem to differ massively from the controls until the 20 sec and 40 sec points and do not reach the levels of spread seen with the 50 μg mL^{-1}. The change in the control is relatively minimal, with the maximum increase seen to be around 1˚C around where the laser was focused. 50 μg mL^{-1} hybrids had values that were relatively well separated in both Figures. As shown in Figure 9, the 50 μg mL^{-1} hybrids had the greatest dissipation overall, with a 2˚C increase from the baseline temperature even 6 mm away from the centre.

Statistical analysis of this data was completed by running separate Kruskal-Wallis H tests, as the data was not normal, as determined by Shapiro-Wilk, nor did it have equality of variances, determined using Levene's test ($p<0.001$). There was found to be no statistically significant difference in the temperature across the agar gel ($p>0.05$), which matches the data obtained. Further, there was found to be a statistically significant difference in the temperature with both concentration ($p<0.05$) and time ($p<0.05$). Pairwise comparisons then determined that the 0 sec time point was statistically significant from all other time points ($p<0.05$). As well as this, there was a statistically significant difference between the 10 and 40 sec time points ($p<0.05$), and all of the concentrations were all found to be statistically significantly different from one another ($p<0.05$). These all generally seem to well explain the data obtained, but it is much harder to tell by eye due to the nature of the graph.

Although these experiments started at ambient room temperature, it is believed from the literature that the extent of heating production remains unchanged when the starting temperature is elevated. With this being said, the temperature increase attained by the silver HNPs was over 10˚C for the 50 µg mL^{-1} HNPs. As body temperature is known to be 37˚C, the 50 µg mL^{-1} hybrids should be able to generate over the 44˚C required to allow for the retro Diels-Alder mediated release of gemcitabine.

Similar experiments have used AuHNPs rather than silver, with testing completed both *in vitro* and *in vivo* in order to determine the success of using a thermally triggered release mechanism (Oluwasanmi *et al.,* 2017; Malekigorji *et al.,* 2017). Curtis *et al.* reported that the 50 µg mL^{-1} AuHNPs were able to produce a 25˚C heat increase, with a maximum temperature of 40˚C reached almost immediately after irradiation had begun. In further studies, 4-6-week-old Nu/Nu female mice with BxPC-3 xenografted tumours were used as a model, with the tumours irradiated for 20 sec each using 1064 nm laser (Malekigorji *et al.,* 2017). There was a clear reduction in tumour volume of the mice when HNPs were used in conjunction with the bisnaphthalamide propyl spermine tetrahydropbromide.

There are obvious pros and cons to the heating profile of the silver HNPs, especially as the AuHNPs were able to heat instantaneously then plateau (Curtis *et al.,* 2016; Malekigorji *et al.,* 2017), whereas silver HNPs heated more steadily over time. The steadier heating period may allow for more controlled release of the gemcitabine from the surface of HNPs in comparison to the AuHNPs, as these have been found to release almost all of the drug at once (Oluwasanmi *et al.,* 2017). However, this would require larger administration of the silver HNPs in order to get the same heating, and therefore the same level of release as shown by the gold. Silver HNPs were also seen to have a wider heat dissipation than the AuHNPs, which may be problematic as there needs to be minimal damage to any healthy surrounding tissues. In order to reach the temperature required to release gemcitabine *via* the

retro Diels-Alder mechanism (44˚C), a heat increase of 7˚C would be required, which may mean that there would need to be a longer irradiation period. In mice studies using the AuHNPs at 50 μg mL^{-1}, the maximum time that the tumours were irradiated was 20 sec (Oluwasanmi *et al.*, 2017). The 50 μg mL^{-1} silver HNPs were able to increase the temperature by 7˚C at the 10 sec time point, which means that these HNPs would be able to release some of the drug within the time frame used. However, the gold hybrids were able to do this at a much faster rate and were able to release a large proportion of the drug (80%) within the time frame (Oluwasanmi *et al.*, 2017). Nevertheless, this could be beneficial if there was a need for the prolonged release of a drug. Potentially, there would be applications if it were possible to attach drugs that were previously too toxic for clinical use even at a low dosage, as silver HNPs could be used as a delivery system and allow for both controlled and slow release of the drug.

It may be possible to tune these HNPs in order to improve the heating profile. Increasing the concentration of the silver may help, as for these nanoparticles, the proportion of loading of silver onto the IONPs was much lower than that of gold, if comparing them based on the concentration of iron. As time progressed, the amount of silver loaded onto the HNPs did increase, as seen in Chapter 2, and the hybrids tested here were the ones with the lowest concentration of silver generated. Hence, further testing is required to determine what the optimum silver shell thickness is in order for these hybrids to heat to a temperature suitable for the thermal release of modified gemcitabine.

Overall, the data obtained imply that the HNPs generated here may be better suited for thermal ablation therapies within the clinical setting rather than for thermally triggered drug release unless there was the need for prolonged release of a drug into tissues.

3.4 Conclusion

This work has shown that the HNPs formed were capable of thermal rise within the temperatures required for elevation to 44˚C. The statistical analysis of the data determined

that there were clear effects of time and concentration of HNPs on the temperature reading of the agar. It was especially clear that there was some form of interaction between the two effects, given the low p-value. Despite the overall results being generally positive and the silver HNPs being able to be used for thermally triggered drug release, caution must be taken to ensure localised heating given the extended irradiation time required and heat dissipation. The next chapter will explore the ability of these HNPs to release the drug gemcitabine, determine the uptake of HNPs into pancreatic cancer cell lines *in vitro*, and determine the cytotoxic effects of HNPs, gemcitabine alone and HNPs with gemcitabine attached.

4.0 Drug loading and drug release

4.1. Introduction

4.11. Thermally labile drug delivery systems

Although nanoparticles of various types have been proven to be successful drug delivery agents, one of the main issues faced is controlling the release of drugs from these systems. For systems where the connections to the nanoparticles are relatively unstable, drug release could occur in any tissues, not just those for which the delivery system was intended. This could cause side effects, like those seen with a generally administered drug. However, systems that release the drug too slowly would also be unfavourable, with a decreased therapeutic effect possible.

One method to combat this is the use of a thermally labile drug delivery system. Here, the drug is attached to the surface of the nanoparticle, which can be done using a variety of methods, then released when exposed to higher temperatures, potentially allowing for the controlled heating of certain tissues. This has been demonstrated using both iron oxide and HNPs.

Oluwasanmi and co-workers used a Diels-Alder linker to attach gemcitabine onto the surface of gold iron oxide HNPs, allowing for the possibility of thermal release *via* reversal of the Diels-Alder mechanism (Oluwasanmi *et al.*, 2017). There was a clear effect of temperature on release, with lower temperatures of 20˚C and 37˚C showing lower rates of release of the gemcitabine than when at 44˚C, where after 60 sec 80% of the drug was released at pH 7, and similar release rates were seen at pH 7.4 and 5.6 over the same period of time.

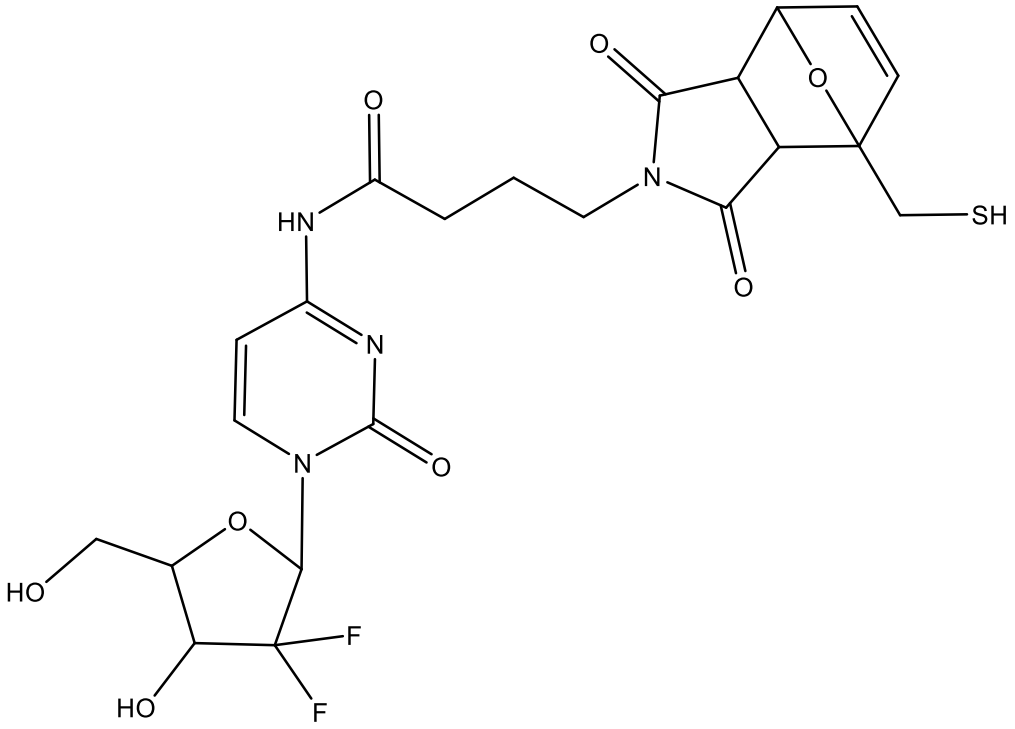

Figure 11: The chemical structure of L-GEM

Most recently, Fuller *et al.* worked on the thermally controlled release of the drug fluorescein in the form of a polymer attached to magnetically controlled nanocarriers, with release *via* a Diels-Alder mechanism (Fuller *et al.*, 2019). Here, superparamagnetic IONPs were combined with a thermally labile polymer, where the drug was loaded onto side chains of the polymers. There was found to be a <1% release of the drug at 37˚C, with minimal release at room temperature (23˚C) when using an alternating magnetic field (AMF). The temperature was found to have an effect on release, with increasing temperature causing an increase in drug release over a period of 1 h. AMF pulses were also used to trigger release, with these being able to release a much greater proportion of the cargo than the control and the temperature of the samples seen to increase to 50˚C.

In this chapter, the initial aim was to complete and determine the loading of the modified gemcitabine (L-GEM), shown in Figure 11, onto the surface of the HNPs. After this, the aims were to determine if release of the drug from the surface was greater with an elevated

temperature. Finally, both the uptake of the drug into the cells and the cytotoxic effects of naked HNPs, free gemcitabine and L-GEM conjugated onto the surface of the HNPs were determined.

4.2 Methods

4.21 Loading of gemcitabine

4.211 Calibration curve of gemcitabine

A calibration curve was generated using known concentrations of gemcitabine plotted against the peak area (R^2 = 0.9989). The procedure used was adapted from Oluwasanmi *et al.* (Oluwasanmi *et al*., 2017). All samples were run using a solvent system of 1:1 acetonitrile/water at a flow rate of 1 mL min^{-1} in a C18 reverse-phase column (150×3mm) [ACE Equivalence] and an injection volume of 10 µL on a UV-HPLC (Shimadzu Prominence). Samples were analysed at 275 nm, with this being gemcitabine's optimum detection wavelength (Kirstein *et al.*, 2006).

4.212 Addition of L-GEM onto the surface of hybrid nanoparticles

L-GEM (20.6 mg) was stirred with 2 mL HNPs (1 mg mL^{-1}) for 1.5 h. The solution was removed, the nanoparticles washed and then redispersed in 2 mL water. The amount of L-GEM successfully loaded onto the surface of the HNPs was determined using HPLC, using the same method as in 4.211. Samples were measured in triplicate and an average value recorded.

4.22 Thermal release study

L-GEM loaded HNPs (1 mL, 0.05 mg mL^{-1} based on L-GEM concentration) were placed into Eppendorf tubes. Samples were either heated at 44˚C or left at room temperature. At the time intervals of 1 min, 5 min, 10 min, 20 min, and 30 min, 100 µL of the sample was removed by holding the HNPs against a magnet. HPLC was then used to determine the

success of release, using the method stated in 4.211. Samples were measured in triplicate and an average value recorded.

4.23 Cell culture

4.231 MTT cytotoxicity assay

BxPC-3 and PANC-1 cells were cultured in RPMI and DMEM media respectively, with media supplemented with 10% foetal bovine serum and 5% penicillin-streptomycin, with 5% L-glutamine also added into DMEM. MEM was substituted for DMEM in this case when the DMEM ran out. BxPC-3 and PANC-1 cells were seeded into 96-well plates at 15,000 cells per well, with three wells used per time interval for each of the cell lines.

L-GEM (70 µL) loaded nanoparticles were diluted in 2.5 mL of DMEM and RPMI respectively, then subsequent dilutions of this and other generated solutions completed to give drug concentrations of 0 µg mL^{-1}, 0.01 µg mL^{-1}, 0.1 µg mL^{-1}, 1 µg mL^{-1}, 5 µg mL^{-1}, 10 µg mL^{-1}, 25 µg mL^{-1}, 50 µg mL^{-1} and 100 µg mL^{-1}. Gemcitabine alone was also made to concentrations of 0 µg mL^{-1}, 0.01 µg mL^{-1}, 0.1 µg mL^{-1}, 1 µg mL^{-1}, 5 µg mL^{-1}, 10 µg mL^{-1}, 25 µg mL^{-1}, 50 µg mL^{-1} and 100 µg mL^{-1}. Dilutions of HNPs were also generated by diluting 24 µL in 5 mL of DMEM and RPMI respectively, then subsequent dilutions of this and other generated solutions completed to give with iron concentrations of 0 µg mL^{-1}, 0.0028 µg mL^{-1}, 0.028 µg mL^{-1}, 0.28 µg mL^{-1}, 1.4 µg mL^{-1}, 2.8 µg mL^{-1}, 7 µg mL^{-1}, 14 µg $mL^{-1}$and 28 µg mL^{-1}.

After confluent growth was determined, 100 µL of each sample and concentration were added into a well, where media and DI water were used for positive and negative controls respectively. One plate for each sample was removed and placed in a separate oven heated to 44˚C for 1 h, then replaced in the incubator for the remaining time. The media/water was then removed, each well was washed with 100 µL media, then fresh media added. 50 µL of MTT was then added into each well, then the plates were replaced in the oven for 4 h. The

solutions were removed from the wells, then 100 µL DMSO added. The samples were scanned using a Tecan Infinite M200 Pro and the Tecan i-Control software. Plates were run under the Absorbance setting, with the wavelength set to 570 nm. Shaking was completed for 10 sec with an amplitude of 1 mm in the "Linear" mode before analysis. Samples were measured in triplicate and an average value recorded.

4.232 Drug uptake study

L-GEM (111 µL) loaded nanoparticles were diluted in 5 mL of DMEM and RPMI respectively, then subsequent dilutions of this and other generated solutions completed to give drug concentrations of 0 µg mL^{-1}, 0.0125 µg mL^{-1}, 1.25 µg mL^{-1}, 50 µg mL^{-1} and 100 µg mL^{-1} based on the concentration of gemcitabine. A control of naked IONPs was generated based on the 100 µg mL^{-1} concentration of gemcitabine, giving an iron concentration of 28 µg mL^{-1}. After the media was removed, 300 µL of each solution was added into a well, then left for 1 h, 6 h and 24 h. After each time interval, the media containing the nanoparticles, and the control, was removed and washed with 1 mL phosphate-buffered saline (PBS). 185 mL trypsin was added to each well, then 1 mL of fresh media added into each when cell detachment was completed.

Cells were lysed using water (1 mL), any nanoparticles removed by magnetisation. The amount of drug released was determined using HPLC, using the same method as in 4.211. Samples were measured in triplicate and an average value recorded.

4.233 Cell counting

The number of live cells was determined by adding 20 µL of cells in media to 100 µL of Trypan Blue, then the cell count determined on a cell counter.

4.24 Statistical analysis

Any graphs generated were created on Microsoft Excel, with the mean value reported and error bars indicating the SD.

Statistical tests were run on the IBM SPSS Statistics 24 software, with the statistical test or tests run stated in the results and discussion.

4.3 Results and discussion

The addition of L-GEM onto the surface of the HNPs was carried with relative ease, as stirring at room temperature for 2 h was enough to facilitate the addition due to the strong bonds formed between silver and sulphur. The nanoparticles were washed after loading in order to accurately determine the amount of L-GEM that successfully attached to the surface of the hybrids.

The loading of L-GEM onto the surface of the HNPs was determined using high-pressure liquid chromatography (HPLC). Calibration standards of the drug gemcitabine were made up in water, then run through the HPLC under conditions adapted from Oluwasanmi *et al.* (Oluwasanmi *et al.*, 2017), with the calibration data shown in Figure 12.

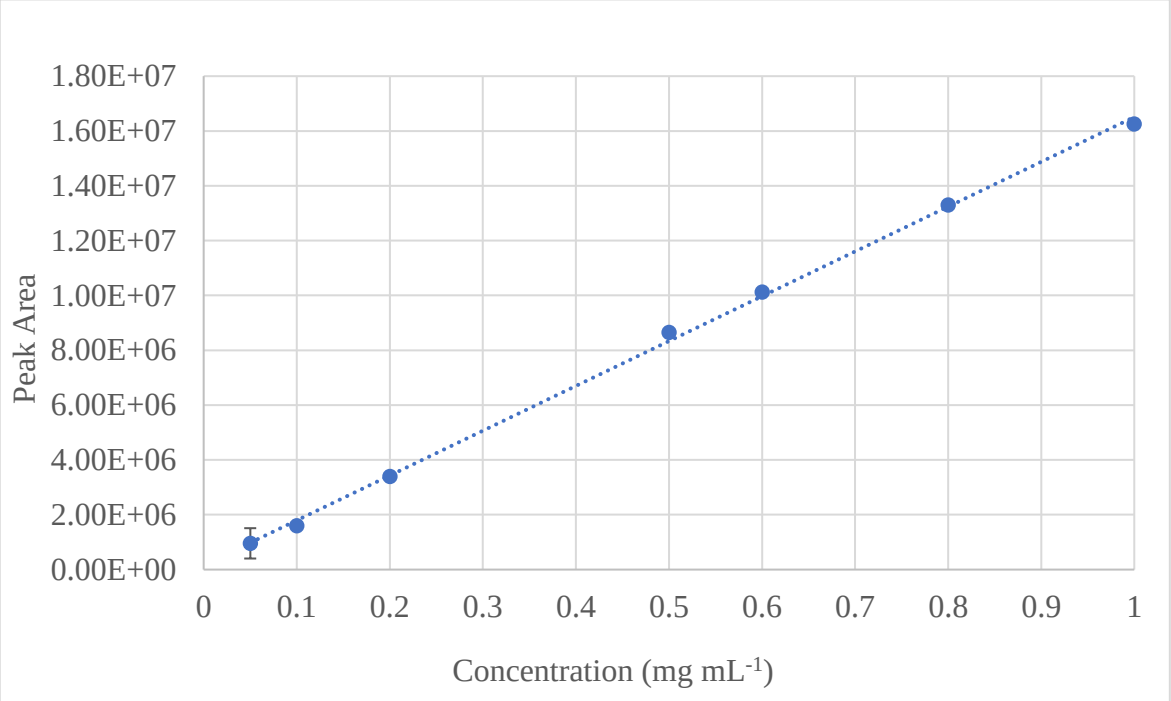

Figure 12: The calibration curve created by plotting the known concentrations of gemcitabine from the peak area obtained from HPLC at a wavelength of 275 nm, where error bars indicate the standard deviation.

The solution removed from the HNPs was then run on the HPLC, giving a concentration for the amount of gemcitabine present in the sample. The concentration of the L-GEM was then back-calculated from this using the molar masses of both gemcitabine and L-GEM respectively. It was determined that 73.8% of the L-GEM was attached to the nanoparticle's surface. Based on this data, it can be said that the ratio of gemcitabine to HNPs, based on the iron concentration, was 3.7:1, which is similar to the 5:1 ratio obtained in the Oluwasanmi *et al.* study (Oluwasanmi *et al.*, 2017).

Subsequently to the successful loading of the drug onto the surface of the HNPs, the uptake, release and cytotoxicity were all established.

Release of the drug from the surface of the HNPs is induced *via* laser irradiation. The ideal temperature to allow for the retro Diels-Alder mechanism to occur is 44˚C, with the mechanism for this seen in Figure X.

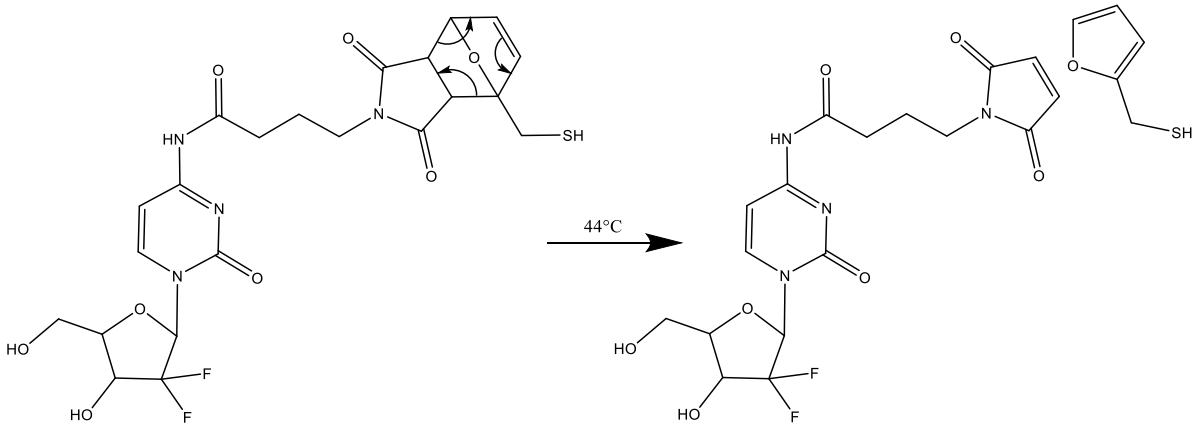

Figure 13: The mechanism of release of modified gemcitabine from the surface of the HNPs. This thermally triggered release occurs at 44˚C when irradiated with a laser.

The results from the release study can be seen in Figure 13, where both the room temperature sample and the 44˚C sample clearly show minimal release. HNPs were able to release a maximum of 0.13% and 1% for the heated and non-heated nanoparticles respectively.

Because the data both deviated from normality and had inequality of variances that could not be fixed using data transformations, an independent samples Kruskal-Wallis H test

was run on the data for both the time and temperature (heated or not heated). It was confirmed that the percentage drug release was the same at each time point ($p>0.05$) but there was a statistically significant difference between the two temperatures ($p<0.001$). Although the statistical analysis did confirm that there was a statistically significantly poorer release of gemcitabine from the heated HNPs that those without heating, in the grand scheme of things, the release was minimal, with the difference between the maximum amount of drug released for each of the samples being less than 1%.

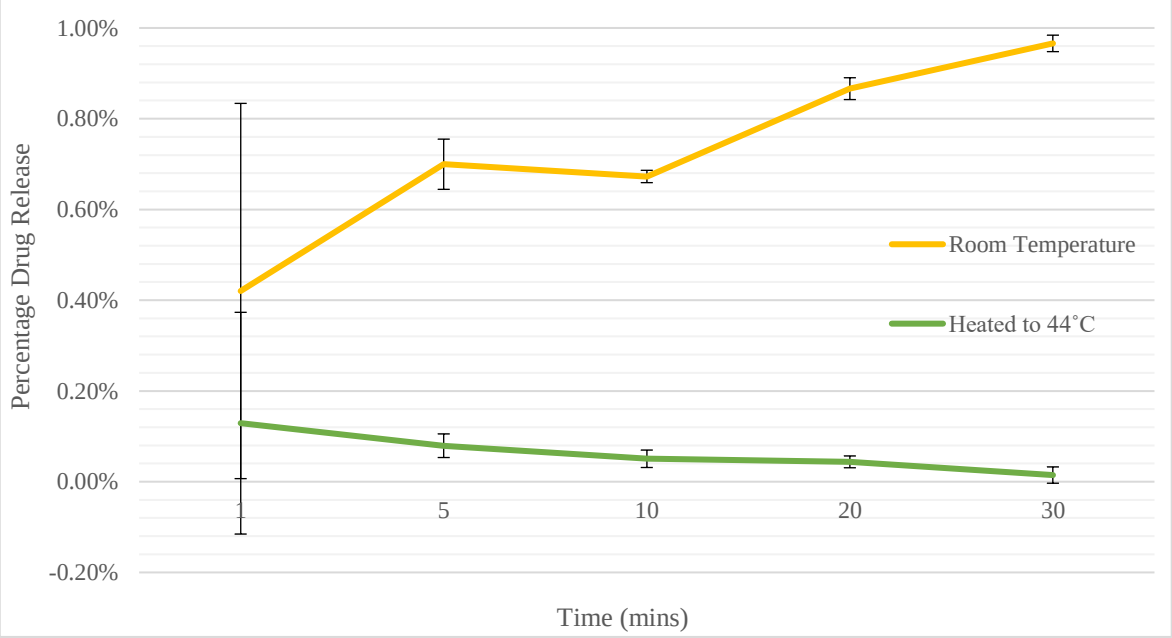

Figure 14: The percentage of L-GEM released from the HNPs.

Oluwasanmi *et al.* completed the same work, using AuHNPs instead of silver (Oluwasanmi *et al.,* 2017). In this study, the release of gemcitabine was measured at three different pH (5.6, 7 and 7.4) in order to better mimic certain biological environments, as well as determining release at three different temperatures (20˚C, 37˚C and 44˚C). Here, pH 7 and two temperatures were used for release, due to a shortage of the L-GEM available to load onto HNPs. There, it was determined that there was an 80% release of the drug at 44˚C compared to a negligible release at 20˚C, showing a much better release profile than the one obtained in this study. This may be due to the different heating abilities of silver and gold, as

demonstrated in Chapter 3, hence the Diels-Alder mechanism cannot go ahead like that in the Oluwasanmi study. As well as this, the concentration of silver present in the hybrids is much lower than that of gold, as discussed in Chapter 2, hence more silver may be required for better heating and therefore greater release of the drug at the higher temperature.

Another study that used the Diels-Alder release mechanism used a thermoresponsive polymer attached to IONPs containing the drug fluorescein, then used an AMF to stimulate heat generation and therefore drug release from the polymer (Fuller *et al.*, 2019). Although the method of release is not entirely the same, the AMF is used to trigger heating and therefore release of the cargo, therefore has an overall similar desired effect. Here, samples were in 25:75 methanol PBS (v/v) then either used AMF to heat the samples to 37˚C, 45˚C, 52.5˚C and 60˚C external heating for an hour. Release of the drug was seen to increase with temperature, with less than 1% release at 37˚C and 4% at 60˚C. The release is much lower in this study due to a layer of PEG-PLA (polyethylene glycol-polylactic acid), which only allowed for the release of the drug at a higher temperature. Although the method here did not work and may need more refinement to allow for release at 44˚C, release at temperatures as high as those used in the Fuller study would most likely not be viable in the clinical setting, due to damage to surrounding tissues caused by the necessary temperature to cause release becoming more likely.

Further, the uptake of gemcitabine into the cells when attached to HNPs has also been measured in both the BxPC-3 and PANC-1 cell lines (Figures 14 and 15 respectively).

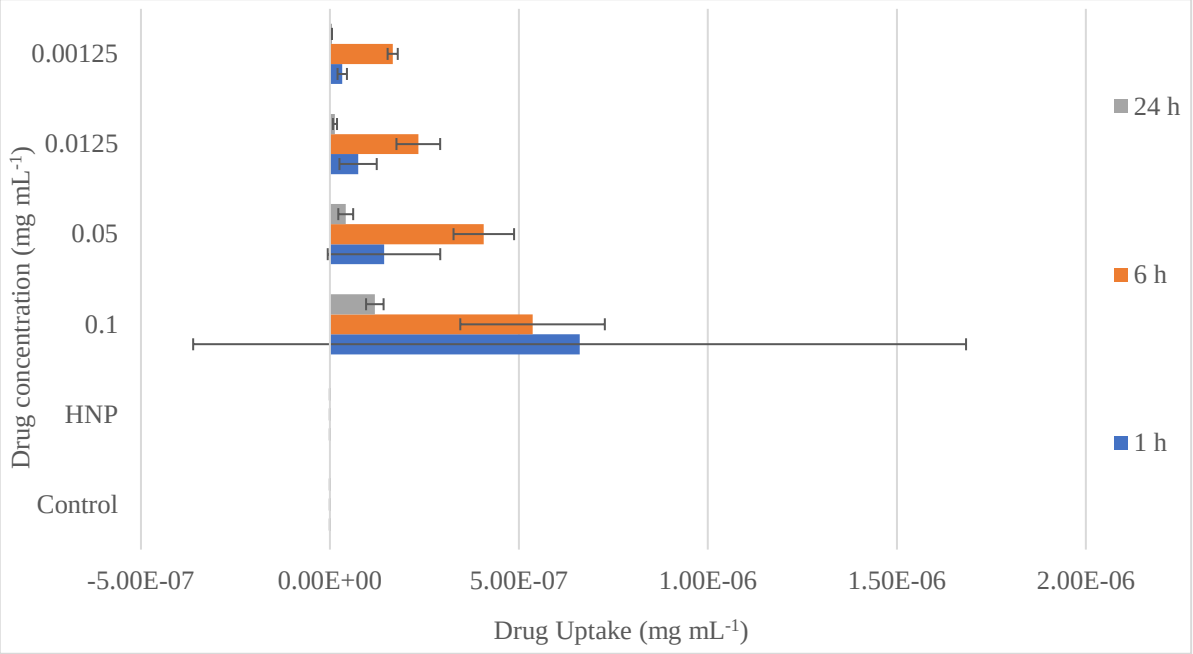

Figure 15: The uptake of the drug gemcitabine into BxPC-3 when attached to HNPs

In the BxPC-3 cell line, the control and naked HNPs showed no uptake of the drug, as expected. The different concentrations of the drug on HNPs also showed different levels of uptake, with these altering between time points in the majority of cases and no overall trend appearing within the data. At the lowest concentration (0.00125 mg mL^{-1}), there was an initial large uptake of the drug, with this decreasing for the 6 h and 24 h time points. However, the proportionally large error bars on the 1 h time point, meaning that this error could make the difference between the uptake not statistically significantly different. The same trend can be seen for the 0.05 mg mL^{-1} drug concentration, with an even larger error than that of the 0.00125 mg mL^{-1} data. For the 0.0125 mg mL^{-1}, each of the time points has a very similar level of uptake, with the error minimal for all time points except 1 h. For the 0.1 mg mL^{-1} data, there seemed to be a clearer uptake of the drug over time, with large error bars on the 1 h sample seen once again.

A two-way ANOVA was attempted on the data, but the data was found to have inequality of variances and deviated from normality, as determined by Levene's test ($p<0.001$) and Shapiro-Wilk ($p<0.05$) respectively. Data transforms were attempted but failed

to have any impact on either of the statistics. Because of this, a Kruskal-Wallis H test was used to analyse the data for both the time and concentration. When looking at the effects of time on the uptake of the drug, it was found that there was a statistically significant difference between the 6 h and 24 h time points, with there being no statistically significant difference between both the 1 h and 6 h and the 1 h and 24 h time points. This means that there was greater uptake of gemcitabine at the 6 h time point than the 24 h time point, which is reflected in the data (Figure 14). It also means that there is no difference in the uptake of gemcitabine between the 1 h and 24 h time points and the 1 h and 6 h time points. This is harder to see when looking at the data initially, until considering the major error in the 1 h data in comparison to the 6 h and 24 h data. For the concentrations, both the control and the naked HNPs were found to be statistically significantly different to 0.0125 mg mL^{-1}, 0.05 mg mL^{-1} and 0.1 mg mL^{-1} samples ($p<0.05$). The control and naked HNPs were not found to be statistically significantly different from one another, as well as to the 0.00125 mg mL^{-1} ($p>0.05$). The two controls clearly were not different from one another when looking at the data, as neither of these should have contained any gemcitabine. The controls not differing from 0.00125 mg mL^{-1} was expected, as the 6 h and 24 h values were quite low and the 1 h value had such large error that it would not end up being statistically significantly different to the controls. The 0.0125 mg mL^{-1}, 0.05 mg mL^{-1} and 0.1 mg mL^{-1} were not statistically significantly different from one another, which also makes sense when looking at error bars in proportion to the average values obtained. The 0.00125 mg mL^{-1} was also found not to be statistically significantly different from 0.1 mg mL^{-1}, 0.05 mg mL^{-1} and 0.0125 mg mL^{-1} ($p>0.05$). This also makes sense when looking at the data, as the three concentrations (0.1 mg mL^{-1}, 0.05 mg mL^{-1} and 0.0125 mg mL^{-1}) clearly have proportionally much larger error bars than the 0.00125 mg mL^{-1}. Overall, though, there was clearly uptake of gemcitabine into the cells, with the peak being at 6 hours.

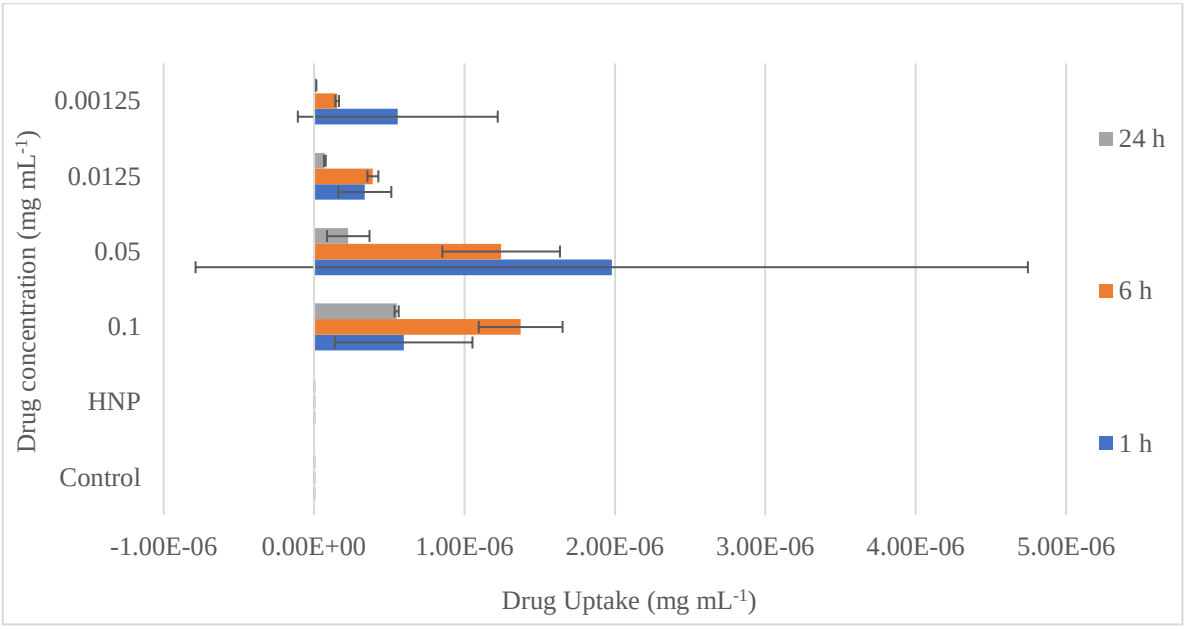

Figure 16: The uptake of the drug gemcitabine into PANC-1 when attached to HNPs

Alike the BxPC-3 cell line, the PANC-1 cells were not found to contain any gemcitabine in the control and HNP only samples (Figure 15). The data here suggest that overall, the uptake was greatest at the 6 h time point, with these levels decreasing at 24 h. The 0.0125 mg mL^{-1} and 0.00125 mg mL^{-1} concentrations had a low influx of the drug, hitting peak uptake at 6 h, then uptake decreasing at 24 h, with low error for each data set. For the 0.05 mg mL^{-1}, the same trend was seen but with the 1 h and 24 h points having a much greater error. Finally, the 0.1 mg mL^{-1} sample was seen to uptake the drug well at 1 h, increase at 6 h, then decreases at 24 h. The error bar for the 1 h sample is clearly much larger than those of the 6 and 24 h, hence statistical analysis is required to determine the significance.

Statistical analysis was then completed on this data. Initially, the data was found to both deviate from normality, determined by Shapiro-Wilk ($p<0.05$), and had inequality of variances, as determined by Levene's test ($p<0.001$). A square root data transformation was able to normalise the data but had no effect on the equality of variances. With the value for the equality of variances still being so low ($p<0.001$), it was not possible to run a two-way ANOVA. Instead, a Kruskal-Wallis H test was used to analyse the statistical significance of the data. When looking at the effect of time, the Kruskal-Wallis H test determined that there

was no difference in drug uptake between any of the time points used. Overall, this means that there was no difference in the uptake of the drug over time, which is well reflected in the data when considering the impact of the error bars.

The two controls clearly were not different from one another when looking at the data, as neither of these should have contained any gemcitabine. The controls not differing from the 0.00125 mg mL^{-1} was expected, as the 6 h and 24 h values were quite low and the 1 h value had such large error that it would not end up being statistically significantly different to the controls. The 0.1 mg mL^{-1}, 0.05 mg mL^{-1} and 0.0125 mg mL^{-1} were not statistically significantly different from one another, which makes sense again when looking at error bars in proportion to the average values obtained. The 0.00125 mg mL^{-1} was also found not to be statistically significantly different from 0.1 mg mL^{-1}, 0.05 mg mL^{-1} and 0.0125 mg mL^{-1} ($p>0.05$). This also makes sense when looking at the data, as the three concentrations (0.1 mg mL^{-1}, 0.05 mg mL^{-1} and 0.0125 mg mL^{-1}) generally either have proportionally much larger error bars than the 0.00125 mg mL^{-1} (0.1 and 0.05 mg mL^{-1}) or have similar average values (0.0125 mg mL^{-1}).

Although the data does appear to show that there was uptake of L-GEM into each of the pancreatic cancer cell lines, repeating this test would be required in order to determine the success of uptake into both pancreatic cancer cell lines used. It could not be done here due to both time constraints and lack of L-GEM to repeat the study.

Oluwasanmi *et al.* determined that there was greater uptake of the modified gemcitabine attached to AuHNPs than when using gemcitabine alone within the BxPC-3 cell line (Oluwasanmi *et al.,* 2017). There was also a clear increase in uptake over time that was not seen within either cell lines used in this study, with the 6 h and 24 h time points both having greater uptake than 1 h. The results of this study are much less concrete as the ones presented by Oluwasanmi *et al.*, hence further studies may be required in order to determine the success of uptake of gemcitabine into cells.

Finally, the cytotoxicity of HNPs, gemcitabine alone and HNPs with gemcitabine were tested on both BxPC-3 and PANC-1 pancreatic cancer cell lines respectively.

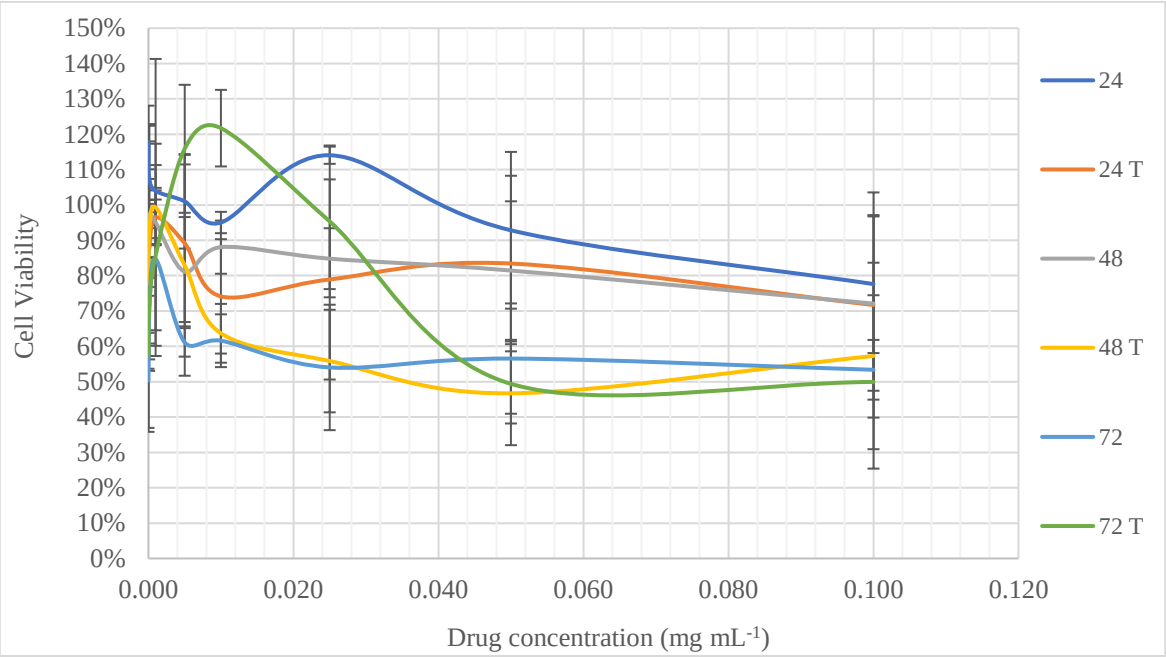

Figure 17: The cell viability of the BxPC-3 cell line when exposed to HNPs at different time intervals (24, 48 and 72 h), with those that also spent 1 h in another over at 44˚C to promote release of the drug indicated by the letter T. The concentrations here are related to the concentration of drug attached to HNPs.

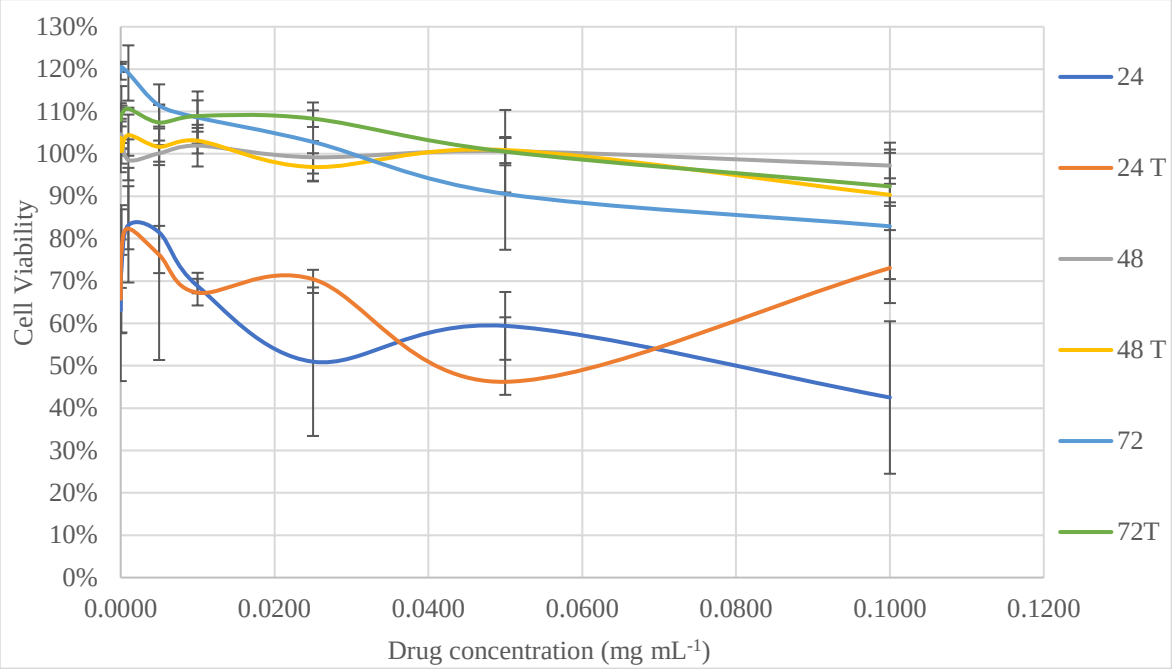

Figure 18: The cell viability of the PANC-1 cell line when exposed to HNPs at different time intervals (24, 48 and 72 h), with those that also spent 1 h in another over at 44˚C to promote release of the drug indicated by the letter T. The concentrations here are related to the concentration of drug attached to HNPs.

The data for the HNPs alone was deemed to be inconclusive due to the variability in the data especially in comparison to the previous studies using AuHNPs (Oluwasanmi *et al.*, 2017).

From the data obtained from the BxPC-3 cell line (Figure 16), it appears that the 24 h and 24 h (T) samples do not appear to be greatly affected by the HNPs, with viability remaining above 70% even when there were dips in viability at low concentrations of HNPs. As time progressed, there was an increase in the cytotoxicity of the HNPs, with 48 h, 48 h (T) and 72 h (T) reaching viabilities below 50%, and 72 h decreasing to lows of around 55%.

For the PANC-1 cell line (Figure 17), the cell viability for both 24 h and 24 h (T) are very varied, with there being clear fluctuations in the data as the concentration increases. Because of this, 24 h and 24 h (T) appear to have two or more IC_{50} values. For these data, there appear to be large error bars for 24 h across the entire graph, with the error bars for 24 h (T) being small until the dip at 0.05 mg mL^{-1} and the increase at 0.1 mg mL^{-1}. The 48, 48 h (T), 72 h and 72 h (T) time points generally seem to decrease with increasing concentration,

but never go below 80%. Because of this, it can be said that at these time points there was no real impact on the cytotoxicity. Overall, the results here are generally inconclusive due to the variability in the graphs obtained, especially when looking between the cell lines. It was expected that the HNPs generated here would have some anti-cancer effects, as the anticancer effects of silver were discussed in Chapter 1. This was expected to occur in the later time points, which was not the case in the PANC-1 cell line.

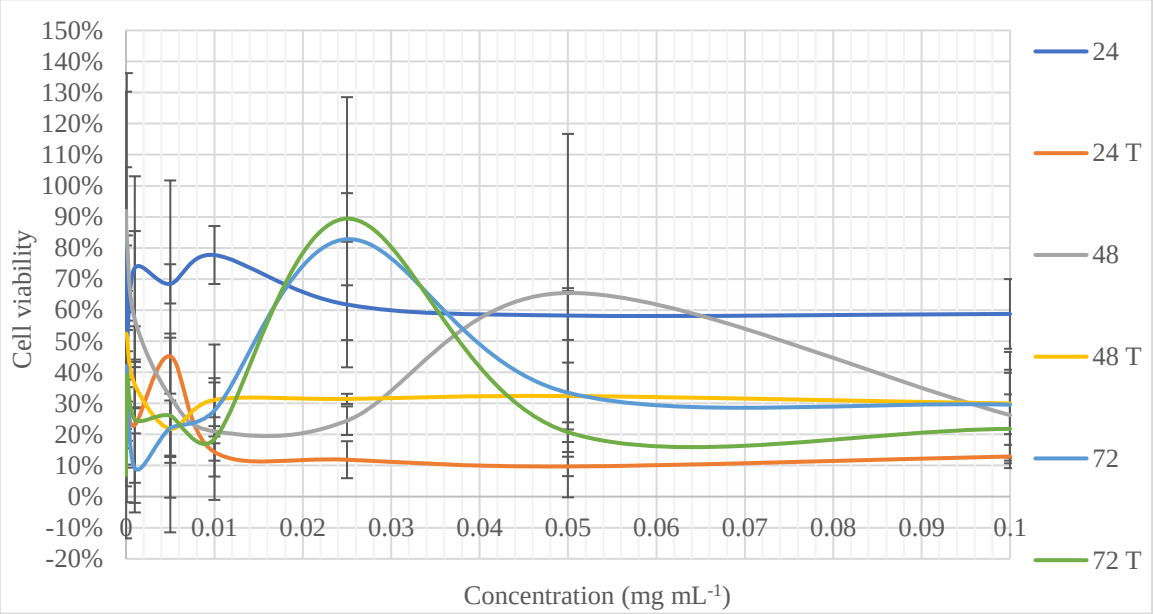

Figure 19: The cell viability of the BxPC-3 cell line when administered difference concentrations of the drug gemcitabine at different time points (24, 48 and 72 h), with those that also spent 1 h in another over at 44˚C to promote the release of the drug indicated by the letter T.

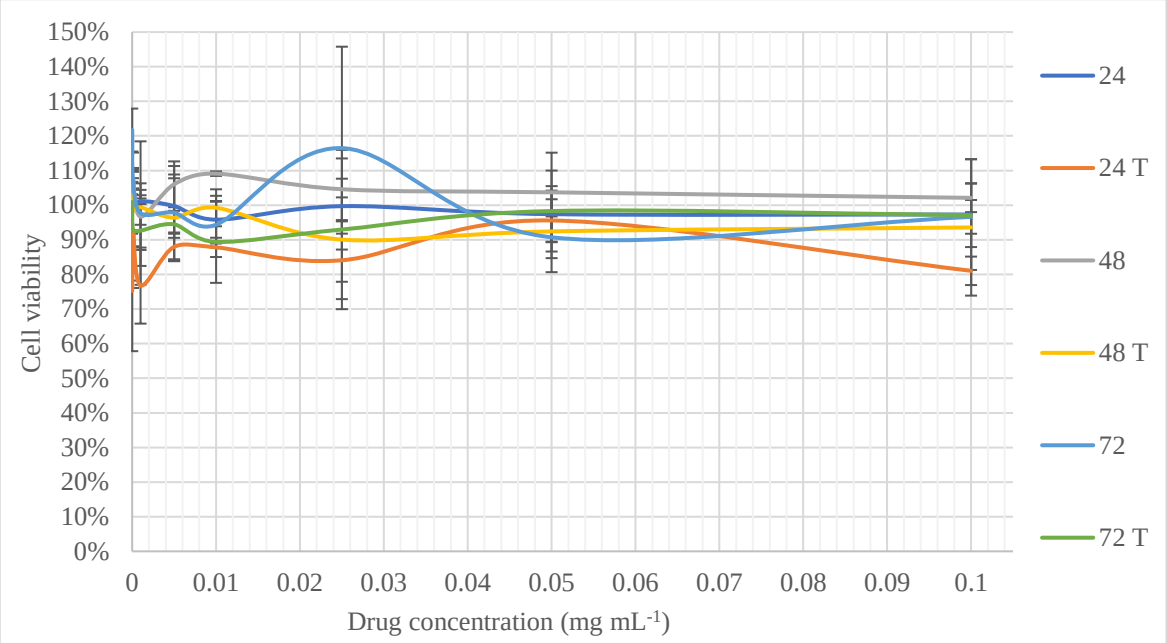

Figure 20: The cell viability of the PANC-1 cell line when administered difference concentrations of the drug gemcitabine at different time points (24, 48 and 72 h), with those that also spent 1 h in another over at 44˚C to promote the release of the drug indicated by the letter T.

The data for gemcitabine alone appears equally inconclusive, with this being more obvious when looking at the two different cell lines.

For the BxPC-3 data (Figure 18), the cell viability for 24 h was the most consistent across all concentrations of the drug, with cytotoxicity never decreasing below 70%. For 24 h (T), there was a much greater cytotoxic effect, with the cell viability being lower than 50% for each concentration. The results for 48 h, 72 h and 72 h (T) were all odd, with the cell viability appearing to increase then decrease, rather than the decrease usually seen. Even more odd is the fact that these increases in viability brought the cell viability above 50% at a much higher concentration of gemcitabine.

For the PANC-1 data (Figure 19), there was a much more consistent cell viability across each of the time points, with none of the data having cell viability of less than 80%. For all of the data, there were clear fluctuations as the concentration of drug increased, with the clearest examples of this being 24 h (T) and 72 h. The most consistent data was seen in at 48 h, where the data initially fluctuated at the lower concentrations, but then plateaued between 0.025 and 0.1 mg mL^{-1}.

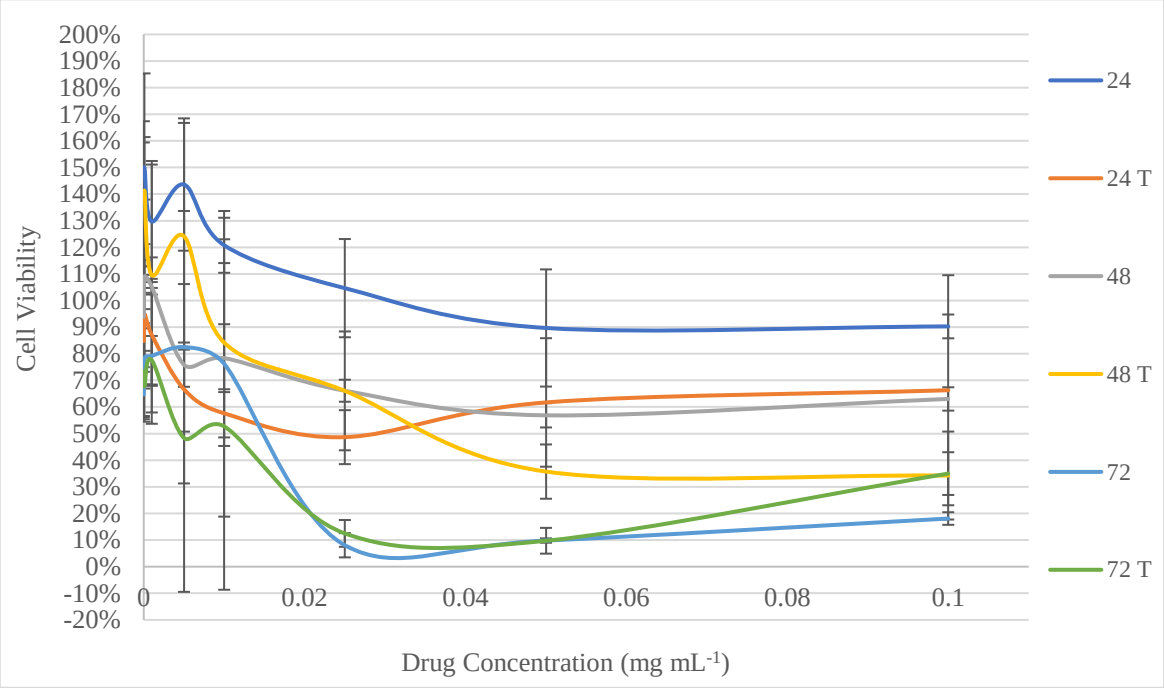

Figure 21: The cell viability of the BxPC-3 cell line when administered difference concentrations of the drug gemcitabine loaded onto HNPs at different time points (24, 48 and 72 h), with those that also spent 1 h in another over at 44˚C to promote the release of the drug indicated by the letter T.

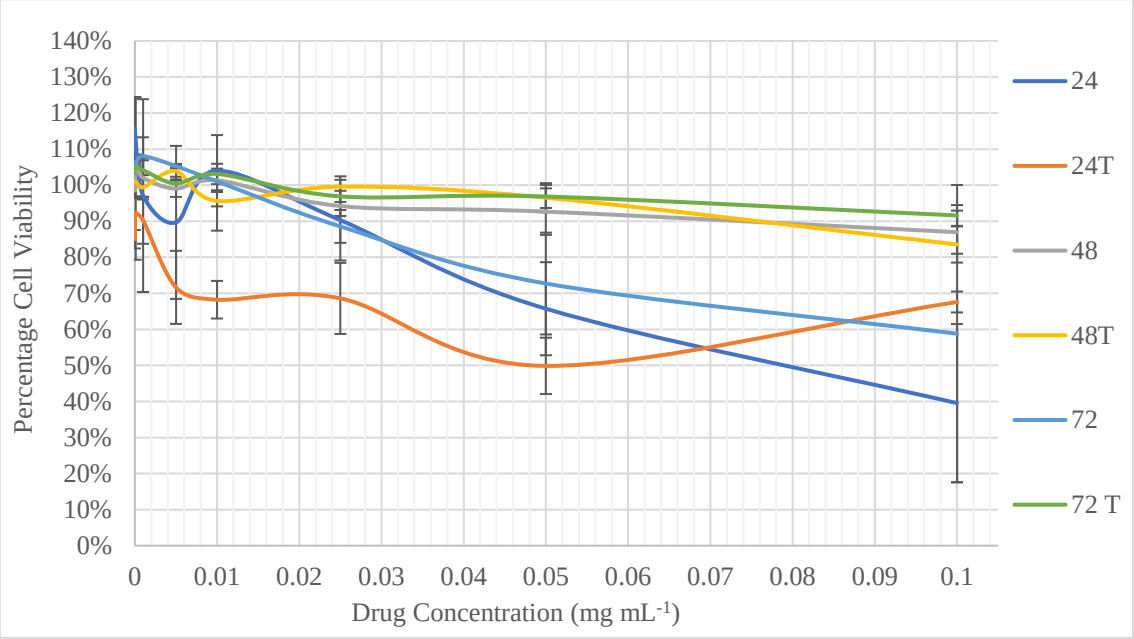

Figure 22: The cell viability of the PANC-1 cell line when administered difference concentrations of the drug gemcitabine loaded onto HNPs at different time points (24, 48 and 72 h), with those that also spent 1 h in another over at 44˚C to promote the release of the drug indicated by the letter T.

The data for the HNPs loaded with gemcitabine also appears to be less inconclusive than for the other data, but there are still some obvious issues with the data obtained, especially when looking at the PANC-1 data.

For the BxPC-3 data (Figure 20), the 24 h time point did have decreasing viability as drug concentration increased, but this did not decrease any lower than 90%. For 24 h (T), there was a much clearer decrease in viability than for the 24 h, but there were only two points where the cell viability decreased below 50%. The results for 48 h were very similar, but the cell viability did not decrease any lower than 60% around 0.05 mg mL^{-1}. For 48h (T), the decrease in viability was much later than that of 48, but the viability decreased to much lower than 40%. For 72 h, there was a clear drop in cell viability to 0.025 mg mL^{-1} that then increased slightly up to 0.05 mg mL^{-1} and 0.1 mg mL^{-1}. For 72 h (T), there was a similar decrease to that seen for 72 h, but there was a clear increase between 0.025 mg mL^{-1} and 0.05 mg mL^{-1}.

For the PANC-1 data (Figure 21), the 24 h time point did have decreasing viability as

drug concentration increased, with this decreasing to a minimum value of 40%. For 24 h (T), the decrease in viability was initially much greater for the lower concentration of the drug, but then the cell viability began to increase after 0.05 mg mL^{-1}. The results for 48 h, 48 h (T) and 72 h (T) all had very similar results, with a decrease in viability over time but the overall viability was greater than 80%. For 72 h, the decrease in viability was more linear, alike 24 h, but did not decrease below 50%.

Table 2: The IC_{50} values of naked HNPs (HNP), gemcitabine alone (Drug) and the gemcitabine conjugated HNPs (HNP+Drug). Dashes (-) denote where the cell viability was above 50%. Where the viability was below 50%, the maximum percentage cell viability has been quoted in brackets. Incidences where 50% was hit twice, both values are listed in the table. (T) indicates where the sample had been heated to 44˚C for 1 hour.

Time (h)	Sample	BxPC-3 IC_{50} value (mg mL^{-1}) ± SD	PANC-1 IC_{50} value (mg mL^{-1}) ± SD
24	HNP	-	0.0230 ± 0.099
24	Drug	-	-
24	HNP+Drug	-	0.0756 ± 0.024
48	HNP	-	-
48	Drug	0.001 ± 0.0014 0.074 ± 0.028	-
48	HNP+Drug	-	-
72	HNP	-	-
72	Drug	0.0145 ± 0.0029 0.0388 ± 0.0182	-
72	HNP+Drug	0.015 ± 0.0089	-
24 (T)	HNP	-	0.0115 ± 0.0344
24 (T)	Drug	0.005 ± 0.003	-
24 (T)	HNP+Drug	0.019 ± 0.012 0.029 ± 0.036	0.0482 ± 0.0385 0.0526 ± 0.0439

48 (T)	HNP	0.01 ± 0.013 0.019 ± 0.012	-
48 (T)	Drug	0.0002 ± 0.00008	-
48 (T)	HNP+Drug	0.035 ± 0.013	-
72 (T)	HNP	0.0138 ± 0.03343	-
72 (T)	Drug	0.015 ± 0.0038 0.0346 ±0.0018	-
72 (T)	HNP+Drug	0.004 ± 0.0023 0.012 ± 0.0083	-

IC_{50} values were then obtained by inspection from the graphs generated, with a summary of these in Table 2. For these data, it was obviously more difficult to determine the IC_{50} values, as there was either no decrease below 50%, the cell viability was already below 50% or there was a trough that meant there were two different possible IC_{50} values.

Statistical analysis was then completed on the cytotoxicity data obtained from the BxPC-3 cell line. Initially, a three-way ANOVA was attempted, but could not be completed due to lack of normality in the data, inequality of variances and data transformations having no impact on either of the aforementioned aspects. Because of this, both Kruskal-Wallis H and Mann-Whitney U tests statistical tests were used to analyse the data, where appropriate.

Time was found to have a statistically significant effect on the cytotoxicity of HNPs ($p<0.05$), HNPs with the drug ($p<0.05$) and the drug alone ($p<0.05$), as determined by a Kruskal-Wallis H test. For the HNPs, there was a significant difference between the 24 and 48 h ($p<0.05$) and the 24 h and 72 h time points ($p<0.05$). For the HNP with L-GEM, there was a statistically significant difference between 24 h and 72 h ($p<0.05$) and 48 and 72 h ($p<0.05$). For gemcitabine alone, there was a statistically significant difference between 48 and 72 h ($p<0.05$).

The temperature was also found to have a statistically significant effect on the

cytotoxicity of the HNP with L-GEM ($p<0.05$) and gemcitabine alone ($p<0.05$), as determined by the Mann-Whitney U test. The temperature did not have a statistically significant effect on the cytotoxicity of the naked HNPs ($p>0.05$).

Concentration was found to have a statistically significant effect on the HNPs ($p<0.05$) and HNPs with L-GEM ($p<0.05$), as determined by the Kruskal-Wallis H test. For the HNPs, there was only found to be a statistically significant difference between the 0.1 and 0.001 mg mL^{-1} concentrations ($p<0.05$). For the HNPs with L-GEM, there were a few results that were statistically significantly different. 0.05 mg mL^{-1} was found to be statistically significantly different to 0.005 mg mL^{-1}, 0.001 mg mL^{-1}, 0.0001 mg mL^{-1}, and 0.00001 mg mL^{-1}. 0.1 mg mL^{-1} was found to be statistically significantly different to 0.001 mg mL^{-1}, 0.0001 mg mL^{-1}, and 0.00001 mg mL^{-1}. Finally, 0.025 mg mL^{-1} was found to be statistically significantly different to 0.001 mg mL^{-1}, 0.0001 mg mL^{-1} and 0.00001 mg mL^{-1} ($p<0.05$).

This statistical analysis of the effects of time, concentration and temperature for the BxPC-3 data seem to well reflect the data obtained. Due to the variability in the data, the results of the statistical analysis were not surprising.

Statistical analysis was then completed on the cytotoxicity data obtained from the PANC-1 cell line. Initially, a three-way ANOVA was attempted, but could not be completed due to lack of normality in the data, inequality of variances and data transformations having no impact on either of the aforementioned aspects. Because of this, both Kruskal-Wallis H and Mann-Whitney U tests statistical tests were used to analyse the data, where appropriate.

Time was found to have a statistically significant effect on the cytotoxicity of HNPs ($p<0.05$), HNPs with the drug ($p<0.05$) and the drug alone ($p<0.05$), as determined by a Kruskal-Wallis H test. For the HNPs, there was a significant difference between the 24 h and 48 h ($p<0.05$), 24 and 72 h ($p<0.05$) and 48 h and 72 h time points ($p<0.05$). For the HNP with L-GEM, there was a statistically significant difference between 24 h and 48 h ($p<0.05$)

and the 24 h and 72 h time points ($p<0.05$). For gemcitabine alone, there was a statistically significant difference between 24 h and 48 h ($p<0.05$).

The temperature was also found to have a statistically significant effect on the cytotoxicity of the gemcitabine alone ($p<0.05$), as determined by the Mann-Whitney U test.

Concentration was found to have a statistically significant effect on the HNPs and HNPs with L-GEM, as determined by the Kruskal-Wallis H test. For HNPs, there was a statistically significant difference between 0.1 mg mL^{-1} and 0.001 mg mL^{-1} ($p<0.05$). For the HNPs with L-GEM, the 0.1 mg mL^{-1} sample was found to be statistically significantly different to 0.01 mg mL^{-1}, 0.005 mg mL^{-1}, 0.001 mg mL^{-1}, 0.1 mg mL^{-1} and 0.0001 mg mL^{-1}. 0.05 mg mL^{-1} was also found to be statistically significantly different to 0.001 mg mL^{-1}, 0.0001 mg mL^{-1}, and 0.00001 mg mL^{-1}. Finally, 0.025 mg mL^{-1} was found to be statistically significantly different to 0.001 mg mL^{-1} ($p<0.05$).

This statistical analysis of the effects of time, concentration and temperature for the PANC-1 data seem to well reflect the data obtained. Due to the variability in the data, the results of the statistical analysis were not surprising.

Finally, statistical analysis was used to determine if there were any statistically significant differences between the cytotoxicity of free gemcitabine and gemcitabine attached to the HNPs. A Mann-Whitney U test was used due to outliers in the data and lack of normality ($p<0.05$).

For the BxPC-3 cell line, there was found to be a statistically significant difference in the cytotoxicity of the two treatments ($p<0.01$), with the data appearing to show that gemcitabine alone had a greater cytotoxic effect than the HNPs with gemcitabine. For the PANC-1 cell line, there was no statistically significant difference between the two treatments ($p>0.05$). This means that the HNPs with gemcitabine had been equally as cytotoxic as free gemcitabine. These results are odd, as it is was expected that the results would be the same across the cell lines considering there is not much difference between them.

Because of the levels of error seen within this study, both the data and the statistical analysis must be taken with a pinch of salt. Repeats could not be attempted to check the results of this study due to production issues with L-GEM, as explained previously. Comparisons between the data, including determining if there were combination effects, were also unable to be completed due to the level of abnormality and error of variances that were found for the data sets. As well as the need to repeat these studies, there is also a need to test these HNPs against normal/non-cancerous cell lines. This is important in order to allow for any further use of these HNPs, as the whole point of delivery systems like these are to ensure that there is minimal damage to surrounding healthy tissues.

The results here do differ to those found in the previous studies using AuHNPs (Oluwasanmi *et al.,* 2017). Within that study, Trypan Blue and MTT assays were both used to look at cell viability within the BxPC-3 cell line. There was no evidence of an IC_{50} value during the 24 h period, other than for the modified gemcitabine alone, which had an IC_{50} of 38 μg mL^{-1}. Both gemcitabine and the hybrids with L-GEM exhibited an IC_{50} value at 48 h, with the 72 h time point giving the lowest IC_{50} values for each treatment type. The HNPs were found to have no IC_{50} value, with relatively consistent cell viability that never decreased far below 80%. This does not match what was seen within this study, as the HNPs were found to have some cytotoxicity at different time points between the two cell lines tested and gemcitabine generally had a better cytotoxic effect at 24 h than the remaining time points for gemcitabine, and there was an apparent increase in the cytotoxicity over time for the BxPC-3 cell line.

The cytotoxicity of the AgNPs has been seen in the literature, with evidence of the cytotoxic effects of silver on pancreatic cancer cell line PANC-1 seen in two different recent studies (Barcińska *et al. et al*., 2018; Zielinska *et al.,* 2018), with other cell lines seeing similar effects within different cancerous cell lines (Yuan, Peng and Gurunathan, 2017; Padinjarathil *et al.,* 2018; Zhang and Jiao, 2018). Because of these previous results, it is

understandable why the HNPs alone were able to cause a reduction in the cell viability of the pancreatic cancer cell lines used within this study.

It is not possible to determine whether uptake of the HNPs increased cytotoxicity, due to the different time points used to in both of the studies. Much shorter time points were used for the uptake study in comparison to the cytotoxicity study. It is only possible to suggest that future work using these HNPs complete cytotoxicity testing and uptake of the HNPs on the same time scale in order to make accurate comparisons between the two.

4.4 Conclusion

Overall, the data obtained here points to the fact that the delivery system used here does not work as well as when using gold hybrids nanoparticles. This has been shown in the drug release, where the drug was unable to be released in the same quantities as seen with gold at the same temperature. Cytotoxicity results were generally unclear, causing confusion as to whether the HNPs themselves were toxic to cancerous cell lines.

Clearly, further testing is required to determine the suitability of the HNPs generated for drug delivery applications, as well as testing on a non-cancerous cell line to determine any significant differences in their effects, which could not be done during this project due to time constraints.

In Chapter 5, a novel targeting agent is tested in order to target pancreatic cancer cell lines, which could be used for both imaging and drug delivery in the clinical setting.

5.0 Targeted drug delivery

5.1 Introduction

5.11 Targeted drug delivery

Drug delivery has become a popular research area, specifically for anti-cancer drugs, with some studies choosing to attach targeting moieties enabling site-specific delivery of payloads. In particular, the use of inorganic nanoparticles, such as IONPs which can be imaged using MRI, has greatly increased (Na, Song and Hyeon, 2009; Estelrich *et al.*, 2015). This allows the delivery of these anticancer drugs to be observed in real-time, tracking the progression of the nanoparticles to the tumour tissues. This targeting of a specific tissue, particularly in cancer therapy, can result in more efficient delivery systems with systemic circulation of toxic moieties reduced. This leads to the reduction of the detrimental side effects that can occur when using such therapies. Once the nanoparticles are at their target site, these inorganic nanoparticulate systems can then be manipulated either internally or externally to release their drug cargo.

Yu and co-workers looked into potential therapies for prostate cancer (Yu *et al.*, 2011). Prostate-specific membrane antigen (PSMA) aptamers were conjugated onto thermally cross-linked superparamagnetic IONPs and then loaded with doxorubicin. These nanoparticles were tested on two prostate carcinoma cell lines. One cell line was PSMA positive and the other negative (LNCaP and PC-3 respectively), as well as in an LNCaP xenograft mouse model. They noted that the majority of doxorubicin (98%) was released over 50 h and that the nanoparticles were target binging both *in vivo* and *in vitro*.

Nagesh and co-workers attached a PSMA, in this case the human antibody marker J591, onto SPIONs as a delivery system of docetaxel for castration-resistant prostate cancer (Nagesh *et al.*, 2016). Both a PSMA positive and negative prostate carcinoma cell lines

(LNCaP C4-2 and PC-3 respectively) were tested against non-targeted and targeted versions of these nanoparticles. Both cell lines were able to both internalise the drug-loaded SPIONs, with a clear cytotoxic effect exhibited in each cell line, which the authors attribute to increased uptake of docetaxel. When using the targeted nanoparticles, internalisation was only seen in the PSMA positive LNCaP C4-2 cell line, hence only caused a cytotoxic effect within these cells. Cytotoxicity in these cells, in both the targeting and non-targeting studies, was linked to morphological changes in the cells, a clear indicator of apoptosis.

Aires *et al*. looked into the selective delivery of IONPs to CD44-positive cancer cells, as CD44 is overexpressed in several cancer cell types, circulating tumour cells and cancer stem cells (Aires *et al*., 2016). IONPs were conjugated with gemcitabine alone or with gemcitabine and anti-CD44, then tested these against pancreatic (PANC-1) and breast cancer (MDA-MB-231) cell lines, both of which have the CD44 marker, and a non-cancerous breast cell line (MCF-10A) as a control. There was deemed to be a standard release of gemcitabine intracellularly (96-98%), with a much poorer rate of release extracellularly (3-5%) after 6-8 h. Using IONPs as a control, it was also verified that the targeting IONPs were surrounding the membranes of the cancerous cells and none were seen surrounding the control cell line. It was also confirmed that the targeting moiety allowed for greater antiproliferative activity and had no effect on the non-cancerous cell line.

In another study, Trabulo *et al*. used IONPs with gemcitabine attached and IONPs with both gemcitabine and anti-CD47 antibodies in an attempt to target pancreatic cancer cell lines PANC-1, PANC-215, and PANC-354 (Trabulo *et al*., 2017). Here, the uptake of the nanoparticles into the cell lines, gemcitabine release, and the cytotoxicity of the two nanoparticle types were all looked into by the researchers. The release of gemcitabine released matched that of the Aires *et al.* study, with the intracellular release being much higher than that extracellularly (96-98% and 3-5% respectively). It was also ascertained that the nanoparticles with the anti-CD47 attached were found in a much higher volume around

the PANC215 and PANC354 than with the IONP alone. The MNPs alone were seen to have little to no impact on cancer cell lines. The gemcitabine attached to the IONPs were found to have the same levels of cytotoxicity as free gemcitabine. Further, CD47 antibodies were used to try and improve this cytotoxicity, determining that there was no extra effect by using the antibodies on the cytotoxic effects.

Olarui *et al.* looked into developing IONPs functionalised with both amine and carboxylic acid groups in order to be able to attach both a fluorescent molecule and the antibody epithelial cell adhesion molecule respectively to allow for targeting imaging in pancreatic cancer (Olariu *et al.,* 2011). It was determined that these IONPs were able to successfully target the pancreatic ductal adenocarcinoma cell line PANC-1 *in vitro*, with internalisation of the nanoparticles seen within an hour and internalisation of other nanoparticles tested not occurring until 24 h.

Carbohydrate-based targeting agents are not a new concept, with many studies previously using these as targets for several types of cancer both *in vitro* and *in vivo*. Many studies have added a sugar moiety onto a drug in order to form a prodrug that could then be used for delivery into cells (Lin *et al.*, 2008; Mikuni *et al.*, 2008; Miot-Noirault *et al.*, 2011).

Lin *et al*. developed four novel prodrugs of paclitaxel, two of which contained glucose and the other two contained glucuronic acid (Lin *et al.*, 2008). These were tested on NCI-H838 (lung adenocarcinoma), Hep-3B (hepatocellular carcinoma), A498 (renal cell carcinoma), MES-SA (uterine corpus sarcoma), HCT-116 (colon carcinoma), NPC-TW01 (nasopharyngeal carcinoma), MKN-45 (gastric adenocarcinoma), HUV-EC-C (umbilical vein/vascular endothelium) and CHO-K1 (Chinese Hamster Ovary). The prodrugs were able to greatly inhibit the growth of HCT-116, MES-SA, NCI-H838, and NPC-TW01. Both of the normal cell lines (CHO-K1 and HUV-EC-C), A498, Hep-3B, and MKN-45 were not affected by the treatments. As well as this, the two glucose and one of the glucuronic acid treatments did not affect the two normal cell lines, but paclitaxel alone did.

Mikuni *et al.* looked attached sugar moieties onto paclitaxel, docetaxel, and 7-Q-xylosylpaclitaxel in order to both improve their solubility and to determine if there were any targeting effects (Mikuni *et al*., 2008). Overall, it was determined that galactose added onto docetaxel was able to increase the antitumor activity and water solubility of the drug, with this determined *in vivo* by injecting P388 mouse lymphoma cells into male CDF1 mice.

Fucose has been identified as a potential targeting agent for pancreatic cancer, as fucosyltransferases have increased expression in pancreatic cancer (Yoshida *et al.*, 2012). Previous work looked at using fucose as a targeting agent for pancreatic cancer Yoshida and co-workers have previously used aminated L-fucose attached onto the surface of liposomes (Yoshida *et al.,* 2012). This was tested *in vivo* in mice with pancreatic ductal adenocarcinoma (AsPC-1) tumour-bearing mice, with the growth of the tumours found to be inhibited when treated with the targeted cisplatin liposomes.

Here, modified fucose (Figure 22) was generated by Dr Gavin Miller's research group at Keele University, attached to the surface of HNPs, and tested on PANC-1 and BxPC-3. Computer modelling, completed by Dr Jóhannes Reynisson at Keele University, clearly identified that modified fucose was able to properly fit into the active site of the 1,3-fucosyltransferase (Figure 23).

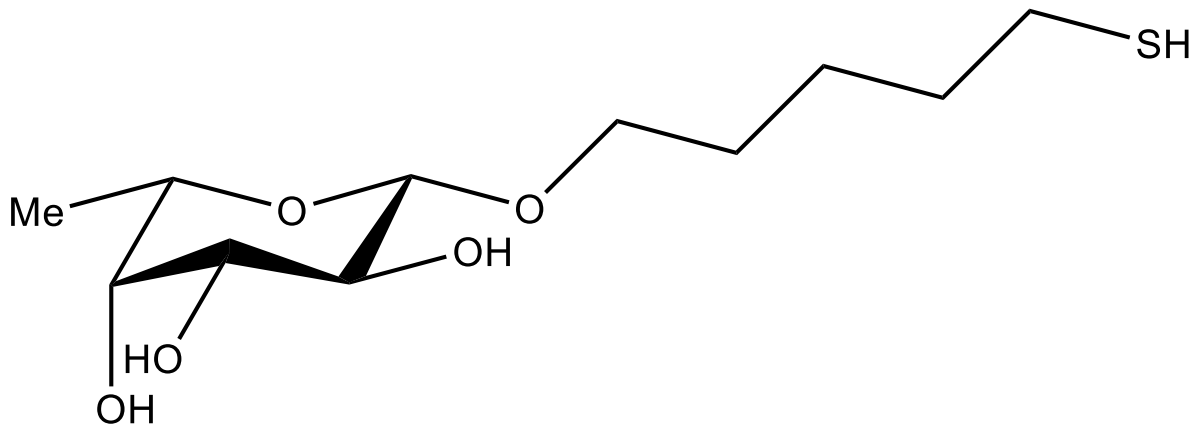

Figure 23: The structure of the targeting ligand attached to the surface of the HNPs

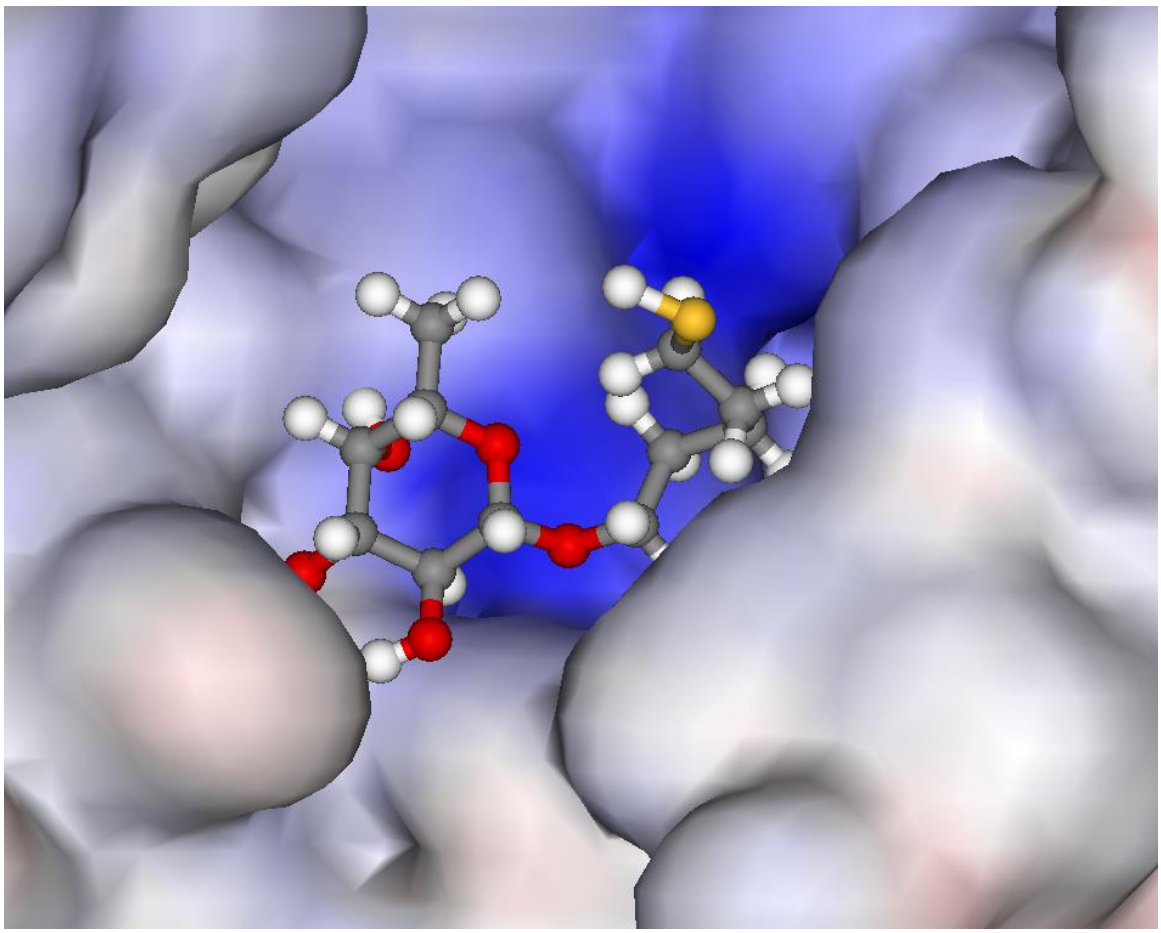

Figure 24: Modified fucose within 1,3-fucosoyltranferase's catalytic site, with a rendered protein surface, shown as a modelled configuration. Hydrophilic and hydrophobic areas are shown using blue and white respectively.

This work aimed to test a novel furan-based carbohydrate linker which is hypothesized to bind onto the surface of pancreatic cancer cells giving preferential uptake. The fucose targeting agents will be irreversibly bound onto the surface of the HNPs *via* dative covalent binding between the thiol in the chain of the fucose and the silver surface of the particles. The ability of these targeted particles to undergo preferential uptake into human pancreatic cancer cells *in vitro* will be evaluated.

5.2 Methods

5.21 Using modified fucose as a targeting agent

The novel fucose targeting agent (10 mg) was dissolved in DI water (100 mL). This solution was then used to create solutions with concentrations of 0.001 mg mL^{-1}, 0.01 mg mL^{-}

^{1}, and 0.02 mg mL^{-1}, allowing for the ratios of 1:1, 5:1, 10:1 and 100:1 of the HNPs to sugar, based on the iron concentration. HNPs were diluted to 0.1 mg mL^{-1} in DI water based on the iron concentration determined by ICP-OES analysis. The water was then removed, then 4.5 mL of each concentration of sugar added into each sample. These were then stirred for 1 h at room temperature, after this time the water was removed and the particles redispersed in 4.5 mL water. It was assumed that all the linker attached due to the low ratios being added onto the surface and the wealth of literature based around thiol-silver binding.

5.22 Cell culture

5.221 Cellular uptake

BxPC-3 and PANC-1 cells were cultured in RPMI and DMEM media respectively, with media supplemented with 10% foetal bovine serum and 1% penicillin-streptomycin, with 1% L-glutamine also added into DMEM. Cells were seeded into 6-well plates at 50,000 cells/well and left to grow until 70% confluency was reached.

Nanoparticle solutions based on the varied Fe:fucose ratios (2.5 mL) were diluted in 10 mL media giving a final iron concentration of 25 μg mL^{-1} and sugar concentrations of 0 μg mL^{-1}, 0.5 μg mL^{-1}, 2.5 μg mL^{-1}, 5 μg mL^{-1} and 25 μg mL^{-1}. The media was removed from the cell wells and replaced with 1 mL of the sample solution and incubated for 1 h, 6 h, and 24 h. After each time interval, the media was removed, and the cells were washed five times with 1 mL PBS. The PBS was removed and trypsin (185 μL) was added to each well. The suspended cells were diluted with 1 mL fresh media and cells were counted using an Invitrogen Countess^{TM} automated cell counter. The number of live cells was determined by adding 20 μL of trypan blue solution to 100 μL of the cell suspension, where the live cell count was used for quantification purposes.

5.222 Quantification of intracellular nanoparticle concentration

Cells (100,000) were isolated from the cell suspension. These were centrifuged for 5 min at 800 rpm using a Hermle Z323 Centrifuge. The supernatant was removed, then 1 mL *Aqua Regia* added to the cell pellets. These were incubated at 90˚C for 1 h, after which the solution was diluted in DI water and metal content was determined using ICP-OES as described in Chapter 2, Section 2.26. Samples were measured in triplicate and an average value recorded.

5.23 Statistical analysis

Any graphs generated were created on Microsoft Excel, with the mean value reported and error bars indicating the SD.

Statistical tests were run on the IBM SPSS Statistics 24 software, with the statistical test or tests run stated in the results and discussion.

5.3 Results and discussion

A novel sugar targeting ligand was synthesised and characterised by the Miller research group at Keele University. The structure of the targeting ligand can be seen in Figure 22. The linker was tethered onto the hybrid nanoparticle surface *via* dative covalent linkage of the thiolated fucose onto the silver surface. The scale at which this work was carried out was too small for FTIR characterisation, hence it was assumed that due to the low loading ratios used and the wealth of literature surrounding dative covalent binding of thiols onto silver surfaces that all the added fucose attached successfully onto the HNPs. Visually, this resulted in a more stable hybrid nanoparticulate suspension with reduced magnetic aggregation and precipitation indicating that attachment had occurred. Targeting is a very important factor when developing new highly toxic formulations using nanotechnologies. The literature has consistently shown that once encapsulated in or attached to the surface of a nanoparticle platform, drugs are more likely to enter the cells more rapidly and *via* alternative mechanisms

(endocytosis) compared to the free drug. Hence, it is very important to target these therapies to their required site of action to not only enhance therapeutic effect but also reduce systemic damage and side effects. In order to determine whether the novel fucose moiety provided was useful as a targeting agent to pancreatic cancer, the HNPs both with and without fucose were incubated with the pancreatic cancer cell lines (BxPC-3 and PANC-1).

The results of the *in vitro* study in PANC-1 cells is shown in Figure 24. The data, upon first inspection, appears to show that there was uptake and retention of the HNPs when using each different concentration of the sugar linker, but also appears to show that there are no differences in the uptake when using different concentrations of the targeting agent and naked HNPs. The uptake of the naked HNPs being better than the HNPs coated in the linker. As well as this, the error bars for the 6 h and 24 h time points are much wider for the linker containing HNPs in comparison to both the control and the naked HNPs. The 1 h time point has the most error, with generally large error bars for each category.

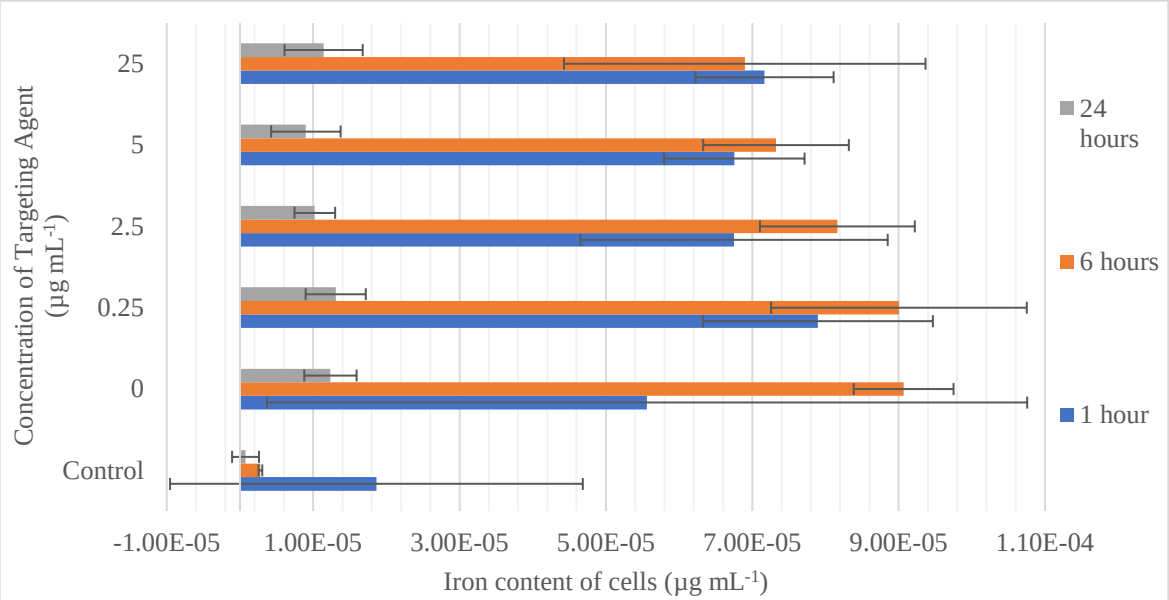

Figure 25: How the use of a sugar linker affects the uptake of HNPs into the pancreatic cancer cell line, PANC-1, with samples taken at time intervals of 1, 6 and 24 h.

The statistical analysis for this data was more complicated, with violations for both the equality of variances and normality. Several data transforms were attempted to counter this

but to no avail. It was decided that the best course of action was to continue with the two-way ANOVA using a lower significance of $p = 0.01$. This was done for the same reasons that were listed in Chapter 3, these being that there was no non-parametric alternative available on the SPSS software, the two-way ANOVA is relatively robust test, and that it was possible to follow up with a Kruskal-Wallis H test to try and gain perspective on the validity of the results could also be completed.

There was found to be a statistically significant effect of both concentration and time on the uptake of the HNPs ($p<0.01$) but there was found to be no interaction effect between the two ($p>0.01$). When looking at the concentration of the targeting agent, there was found to be a statistically significant difference between the control and all other samples ($p<0.01$). There was found to be no statistically significant difference between any other samples ($p>0.01$). When looking at the time, there was found to be a statically significant difference between the 1 h & 24 h and 6 h & 24 h time points ($p<0.01$), with the 1 h and 6 h time points found to be not statistically significantly different ($p>0.01$).

The Kruskal-Wallis H test was subsequently run in order to determine any significant difference in the impact of time on the HNP uptake and the concentration of the linker of the HNP uptake, without being able to determine if there were any joint effects on the uptake. Both data sets were not found to be evenly distributed when looking at box plots, so the distributions were compared rather than the median values. The output gave a statistically significant effect of both the targeting ligand's concentration and the time on the uptake of the HNPs, with the control found to be statistically significantly different all samples except for the 5 $\mu g\ mL^{-1}$. Alike the Two-way ANOVA, the 1 h and 6 h time points were not statistically significantly different, but both of these time points were found to be statistically significantly different to 24 h ($p>0.05$).

For the BxPC-3 data (Figure 25), there was also no evidence that the sugar linker had an effect on the uptake and retention of the HNPs, as the naked HNPs appeared to uptake the

most nanoparticles at the initial 1 h period, then lose these over the 6 h and 24 h time points. For the HNPs with the sugar linker, there was a more obvious increase between the 1 h and 6 h time points in uptake. There was then a more rapid decrease in the HNPs, decreasing to levels below that of the 1 h time point.

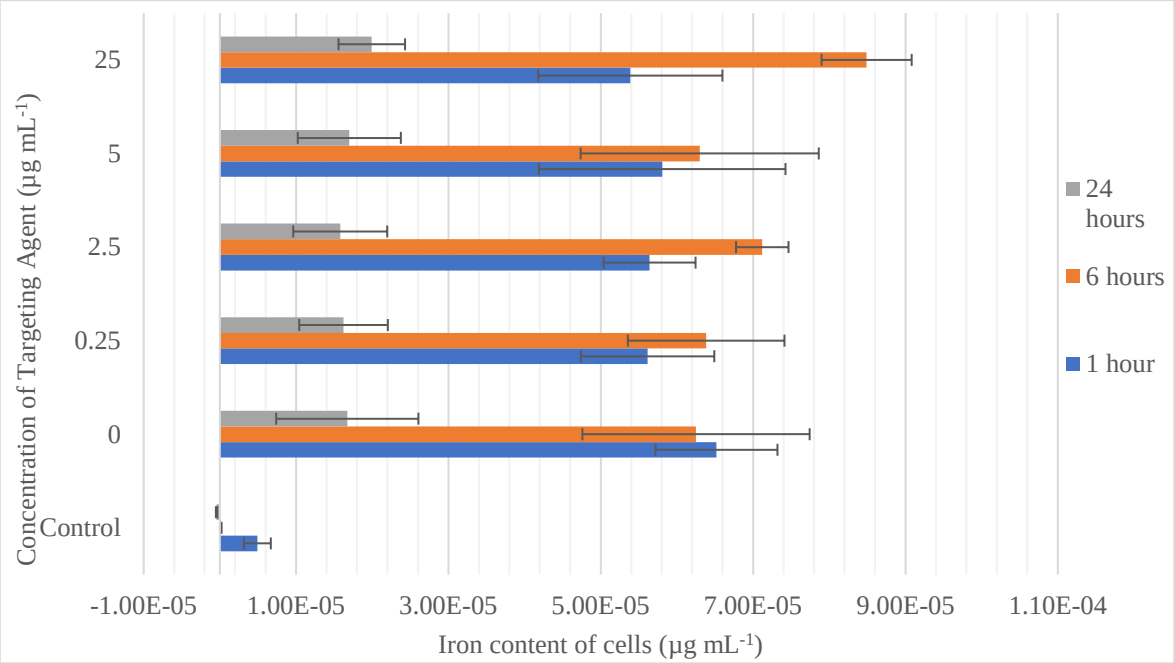

Figure 26: How the use of a sugar linker affects the uptake of HNPs into the pancreatic cancer cell line, BxPC-3, with samples taken at time intervals of 1, 6 and 24 h

A Two-way ANOVA with a square root data transform applied was used to determine any statistically significant outputs. The data transform was applied in order to ensure equality of variance, as indicated by Levene's test. The transformed data was found to be normal according to the Shapiro-Wilk test ($p>0.05$). The initial results determined that the concentration of the linker, time and the two in combination had a statistically significant effect on the uptake of the HNPs ($p>0.01$).

Pairwise comparisons were also looked at to determine if there were any significant differences in the HNP uptake at each time point between each of the concentrations. For the control sample, the 1 h time point was found to be statistically significantly different to both the 6 h and 24 h time points. For the 25 µg mL^{-1}, all of the time points were found to be

statistically significantly different from each other. For the remaining data (0 μg mL^{-1}, 0.25 μg mL^{-1}, 2.5 μg mL^{-1}, and 5 μg mL^{-1}), the 24 h point was found to be statistically significantly different both the 1 h and 6 h time points ($p<0.05$). Pairwise comparisons also looked at any significant differences in the HNP uptake at each time point between each of the concentrations and the control. At all of the time points, the control was found to be statistically significantly different to all of the other samples ($p<0.001$), with the other samples only found to be statistically significantly different to the control for each time point ($p>0.05$).

Overall, the statistical analysis for both the PANC-1 and BxPC-3 data was able to back up what was presented in the data (Figures 23 and 24), meaning that there was no significant difference in the uptake of the HNPs when using the targeting linker, and that there was no clear difference in the uptake of the HNPs within the 1 h and 6 h time points, but these time point both were able to retain more HNPs that the cells at the 24 h time points.

Other studies have had more success in generating targeting agents for drug delivery applications for several cancerous cell lines, with results demonstrated both *in vitro* and *in vivo* in one case (Yu *et al.*, 2011).

One of the potential reasons that the targeting ligand was unable to successfully force cells to uptake and retain the HNPs is possibly due to the chain length. Computational modelling completed by Dr Jóhannes Reynisson suggested that the chain length needed to be longer in order to better penetrate and "stick" into the cells, allowing the HNPs better uptake and retention. The molecular dynamics approach was used to model fucose. This was done using the catalytic pocket of the enzyme 1,3-fucosyltransferase (PDB ID: 2NZY resolution 2.05 Å) (Sun *et al.*, 2007).

It was assumed that the sugar moiety was bound in the same way as fucose, as the only difference is the addition of the hydrocarbon chain, holding the ring of fucose and the protein static. Bond formation to silver can occur due to the thiol pointing towards the

aqueous phase.

As well as this, the targeting ligands used in these studies have often been tested on other cell lines, or have well-defined biological actions, such as antibodies and antigens (Dilnawaz *et al.*, 2010; Yu *et al.*, 2011; Aires *et al*., 2016; Nagesh *et al.*, 2016; Trabulo *et al*., 2017), that have receptor sites on the surface of the cells, allowing for the great targeting ability seen within these studies.

5.4 Conclusion

The potential of the novel fucose targeting ligand for enhanced uptake in pancreatic cells has been fully explored *in vitro* in two different pancreatic cancer cell lines, with computer modelling data used to explain a potential reason as to why this particular targeting moiety did not work. Further optimisation using different chain lengths is required in order to determine if the sugar used here could be used as a targeting agent for pancreatic cancer, as well as using this *in vivo*, as this is normally a stronger model than using the cell line alone, even though not all *in vitro* and *in vivo* successes translate in the clinical setting.

Chapter 6 details the antibacterial properties of the generated HNPs, with testing on three gram-negative bacterial strains used to determine if these HNPs would successfully kill intratumoral bacteria.

6.0 Antimicrobial studies

6.1 Introduction

6.11 Silver as an antibacterial agent

Because of the rise in resistance to antibiotics, other antibacterial agents may be required when treating pancreatic cancer. The antibacterial properties of AgNPs are well known, with silver ions having several modes of action by which they can inhibit bacteria, such as affecting DNA replication (Marini *et al.*, 2007), interfering with the permeability of bacterial membranes and respiratory chain enzyme inhibition (Lok *et al*., 2007).

Adherence of AgNPs onto the surface of *Pseudomonas aeruginosa* has also been noted, with these nanoparticles then able to enter the bacterial cells and cause more damage (Morones *et al*., 2005). The distribution of silver differs, with 40% only surface binding and 60% entering the bacteria (Holt and Bard, 2005). The ability of AgNPs to enter cells has also been seen in a multidrug-resistant *Pseudomonas aeruginosa* (Liao *et al.*, 2019).

The release of silver ions has also been documented to be a method by which AgNPs kill bacteria, with this seen to be the only cause of AgNPs antibacterial effect in one study (Xiu *et al*., 2012). Other studies have seen a synergistic effect between the release of silver ions and particle-specific effects, including protein expression not seen when using a source of silver ions alone (Yan *et al.*, 2018). The formation of ‘pits’ or pores in the cellular membrane have also been seen in studies using both *Escherichia coli* (Sondi and Salopek, 2004) and *Vibrio cholerae* (Gahlawat *et al.*, 2016). This led to an increase in the permeability of the cell wall, eventually causing cell death. Free radical production has also been implicated as the cause of AgNPs antibacterial efficacy in studies using *Escherichia coli* (Kim *et al.*, 2007) and *Pseudomonas aeruginosa* (Liao *et al.*, 2019; Yan *et al.*, 2018), leading to oxidative stress.

Whether the bacteria are Gram-positive or Gram-negative is another important factor in the efficacy of AgNPs, with the majority of research finding that Gram-negative bacteria are more susceptible to AgNPs bactericidal effects than gram-positive bacteria (Morones *et al.*, 2005; Kim *et al.*, 2007), with this thought to be due to the differences in their cell walls. These effects extend to silver and silver products generally (Jung *et al.*, 2008; Otari *et al.*, 2013; Acharya *et al.*, 2017). In this research, the focus will be on gram-negative bacteria, as these were most commonly found in the PDAC tissues, as described in Geller *et al.* (Geller *et al.*, 2017).

Here, the HNPs generated were tested against gram-negative bacterial strains from the *Enterobacteriaceae* and *Pseudomonadaceae* families to determine whether the hybrids have an antibacterial effect.

6.2 Methods

6.21 Dilutions

The solutions created were based on the concentration of the gemcitabine using its IC_{50} value. The concentration of silver was looked at in this case as silver is the component that has the antibacterial effect, not iron oxide.

Gemcitabine (50 mg) was dissolved in water (10 mL, 5 mg mL^{-1}). 0.1 mL of this was then diluted to 10 mL using water to generate a 0.05 mg mL^{-1} solution. A corresponding concentration of HNPs with gemcitabine was subsequently made by diluting 135 µL to 10 mL, giving a silver concentration of 8.1 µg mL^{-1}. Hence, 54 µL of HNPs (1.5 mg mL^{-1}, silver) was made up to 10 mL in order to gain 8.1 µg mL^{-1} of silver.

6.22 Silver as an Antibacterial Agent

The method here was adapted from the EUCAST disk diffusion method of antimicrobial susceptibility testing (EUCAST, 2019), with the preparation of the agar plates,

the growth of the bacteria, McFarland standard and swabbing of the bacteria onto the plates were all completed by Rebecca Harrison and her laboratory technicians.

The bacteria used were either wild-type clinical isolates (PS995433 and ECO995530) or were obtained from the National Collection of Type Cultures (ECO12241) in order to have a control strain that has known susceptibility to certain antibiotics.

Bacteria were initially grown in an incubator at 36˚C for around 8 h. An inoculum suspension of a 0.5 McFarland standard was generated for each bacterial strain; wild-type *Escherichia coli* (ECO995530), wild-type *Pseudomonas aeruginosa* (PS995433), and *Escherichia coli* (ECO12241). The suspensions were then added onto the plate using a cotton swab to wipe the bacteria onto the centre of the plate in three different directions in order to promote confluent growth. The plates were incubated at 36˚C overnight with the 100 µL of HNPs, gemcitabine, and HNPs loaded with gemcitabine loaded onto plates with each bacteria type. The plates were then removed from the incubator and the zone of inhibition (diameter, mm) measured using callipers.

Samples were measured in triplicate and an average value recorded.

6.23 Statistical Analysis

Any graphs generated were created on Microsoft Excel, with the mean value reported and error bars indicating the SD.

Statistical tests were run on the IBM SPSS Statistics 24 software, with the statistical test or tests run stated in the results and discussion.

6.3 Results and Discussion

In order to determine if the HNPs were showed antibacterial activity, testing was completed on three strains of bacteria. The bacteria used for this study were chosen for several different reasons. Initially, the bacteria have to belong to the families *Enterobacteriaceae* and *Pseudomonadaceae*, as these were found to be present in the PDAC

tissues tested by Geller and co-workers (Geller *et al*., 2017). Secondly, *Escherichia coli* and *Pseudomonas aeruginosa* are relatively common and well-known bacteria, meaning that they were likely to appear within these tissues. Finally, two wild type strains of *Escherichia coli* and *Pseudomonas aeruginosa* (ECO995530 and PS995433 respectively) and a control strain of *Escherichia coli* (ECO12241) were used to test for any antibacterial effects. Here, the control strain has a well-defined pattern of antimicrobial resistance, whereas the wild-type strains do not, so the resistance levels may differ.

Figure 26 shows images taken of the plates approximately 16 h after each solution was applied, with these being used as the initial run to determine if the volume of the solution used was enough to cause inhibition.

Because all of the samples were in water, it was difficult to get the usual zone of inhibition seen in other studies. It also meant that the procedure had to be adapted. The plates are usually placed into the incubator upside-down in order to avoid condensation dripping onto the plate and affecting the concentration of the sample. In this case, the plates could not be stored upside-down, due to the samples being water-based.

In spite of this, the clear lack of growth in the areas of the plate where the nanoparticle solution was applied are quite obvious for the hybrids alone and the hybrids in combination with gemcitabine. Gemcitabine alone was not seen to have any impact on any of the bacterial strains, which was expected due to the nature of this work was to protect gemcitabine from being degraded by bacteria. There was also no sign of a synergistic effect between the gemcitabine and the hybrids, with the zone of inhibition either remaining the same, as in the case of the *Pseudomonas aeruginosa* or decreasing, as seen with both *Escherichia coli* species.

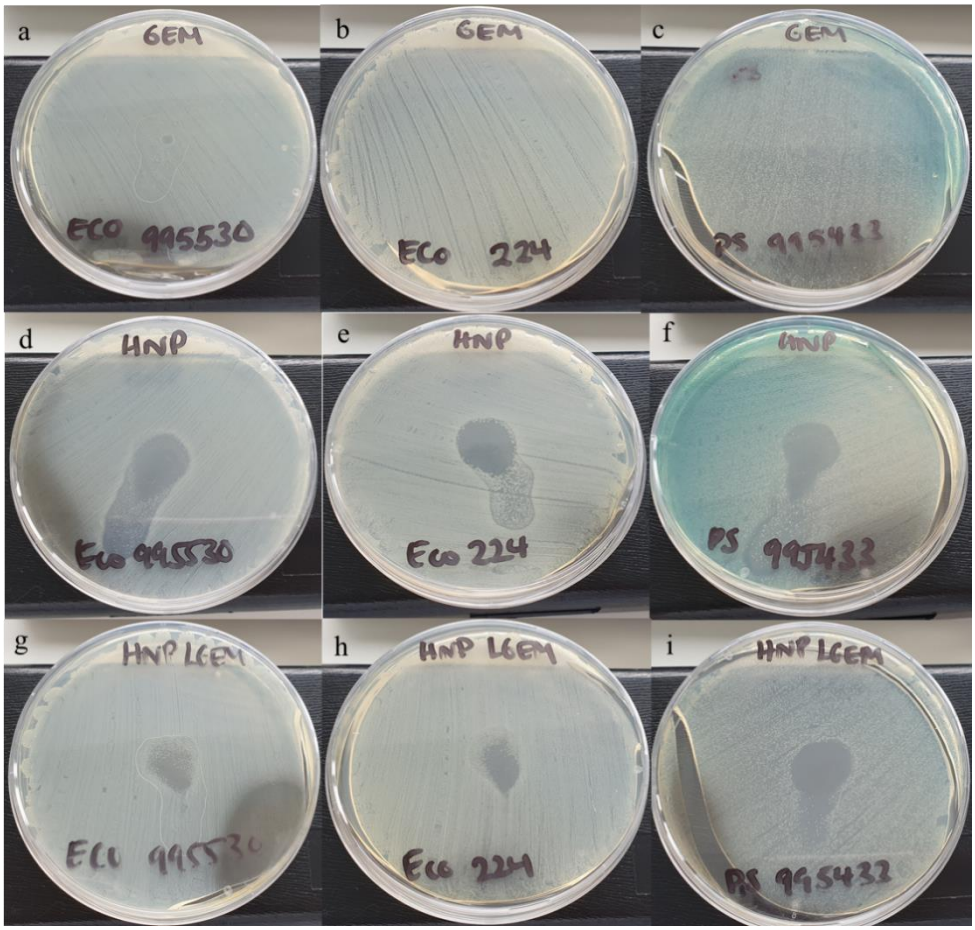

Figure 27: Testing the antibacterial capabilities of gemcitabine (a, b and c), the HNPs (d, e, and f) and the HNPs with L-GEM attached (g, h, and i), against a clinical isolate of *Escherichia coli* (a, d, and g), a control strain of *Escherichia coli* (b, e, and h) and a clinical isolate of *Pseudomonas aeruginosa* (c, f, and i).

Upon initial observation of the zones of inhibition for all of the bacteria, the differences appear to be relatively obvious, with the naked HNPs having a greater effect on ECO12241 and ECO995530. The HNPs and HNP with gemcitabine seemed to have no difference in effect on PS995433. However, Figure 27 shows the error bars for the combination treatment were large for both *Escherichia coli* strains tested, as was the error bar on the naked HNPs for ECO995530, hence it could not be said with absolute certainty that the results truly differed until statistical analysis of the data was undertaken.

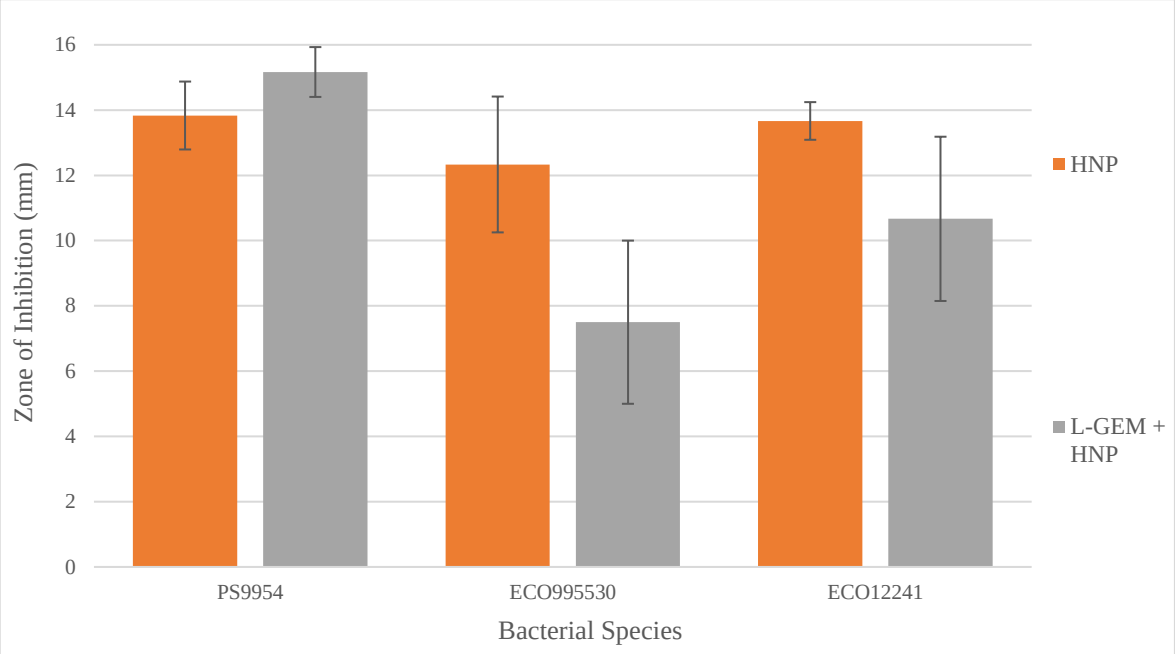

Figure 28: The average zone of inhibition found for the HNPs (HNP) and the HNPs with gemcitabine attached to the surface (L-GEM + HNP) for wild type *Pseudomonas aeruginosa* (PS995433), wild-type *Escherichia coli* (ECO99530) and *E coli* (ECO12241). Gemcitabine is not shown as it did not cause a zone of inhibition in the bacteria used.

A Kruskal-Wallis H test was used for statistical analysis of the data, as the data was found to seriously deviate from normality and had inequality of variance, based on the Levene's test ($p<0.001$). From this, it was determined that there was not a statistically significant difference in the zone of inhibition between the different strains of bacteria ($p>0.05$). There was, however, found to be a statistically significant difference in the zone of inhibition depending on the treatment given, where the treatments were gemcitabine alone, HNPs alone, or the HNP with the drug attached. Pairwise comparisons were able to determine that gemcitabine alone was statistically significantly different to both HNPs ($p<0.05$) and HNPs with gemcitabine ($p<0.001$). Hence, it was also determined that there was not a statistically significant difference in the effects of HNPs and HNPs with gemcitabine on the zone of inhibition ($p>0.05$). The statistical analysis in part reflected in the results shown in Figure 26.

When looking at the data and the statistical analysis, it is clear that gemcitabine alone

had no effect on any of the bacteria tested in this study. As well as this, there was a clear effect of both HNPs and the combination treatment on all of the bacteria, with no statistically significant difference or observationally obvious difference between the two.

A clear issue with this technique is measuring the zone of inhibition by eye, as this is not the most accurate way to gain information due to obvious errors that could occur, especially between researchers. As well as this, there will be issues related to changing the procedure to fit the solutions used, such as the potential for water droplets to decrease the concentrations of the samples on the plate and the issue of the solutions being able to spread easily across the plate, thereby affecting the results. Future studies could be completed using other antibacterial testing techniques, such as the minimum inhibitory concentration (MIC), in order to confirm the results obtained here.

The use of the disk-diffusion assay has been previously completed to determine the antibacterial effect of AgNPs on *Escherichia coli* strains. A study by Vu *et al.,* in which 8 nm AgNPs were tested for their antibacterial efficacy on both *Escherichia coli* and *Staphylococcus aureus* (Vu *et al*., 2018), there was an average zone of inhibition of 7.7 mm for *Escherichia coli*, which is lower than the averages obtained in this study for both the control and wild-type studies both HNPs (12.3 and 13.7 mm) and HNPs with gemcitabine (7.5 mm and 10.7 mm). The strains of *Escherichia coli* used in this study are not clearly stated, so it is harder to compare the results, especially as different strains of *Escherichia coli* have different types of resistance to antibiotics. Another study also measured the zone of inhibition for both *Pseudomonas aeruginosa* and *Escherichia coli*, finding a zone of inhibition of 14.5 mm and 13 mm respectively (Singh *et al.,* 2018). These closely match the values obtained for the wild type *Pseudomonas aeruginosa* using HNPs and gemcitabine HNPs (13.8 mm and 15 mm), wild-type *Escherichia coli* (12.3 mm and 7.5 mm) and the control *Escherichia coli* (13.6 mm and 10.7 mm). Again, different strains may have been used so comparisons can be difficult.

Several other studies have been able to also show the success of AgNPs as antibacterial agents, with the data presented using several different methods, including looking at the MIC (Kim *et al*., 2007; Liao *et al.,* 2019), the IC_{50} (Yan *et al*., 2018), and minimal bactericidal concentration (Liao *et al*., 2019). Kim *et al*. determined that there was a MIC of over 3.3 nM for *Escherichia coli*, a much lower concentration than the one used in this study (Kim *et al.,* 2007). For *Pseudomonas aeruginosa*, the MIC was found to be 2.285 ± 1.492 µg mL^{-1} for the multidrug-resistant strain and 2.596 ± 1.126 µg mL^{-1} for the drug-resistant strain, with minimal bactericidal concentration of 3.165 ± 0.994 µg mL^{-1} and 3.246 ± 1.056 µg mL^{-1}, respectively when completing an agar dilution test (Liao *et al.,* 2019). Yan *et al.* determined that there was an IC_{50} of 0.88 µg mL^{-1} when using AgNPs against *Pseudomonas aeruginosa* (Yan *et al*., 2018). Although the methods and types of nanoparticles differ from the one used here, all of the data together shows the power of silver, especially AgNPs, as an antibacterial agent and confirms the results obtained in this study.

These results clearly show the potential for these hybrids to be used in order to kill intratumoral bacteria, but further studies, including *in vivo* modelling, would be required before application in the clinical setting.

6.4 Conclusion

Overall, there was a clear effect of both HNPs and drug conjugated HNPs on the bacterial strains tested, with no effect found when using gemcitabine alone. This was expected as several studies have proven the efficacy of silver as an antibacterial agent.

7.0 Conclusions and Future Work

The synthesis and characterisation of HNPs composed of an iron oxide core and silver coatings was successfully completed, with several analytical techniques used to confirm this. As mentioned in Chapter 2, the optimisation of the synthesis is required for these hybrids to be used clinically. One possible way in which more consistent coating of the hybrids could be achieved is through the use of microfluidics, which would allow greater control of the size and size distribution of the HNPs, as well as allowing for greater reproducibility.

The ability of these HNPs to be used for laser ablation were also explored, with the results indicating that it is plausible to use these HNPs as thermal triggers for the release of gemcitabine *via* the Diels-Alder mechanism. There were some issues with this, one being the spread of the heat and the other the time it took for the HNPs to heat to the appropriate temperature required for release, especially when compared to AuHNPs. Future work may involve the use of a laser set at a different wavelength, like the one used here better-suited gold due to its surface plasmon resonance. Other issues relate to the silver coating, which was a much lower concentration proportionally to that on the AuHNPs, therefore needing further optimisation.

The drug loading and release of these hybrids have also been tested, as well as the cytotoxicity. Drug loading was successful, with over 70% of L-GEM successfully attached to the surface of the HNPs. However, there were clear issues with the release of the drug, with thermal release at 44˚C unable to release the gemcitabine using the Diels-Alder mechanism previously described. The cytotoxicity data was also relatively inconclusive, with gemcitabine, HNPs and HNPs loaded with L-GEM all having varied toxic effects on both cell lines tested. Due to issues related to the production of L-GEM, it was not possible to repeat any of the tests listed here, therefore future work would be to repeat these tests.

The ability of the modified fucose to target pancreatic cancer cell lines was attempted,

where the results clearly showed that there was no difference in the uptake of the HNPs with or without the linker. Modifications to the molecule may be required to get the desired effect.

Antibacterial testing of the HNPs was completed in order to determine if these HNPs were able to provide a dual therapy within tumour tissues. As expected, gemcitabine alone was unable to exhibit an antibacterial effect. Both the HNPs and the HNPs with L-GEM were able to cause a zone of inhibition on all of the bacteria tested, with L-GEM not affecting the antibacterial efficacy of the HNPs according to statistical testing. Further work would require testing *in vivo* to see if these HNPs would be able to kill bacteria in a more physiologically accurate environment.

Overall, the results obtained here are relatively mixed, with both positive and negative outcomes throughout. The highlights of this work include the successful synthesis of the HNPs, their antibacterial efficacy, and the potential success of the targeting ligand, after some adjustments to its structure. The majority of this work will need optimisation in order for these HNPs to be used within the clinical setting, work that was not possible to complete due to the time constraints of a master's qualification. However, the work here is promising and has shown what is possible for the future of pancreatic cancer treatments.

References

Acharya, C., Panda, C. R., Bhaskara, P. K., Sasmal, A., Shekhar, S. and Sen, A. K. (2017) Physicochemical and antimicrobial properties of sodium alginate/gelatin-based silver nanoformulations, *Polymer Bulletin*, 74(3), pp.689-706.

Agnihotri, S., Mukherji, S. and Mukerji, S. (2014) Size-controlled silver nanoparticles synthesized over the range 5–100 nm using the same protocol and their antibacterial efficacy, *RSC Advances*, 4(8), pp.3974-3983.

Ahamed, M., AlSalhi, M. S. and Siddiqui, M. K. J. (2010) Silver nanoparticle applications and human health, *Clinica Chimica Acta*, 411(23-24), pp.1841-1848.

Aires, A., Ocapmo, S. M., Simões, B. M., Rodrígues, M. J., Cadenas, J. F., Couleaud, P., Spence, K., Latorre, A., Miranda, R., Somoza, A., Clarke, R. B., Carrscosa, J. L. and Cortajarena, A. L. (2016) Multifunctionlized iron oxide nanoparticles for selective drug delivery to CD44-positive cancer cells, *Nanotechnology*, 27(6), pp.065103(1-10).

Alarifi, S., Ali, D., Alkahtani, S. and Alhader, M. S. (2014) Iron Oxide Nanoparticles Induce Oxidative Stress, DNA Damage, and Caspase Activation in the Human Breast Cancer Cell Line, *Biological Trace Element Research*, 159(1-3), pp.416-424.

Ali, A. A., Hsu, F. T., Hsieh, C. L., Shiau, C. Y., Chiang, C. H., Wei, Z. H., Chen C. Y. and Huang, H. S. (2016) Erlotinib-conjugated iron oxide nanoparticles as a smart cancer-targeted theranostic probe for MRI, *Scientific Reports*, 6, pp.36650(1-16).

Apte, M. V., Haber, P. S., Applegate, T. L., Norton, I. D., McCaughan, G. W., Korsten, M. A., Pirola, R. C. and Wilson, J. S. (1998) Periacinar stellate shaped cells in rat pancreas: identification, isolation, and culture, *Gut*, 43(1), pp.128–133.

Apte, M. V., Park, S., Phillips, P. A., Santucci, N., Goldstein, D., Kumar, R. K., Ramm, G. A., Buchler, M., Friess, H., McCarroll, J. A., Keogh, G., Merrett, N., Pirola R. and Wilson, J. S. (2004) Desmoplastic reaction in pancreatic cancer: role of pancreatic stellate cells, *Pancreas*, 29(3), pp.179–187.

Aranda-Lara, L., Torres-Garcia, E. and Oros-Pantoja, R. (2014) Biological tissue modelling with agar gel phantom for radiation dosimetry with ^{99m}Tc, *Open Journal of Radiology*, 4(1), pp.44-52.

Barcińska, E., Wierzbicka, J., Zauszkiewicz-Pawlak, A., Jacewicz, D., Dabrowska, A. and Inkielewicz-Stepniak, I. (2018) Role of Oxidative and Nitro-Oxidative Damage in Silver Nanoparticles Cytotoxic Effect against Human Pancreatic Ductal Adenocarcinoma Cells, *Oxidative Medicine and Cellular Longevity*, 2018, pp.8251961(1-15).

Ben, Q., Xu, M., Ning. X., Liu, J., Hong, S., Huang, W., Zhang, H. and Li Z. (2011) Diabetes mellitus and risk of pancreatic cancer: A meta-analysis of cohort studies, *European Journal of Cancer*, 47(13), pp.1928–1937.

Bray, F., Ferlay, J., Soerjomataram, I., Siegel, R., Torre, L. and Jemal, A. (2018) Global cancer statistics 2018: GLOBOCAN estimates of incidence and mortality worldwide for 36 cancers in 185 countries, *CA: A Cancer Journal for Clinicians*, 68(6), pp.394-424.

Brown, A. N., Smith, K., Samuels, T. A., Lu, J., Obare, S. O. and Scott, M. E. (2012) Nanoparticles functionalized with ampicillin destroy multiple-antibiotic-resistant isolates of Pseudomonas aeruginosa and Enterobacter aerogenes and methicillin-resistant Staphylococcus aureus, *Environmental Microbiology*, 78(8), pp.2768–2774.

Burrell, R. A., McGranahan, N., Bartek, J. and Swanton, C. 2013 The causes and consequences of genetic heterogeneity in cancer evolution, *Nature*, 501, pp.338-345.

Burris 3rd, H. A., Moore, M. J., Andersen, J., Green, M. R., Rothenberg, M. L., Modiano, M. R., Cripps, M. C., Portenoy, R. K., Storniolo, A. M., Tarassoff, P., Nelson, R., Dorr, F. A., Stephens, C. D. and Von Hoff, D. D. (1997) Improvements in survival and clinical benefit with gemcitabine as first-line therapy for patients with advanced pancreas cancer: a randomized trial, *Journal of Clinical Oncology*, 15(6), pp.2403-2413.

Cameron, P., Gaiser, B. K., Bhandari, B., Bartley, P. M., Katzer, F. and Bridle, H. (2016) Silver nanoparticles decrease the viability of Cryptosporidium parvum Oocysts, *Applied Environmental Microbiology,* 82, pp.431-437.

Chand, S., O'Hayer, K., Blanco, F. F., Winter, J. M. and Brody, J. R. (2016) The Landscape of Pancreatic Cancer Therapeutic Mechanisms, *International Journal of Biological Sciences*, 12(3), pp.237-282.

Chen, G., Lu, J., Lam, C. and Yu, Y. (2014) A novel green synthesis approach for polymer nanocomposites decorated with silver nanoparticles and their antibacterial activity, *Analyst*, 139(22), pp.5795-5799.

Chiaravalli, M., Reni M. and O'Reilly, E. M. (2017) Pancreatic ductal adenocarcinoma: State-of-the-art 2017 and new therapeutic strategies, *Cancer Treatment Reviews*, 60, pp.32-43.

Chin, S. F., Iyer, S. and Raston, C. L. (2009) Facile and Green Approach To Fabricate Gold and Silver Coated Superparamagnetic Nanoparticles, *Crystal Growth and Design,* 9(6), pp.2685-2689.

Conroy, T., Bachet, J. B., Ayav, A., Huguet, F., Lambert, A., Caramella, C., Maréchal, R., Van Laethem, J. L. and Ducreux, M. (2016) Current standards and new innovative approaches for treatment of pancreatic cancer, *European Journal of Cancer*, 57, pp.10-22.

Conroy, T., Desseigne, F., Ychou, M., Bouché, O., Guimbaud, R., Bécouarn, Y., Adenis, A., Raoul, J. L., Gourgou-Bourgade, S., de la Fouchardière, C., Bennouna, J., Bachet, J. B.,

Khemissa-Akouz, F., Péré-Vergé, D., Delbaldo, C., Assenat, E., Chauffert, B., Michel, P., Montoto-Grillot, C. and Ducreux, M. (2011) FOLFIRINOX *versus* Gemcitabine for Metastatic Pancreatic Cancer, *The New England Journal of Medicine*, 364(19), pp.1817-1825.

Cunningham, D., Chau, I., Stocken, D. D., Valle, J. W., Smith, D., Steward, W., Harper, P. G., Dunn, J., Tudur-Smith, C., West, J., Falk, S., Crellin, A., Adab, F., Thompson, J., Leonard, P., Ostrowski, J., Eatock, M., Scheithauer, W., Herrmann, R. and Neoptolemos, J. P. (2009) Phase III Randomized Comparison of Gemcitabine Versus Gemcitabine Plus Capecitabine in Patients With Advanced Pancreatic Cancer, *Journal of Clinical Oncology*, 27(33), pp.5513–5518.

Curtis, A., Malekigorji, M., Holman, J., Skidmore, M., and Hoskins, C. (2015) Heat Dissipation of Hybrid Iron Oxide-Gold Nanoparticles in an Agar Phantom, *Journal of Nanomedicine and Nanotechnology*, 6(6), pp.1000335(1-7)

Dabbagh, A., Abdullah, B. J., Ramasindarum, C. and Abu Kasim, N. H. (2014) Tissue-mimicking gel phantoms for thermal therapy studies, *Ultrasonic Imaging*, 36(4), pp.291-316.

de Visser, K. E., Korets, L. V. and Coussens, L. M. (2005) De novo carcinogenesis promoted by chronic inflammation is B lymphocyte dependent, *Cancer Cell*, 7(5), pp.411–423.

Dewhirst, M. W., Cao, Y. and Moeller, B. (2008) Cycling hypoxia and free radicals regulate angiogenesis and radiotherapy response, *Nature Reviews Cancer*, 8(6), pp.425-437.

Dilnawaz, F., Singh, A., Mohanty, C. and Sahoo, S. K. (2010) Dual drug loaded superparamagnetic iron oxide nanoparticles for targeted cancer therapy, *Biomaterials*, 31(13), pp.3694-3706.

Ducreux, M., Cuhna, A. S., Caramella, C., Hollebecque, A., Burtin, P., Goéré, D., Seufferlein, T., Haustermans, K., Van Laethaem, J. L., Conroy, T. and Arnold, D. (2015) Cancer of the

pancreas: ESMO Clinical Practice Guidelines for diagnosis, treatment and follow-up, *Annals of Oncology*, 2015, 26(Suppl. 5), pp.56-68.

Ducreux, M., Mitry, E., Ould-Kaci, M., Boige, V., Seitz, J. F., Bugat, R., Breau, J. L., Bouché, O., Etienne, P. L., Tigaud, J. M., Morvan, F., Cvitkovic E. and Rougier P. (2004) Randomized phase II study evaluating oxaliplatin alone, oxaliplatin combined with infusional 5-FU, and infusional 5-FU alone in advanced pancreatic carcinoma patients, *Annals of Oncology*, 15(3), pp.467-473.

Elechiguerra, J. L., Burt, J. L., Morones, J. R., Camacho-Bragado, A., Gao, X., Lara, H. H. and Yacaman, M. J. (2005) Interaction of silver nanoparticles with HIV-1, *Journal of Nanobiotechnology*, 3(6), pp.1-10.

Erez, N., Truitt, M., Olson, P., Arron, S. T. and Hanahan, D. (2010) Cancer-Associated Fibroblasts Are Activated in Incipient Neoplasia to Orchestrate Tumor-Promoting Inflammation in an NF-kappaB-Dependent Manner, *Cancer Cell*, 17(2), pp.135-147.

Erkan, M., Hausmann, S., Michalski, C. W., Fingerle, A. A., Dobritz, M., Kleeff, J. and Friess, H. (2012) The role of stroma in pancreatic cancer: diagnostic and therapeutic implications, *Nature Reviews Gastroenterology and Hepatology*, 9, pp.454-467.

Erkan, M., Michalski, C. W., Rieder, S., Reiser-Erkan, C., Abiatari, I., Kolb, A., Giese, N. A., Esposito, I., Friess, H. and Kleeff, J. (2008) The Activated Stroma Index Is a Novel and Independent Prognostic Marker in Pancreatic Ductal Adenocarcinoma, *Clinical Gastroenterology and Hepatology*, 6(10), pp.1155-1161.

Estelrich, J., Sánchez-Martín, M. J. and Busquets, M. A. (2015) Nanoparticles in magnetic resonance imaging: from simple to dual contrast agents, *International Journal of Nanomedicine*, 10, pp.1727-1741.

EUCAST Disk Diffusion Method for Antimicrobial Susceptibility Testing [Internet]. 7th ed. EUCAST; 2019 [cited 9 July 2019]. Available from: http://www.eucast.org/fileadmin/src/media/PDFs/EUCAST_files/Disk_test_documents/2019_manuals/Manual_v_7.0_EUCAST_Disk_Test_2019.pdf

Everett, M. J., Jin, Y. F., Ricci V. and Piddock, L. J. (1996) Contributions of individual mechanisms to fluoroquinolone resistance in 36 Escherichia coli strains isolated from humans and animals, *Antimicrobial Agents and Chemotherapy*, 40(10), pp.2380-2386.

Fayaz, A. M., Balaji, K., Girilal, M., Yadav, R., Kalaichelvan, P. T. and Venketesan, R. (2010) Biogenic synthesis of silver nanoparticles and their synergistic effect with antibiotics: a study against gram-positive and gram-negative bacteria, *Nanomedicine: NBM*, 6(1), pp.103–109.

Ferreira, C. G., Span, S. W., Peters, G. J., Kruyt, F. A. and Giaccone, G. (2000) Chemotherapy triggers apoptosis in a caspase-8-dependent and mitochondria-controlled manner in the non-small cell lung cancer cell line NCI-H460, *Cancer Research*, 60(24), pp.7133-7141.

Filmus, J. and Selleck, S. B. (2001) Glypicans: proteoglycans with a surprise, *Journal of Clinical Investigations*., 108(4), pp.497-501.

Foldbjerg, R., Dang, D. A. and Autrup, H. (2011) Cytotoxicity and genotoxicity of silver nanoparticles in the human lung cancer cell line, A549, *Archives of Toxicology*, 85(7), pp.743–750.

Franco-Molina, M. A., Mendoza-Gamboa, E., Sierra-Rivera, C. A., Gómez-Flores, R. A., Zapata-Benavides, P., Castillo-Tello, P., Alcocer-González, J. M., Miranda-Hernández, D. F., Tamez-Guerra, R. S. and Rodríguez-Padilla, C. (2010) Antitumor activity of colloidal silver

on MCF-7 human breast cancer cells, *Journal of Experimental and Clinical Cancer Research*, 29, pp.148–154.

Fuller, E. G., Sun, H., Dhavalikar, R. D., Unni, M., Scheutz, G. M., Sumerlin, B. S. and Rinaldi, C. (2019) Externally Triggered Heat and Drug Release from Magnetically Controlled Nanocarriers, *ACS Applied Polymer Materials*, 1(2), pp.211-220.

Gahlawat, G., Shikha, S., Chaddha, B. S., Chaudhuri, S. R., Mayilraj, S. and Choudhury, A. R. (2016) Microbial glycolipoprotein-capped silver nanoparticles as emerging antibacterial agents against cholera, *Microbial Cell Factories*, 15, pp.25(1-14)

Garrido-Laguna, I. and Hidalgo, M. (2015) Pancreatic cancer: from state-of-the-art treatments to promising novel therapies, *Nature Reviews Clinical Oncology*, 12(6), pp.319-334.

Geller, L. T., Barzily-Rokni, M., Danino, T., Jonas, O. H., Shental, N., Nejman, D., Gavert, N., Zwang, Y., Cooper, Z. A., Shee, K., Thaiss, C. A., Reuben, A., Livny, J., Avraham, R., Frederick, D. T., Ligorio, M., Chatman, K., Johnston, S. E., Mosher, C. M., Brandis, A., Fuks, G., Gurbatri, C., Gopalakrishnan, V., Kim, M., Hurd, M. W., Katz, M., Fleming, J., Maitra, A., Smith, D. A., Skalak, M., Bu, J., Michaud, M., Trauger, S. A., Barshack, I., Golan, T., Sandbank, J., Flaherty, K. T., Mandinova, A., Garrett, WS., Thayer, S. P., Ferrone, C. R., Huttenhower, C., Bhatia, S. N., Gevers, D., Wargo, J. A., Golub, T. R. and Straussman, R. (2017) Potential role of intratumor bacteria in mediating tumor resistance to the chemotherapeutic drug gemcitabine, *Science*, 357(6356), pp.1156-1160.

Gourgou-Bourgade, S., Bascoul-Mollevi, C., Desseigne, F., Ychou, M., Bouché, O., Guimbaud, R., Bécouarn, Y., Adenis, A., Raoul, J. L., Boige, V., Bérille, J. and Conroy, T. (2013) Impact of FOLFIRINOX compared with gemcitabine on quality of life in patients with metastatic pancreatic cancer: results from the PRODIGE 4/ACCORD 11 randomized trial, *Journal of Clinical Oncology*, 31(1), pp.23-29.

Granqvist, N., Liang, H., Laurila, T., Sadowski, J., Yliperttula, M. and Viitala, T. (2013) Characterizing Ultrathin and Thick Organic Layers by Surface Plasmon Resonance Three Wavelength and Waveguide Mode Analysis, *Langmuir*, 29(27), pp.8561-8571.

Grippo, P. J. and Sandgren, E. P. (2012) Acinar-to-ductal metaplasia accompanies c-myc-induced exocrine pancreatic cancer progression in transgenic rodents, *International Journal of Cancer*, 131(5), pp.1243-1248.

Guimarães Sá Correia, M., Briuglia, M. L., Niosi, F. and Lamprou, D. A. (2017) Microfluidic manufacturing of phospholipid nanoparticles: Stability, encapsulation efficacy, and drug release, *International Journal of Pharmaceutics*, 516(1-2), pp.91-99.

Guo, D., Zhu, L., Huang, Z., Zhou, H., Ge, Y., Ma, W., Wu, J., Zhang, X., Zhou, X., Zhang, Y., Zhao, Y. and Gu, N. (2013) Anti-leukemia activity of PVP-coated silver nanoparticles via generation of reactive oxygen species and release of silver ions, *Biomaterials*, 34(32), pp.7884-7894.

Gurunathan, S., Choi, Y. J. and Kim, J. H. (2018) Antibacterial Efficacy of Silver Nanoparticles on Endometritis Caused by Prevotella melaninogenica and Arcanobacterum pyogenes in Dairy Cattle, *International Journal of Molecular Sciences*, 19(4), pp.1210(1-20).

Haes, A. J. and Van Duyne, R. P. (2002) A Nanoscale Optical Biosensor: Sensitivity and Selectivity of an Approach Based on the Localized Surface Plasmon Resonance Spectroscopy of Triangular Silver Nanoparticles, *J. Am. Chem. Soc.*, 124(35), pp.10596-10604.

Hagemann, T., Wilson, J., Burke, F., Kulbe, H., Li, N. F., Plüddemann, A., Charles, K., Gordon S. and Balkwill, F. R. (2006) Ovarian cancer cells polarize macrophages toward a tumor-associated phenotype, *Journal of Immunology*, 176, pp.5023-5032.

Hatiz, P., Al-Madhoon, A. S., Jüllig, M., Petrakis, T. G., Eriksson, S. and Talianidis, I. (1998) The intracellular localization of deoxycytidine kinase, *Journal of Biological Chemistry,* 273(46), pp.30239-30243.

Heinemann, V., Hertelm L. W., Grindey, G. B. and Plunkett, W. (1988) Comparison of the Cellular Pharmacoldnetics and Toxicity of 2',2'-Difluorodeoxycytidine and 1-β-D-Arabinofuranosylcytosine, *Cancer Research*, 48(14), pp.4024-4031.

Heinemann, V., Xu, Y. Z., Chubb, S., Sen, A., Hertel, L. W., Grindley, G. B. and Plunkett, W. (1992) Cellular elimination of 2',2'-difluorodeoxycytidine 5'-triphosphate: a mechanism of self-potentiation, *Cancer Research*, 52(3), pp.553-539.

Hermann, P. C., Huber, S. L., Herrler, T., Aicher, A., Ellwart, J. W., Guba, M., Bruns, C. J. and Heeschen, C. (2007) Distinct populations of cancer stem cells determine tumor growth and metastatic activity in human pancreatic cancer, *Cell Stem Cell*, 1(3), pp.313-323.

Hidalgo, M., Cascinu, S., Kleeff, J., Labianca, R., Löhr, J. M., Neoptolemos, J., Real, F. X. Van Laethem, J. L. and Heinemann. V. (2015) Addressing the challenges of pancreatic cancer: future directions for improving outcomes, *Pancreatology*, 15(1), pp.8-18.

Holt, K. B. and Bard, A. J. (2005) Interaction of silver(I) ions with the respiratory chain of Escherichia coli: an electrochemical and scanning electrochemical microscopy study of the antimicrobial mechanism of micromolar Ag^{+}, *Biochemistry,* 44(39), pp.13214-13223.

Hoskins, C., Min, Y., Gueorguieva, M., McDougall, C., Volovick, A., Prentice, P., Wang, Z., Melzer, A., Cuschieri, A. and Wang, L. (2012) Hybrid gold-iron oxide nanoparticles as a multifunctional platform for biomedical application, *Journal of Nanobiotechnology*, 10, pp.27(1-12).

Hruban, R. H., Adsay, N. V., Albores-Saavedra, J., Compton, C., Garrett, E. S., Goodman, S. N., Kern, S. E., Klimstra, D. S., Klöppel, G., Longnecker, D. S., Lüttges, J. and Offerhaus, G.

J. (2001) Pancreatic intraepithelial neoplasia: a new nomenclature and classification system for pancreatic duct lesion, *American Journal of Surgical Pathology*, 25(5), pp.579-586.

Hu, F. X. , Neoh K. G., and Kang, E. T. (2006) Synthesis and in vitro anti-cancer evaluation of tamoxifen-loaded magnetite/PLLA composite nanoparticles, *Biomaterials*, 27(33), pp.5725-5733.

Huang, P., Chubb, S., Hertel, L. W., Grindley, G. B. and Plunkett, W. (1991) Action of 2',2'-difluorodeoxycytidine on DNA synthesis, *Cancer Research*, 51(22), pp.6110-6117.

Hwang, R. F., Moore, T., Arumugam, T., Ramachandran, V., Amos, K. D., Rivera, A., Ji, B., Evans, D. B. and Logsdon, C. D. (2008) Cancer-associated stromal fibroblasts promote pancreatic tumor progression, *Cancer Res.*, 68(3), pp.918-926.

Iglesias-Silva, E., Rivas, J., León Isidro, L. M. and López-Quintela, M. A. (2007) Synthesis of silver-coated magnetite nanoparticles, *Journal of Non-Crystalline Solids*, 353(8-10), pp.829-831.

Iozzo, R. V. (2001) Series Introduction: Heparan sulfate proteoglycans: intricate molecules with intriguing functions, *Journal of Clinical Investigations*, 108(2), pp.165-167.

Iozzo, R. V. and Schaefer, L. (2010) Proteoglycans in health and disease: novel regulatory signaling mechanisms evoked by the small leucine-rich proteoglycans, *The FEBS Journal*, 277(19), pp.3864-3875.

Jacobs, E. J., Chanock, S. J., Fuchs, C. S., Lacroix, A., McWilliams, R. R., Steplowski, E., Stolzenberg-Solomon, R. Z., Arslan, A. A., Bueno-de-Mesquita, H. B., Gross, M., Helzlsouer, K., Petersen, G., Zheng, W., Agalliu, I., Allen, N. E., Amundadottir, L., Boutron-Ruault, M. C., Buring, J. E., Canzian, F., Clipp, S., Dorronsoro, M., Gaziano, J. M., Giovannucci, E. L., Hankinson, S. E., Hartge, P., Hoover, R. N., Hunter, D. J., Jacobs, K. B., Jenab, M., Kraft, P., Kooperberg, C., Lynch, S. M., Sund, M., Mendelsohn, J. B., Mouw, T., Newton, C. C.,

Overvad, K., Palli, D., Peeters, P. H., Rajkovic, A., Shu, X. O., Thomas, G., Tobias, G. S., Trichopoulos, D., Virtamo, J., Wactawski-Wende, J., Wolpin, B. M., Yu, K. and Zeleniuch-Jacquotte A (2010) Family history of cancer and risk of pancreatic cancer: a pooled analysis from the Pancreatic Cancer Cohort Consortium (PanScan), *International Journal Cancer*, 127(6), pp.1421–1428.

Jain, T. K., Morales, M. A., Sahoo, S. K., Leslie-Pelecky D. L. and Labhasetwar, V. (2005) Iron oxide nanoparticles for sustained delivery of anticancer agents, *Molecular Pharmaceutics*, 2(3), pp.194-205.

Jeyaraj, M., Sathishkumar, G., Sivanandhan, G., MubarakAli, D., Rajesh, M. Arun, R., Kapildev, G., Manickavasagam, M., Thajuddin, N., Premkumar, K. and Ganapathi, A. (2013) Biogenic silver nanoparticles for cancer treatment: An experimental report, *Colloids and Surfaces B Biointerfaces*, 106, pp.86-92.

Jiao, L., Berrington de Gonzalez, A., Hartge, P., Pfeiffer, R., Park, Y., Freedman, D., Gail, M., Alavanja, M., Albanes, D., Beane Freeman, L., Chow, W., Huang, W., Hayes, R., Hoppin, J., Ji, B., Leitzmann, M., Linet, M., Meinhold, C., Schairer, C., Schatzkin, A., Virtamo, J., Weinstein, S., Zheng, W. and Stolzenberg-Solomon, R. (2010) Body mass index, effect modifiers, and risk of pancreatic cancer: a pooled study of seven prospective cohorts, *Cancer Causes & Control*, 21(8), pp.1305-1314.

Johnston, K. S., Karlsen, S. R., Jung, C. C. and Yee, S. S. (1995) New analytical technique for characterisation of thin films using surface plasmon resonance, *Materials Chemistry and Physics*, 42(4), pp.242-246.

Jung, W. K., Koo, H. C., Kim, K. W., Shin, S., Kim, S. H. and Park, Y. H. (2008) Antibacterial Activity and Mechanism of Action of the Silver Ion in Staphylococcus aureus and Escherichia coli, *Applied Environmental Microbiology*, 74(7), pp.2171-2178.

Kaur, D. C. and Chate, S. S. (2015) Study of Antibiotic Resistance Pattern in Methicillin Resistant Staphylococcus Aureus with Special Reference to Newer Antibiotic, *Journal of Global Infectious Diseases*, 7(2), pp.78-84.

Khan, M. I., Mohammad, A., Patil, G., Naqvi, S. A., Chauhan, L. K., and Ahmad, I. (2012), Induction of ROS, mitochondrial damage and autophagy in lung epithelial cells by iron oxide nanoparticles, *Biomaterials*, 33(5), pp.1477-1488.

Kim, J. S., Kuk, E., Yu, K. N., Kim, J. H., Park, S. J., Lee, H. J., Kim, S. H., Park, Y. K., Hwang, C. Y., Kim, Y. K., Lee, Y. S., Jeong, D. H. and Cho, M. H. (2007) Antimicrobial effects of silver nanoparticles, *Nanomedicine,* 3(1), pp.95-101.

Kim, S., Choi, J. E., Choi, J., Chung, K. H., Park, K., Yi, J. and Ryu, D. Y. (2009a) Oxidative stress-dependent toxicity of silver nanoparticles in human hepatoma cells, *Toxicology In Vitro*, 23(6), pp.1076-1084.

Kim, S., Takahashi, H., Lin, W. W., Descargues, P., Grivennikov, S., Kim, Y., Luo, J. L. and Karin M. (2009b) Carcinoma-produced factors activate myeloid cells through TLR2 to stimulate metastasis, *Nature,* 457, pp.102-106.

Kim, S. W., Jung, J. H., Lamsal, K., Kim, Y. S., Min, J. S. and Lee, Y. S. (2012a) Antifungal Effects of Silver Nanoparticles (AgNPs) against Various Plant Pathogenic Fungi, *Mycobiology*, 40(1), pp.53-58.

Kim, Y. L., Wang, K. U., Choi, W. B., Kim, H. J., Hwang, J. Y., Lee, J. H. and Kim, S. W. (2012b) Efficacy and Safety of 1,064 nm Q-switched Nd:YAG Laser Treatment for Removing Melanocytic Nevi, *Annals of Dermatology*, 24(2), pp.162–167.

Kirstein, M. N., Hassan, I., Guire, D. E., Weller, D. R., Dagit, J. W., Fisher, J. E. and Remmel, R. P. (2006) High-performance liquid chromatographic method for the

determination of gemcitabine and 2′,2′-difluorodeoxyuridine in plasma and tissue culture media, *Journal of Chromatography B*, 835(1-2), pp.136-142.

Kleeff, J., Korc, M., Apte, M., La Vecchia, C., Johnson, C. D., Biankin, A. V., Neale, R. E., Tempero, M., Tuveson, D. A., Hruban R. H. and Neoptolemos, J. P. (2016) Pancreatic Cancer, *Nature Reviews Disease Primers*, 2, pp.16022(1-22).

Klemm, F. and Joyce, J. A. (2015) Microenvironmental regulation of therapeutic response in cancer, *Trends in Cellular Biology*, 25(4), pp.198–213.

Kong, H. and Jang, J. (2008) Antibacterial Properties of Novel Poly(methyl methacrylate) Nanofiber Containing Silver Nanoparticles, *Langmuir*, 24(5), pp.2051-2056.

Korhonen, K., Granqvist, N., Ketolainen, J. and Laitinen, R. (2015) Monitoring of drug release kinetics from thin polymer films by multi-parametric surface plasmon resonance, *International Journal of Pharmaceutics*, 494(1), pp.531-536.

Kosmidis, C., Schindler, B. D., Jacinto, P. L., Patel, D., Bains, K., Seo, S. M. and Kaatz, G. W. (2012) Expression of multidrug resistance efflux pump genes in clinical and environmental isolates of Staphylococcus aureus, *International Journal of Antimicrobial Agents*, 40(3), pp.204-209.

Kumar, P., Yuvkkumar, R., Vijayakumar, S. and Vaseeharan, B. (2018) Cytotoxicity of phloroglucinol engineered silver (Ag) nanoparticles against MCF-7 breast cancer cell lines, *Mater. Chem. Phys.*, 220, pp.402-408.

Kumar, S. R., Priyatharshni, S., Babu, V. N., Mangalaraj, D., Viswanathan, C., Kannan, S. and Ponpandian, N. (2014) Quercetin conjugated superparamagnetic magnetite nanoparticles for in-vitro analysis of breast cancer cell lines for chemotherapy applications, *Journal of Colloid and Interface Science*, 436, pp.234-242.

Lara, H. H., Ayala-Nuñez, N. V., Ixtepan-Turrent, L. and Rodriguez-Padilla, C. (2010) Mode of antiviral action of silver nanoparticles against HIV-1, *Journal of Nanobiotechnology*., 2010, 8, pp.1-10.

Larsson, S., Orsini, N. and Wolk, A. (2007) Body mass index and pancreatic cancer risk: A meta-analysis of prospective studies, *International Journal of Cancer*, 120(9), pp.1993-1998.

Lee, E. S. and Lee, J. M. (2014) Imaging diagnosis of pancreatic cancer: a state-of-the-art review, *World Journal of Gastroenterology*, 20(24), pp.7864-7877.

Lehouritis, P., Cummins, J., Stanton, M., Murphy, C. T., McCarthy, F. O., Reid, G., Urbaniak, C., Byrne, W. L. and Tangney, M. (2015) Local bacteria affect the efficacy of chemotherapeutic drugs, *Scientific Reports*, 2015, 5, pp.14554(1-12).

Li, C., Heidt, D. G., Dalerba, P., Burant, C. F., Zhang, L., Adsay, V., Wicha, M., Clarke M. F. and Simeone D. M. (2007) Identification of pancreatic cancer stem cells, *Cancer Research*, 67(3), pp.1030-1037.

Liao, S., Zhang, Y., Pan, X., Zhu, F., Jiang, C., Liu, Q., Cheng, Z., Dai, G., Wu, G., Wang, L. and Chen, L. (2019) Antibacterial activity and mechanism of silver nanoparticles against multidrug-resistant Pseudomonas aeruginosa, *International Journal of Nanomedicine*, 2019(14), pp.1469-1487.

Lim, D. H., Jang, J., Kim, S., Kang, T., Lee, K. and Choi, I. H. (2012) The effects of sub-lethal concentrations of silver nanoparticles on inflammatory and stress genes in human macrophages using cDNA microarray analysis, *Biomaterials*, 33(18), pp.4690-4699.

Lim, H. K., Gurung, R. L. and Hande, M. P. (2017) DNA-dependent protein kinase modulates the anti-cancer properties of silver nanoparticles in human cancer cells, *Mutation Research Genetic Toxicology and Environmental Mutagenesis*, 824, pp.32-41.

Lin, W. C. Rajbhandari, N., Liu, C., Sakamoto, K., Zhang, Q., Triplett, A. A., Batra, S. K., Opavsky, R., Felsher, D. W., DiMaio, D. J., Hollingsworth, M. A., Morris, J. P., Hebrok, M., Witkiewicz, A. K., Brody, J. R., Rui, H. and Wagner, K. U. (2013) Dormant cancer cells contribute to residual disease in a model of reversible pancreatic cancer, *Cancer Research*, 73(6), pp.1821-1830.

Lin, Y. S., Tungpradit, R., Sinchaikul, S., An, F. M., Liu, D. Z., Phutrakul, S. and Chen, S. T. (2008) Targeting the Delivery of Glycan-Based Paclitaxel Prodrugs to Cancer Cells via Glucose Transporters, *Journal of Medicinal Chemistry*, 51(23), pp.7428-7441

Loges, S., Schmidt, T., Tjwa, M., van Geyte, K., Lievens, D., Lutgens, E., Vanhoutte, D., Borgel, D., Plaisance, S., Hoylaerts, M., Luttun, A., Dewerchin, M., Jonckx, B. and Carmeliet, P. (2010) Malignant cells fuel tumor growth by educating infiltrating leukocytes to produce the mitogen Gas6, *Blood*, 115(11), pp.2264-2273.

Lok, C. N., Ho, C. M., Chen, R., He, Q. Y., Yu, W. Y., Sun, H., Tam, P. K., Chiu, J. F. and Che, C. M. (2007) Silver nanoparticles: partial oxidation and antibacterial activities, *Journal of Biological Inorganic Chemistry*, 12(4), pp.527-534.

Lu, L., Sun, R. W., Chen, R., Hui, C. K., Ho, C. M., Luk, J. M., Lau, G. K. and Che C. M. (2008) Silver nanoparticles inhibit hepatitis B virus replication, *Antiviral Therapy*, 13(2), pp.253-262.

Macgregor-Das A. M. and Iacobuzio-Donahue C. A. (2013) Molecular pathways in pancreatic carcinogenesis, *Journal of Surgical Oncology*, 107(1), pp.8-14.

Mahmoudi, M. and Serpooshan, V. (2012) Silver-Coated Engineered Magnetic Nanoparticles Are Promising for the Success in the Fight against Antibacterial Resistance Threat, *ACS Nano*, 6(3), pp.2656-2664.

Malekigorji, M., Alfahad, M., Lin, P. K. T., Jones, S., Curtis, A. and Hoskins, C. (2017) Thermally triggered theranostics for pancreatic cancer therapy, *Nanoscale*, 9(34), pp.12735-12745.

Mandal, M., Kundu, S., Ghosh, S. K., Panigrahi, S., Sau, T. K., Yusuf, S. M. and Pal, T. (2005) Magnetite nanoparticles with tuneable gold or silver shell, *Journal of Colloid and Interface Science*, 286(1), pp.187-194.

Mantovani, A. and Sica, A. (2010) Macrophages, innate immunity and cancer: balance, tolerance, and diversity, *Current Opinions Immunology*, 22(2), pp.231-237.

Mantovani, A., Allavena, P., Sica A. and Balkwill, F. (2008) Cancer-related inflammation, *Nature*, 454, pp.436-444.

Marini, M., De Niederhausern, S., Iseppi, R., Bondi, M., Sabia, C., Toselli, M. and Pilati, F. (2007) Antibacterial activity of plastics coated with silver-doped organic-inorganic hybrid coatings prepared by sol-gel processes, *Biomacromolecules*, 8(4), pp.1246–1254.

Martínez-Castañón, G. A., Niño-Martínez, N., Martínez-Gutierrez, F., Martínez-Mendoza, J. R. and Ruiz, F. (2008) Synthesis and antibacterial activity of silver nanoparticles with different sizes, *Journal of Nanoparticle Research*, 10(8), pp.1343-1348.

Matthaei, H., Schulick, R. D., Hruban, R. H. and Maitra A. (2011) Cystic precursors to invasive pancreatic cancer, *Nature Reviews Gastroenterology and Hepatology*, 8(3), pp.141-150.

Mazur, P. K., Einwächter, H., Lee, M., Sipos, B., Nakhai, H., Rad, R., Zimber-Strobl, U., Strobl, L. J., Radtke, F., Klöppel, G., Schmid, R. M. and Siveke, J. T. (2010) Notch2 is required for progression of pancreatic intraepithelial neoplasia and development of pancreatic ductal adenocarcinoma, *Proceedings of the National Academy of Sciences of the United States of America*, 107(30), pp.13438–13443.

McFarland, A. D. and Van Duyne, R. P. (2003) Single Silver Nanoparticles as Real-Time Optical Sensors with Zeptomole Sensitivity, *Nano Letters*, 3(8), pp.1057-1062.

Michaud, D. S., Vrieling, A., Jiao, L., Mendelsohn, J. B., Steplowski, E., Lynch, S. M., Wactawski-Wende, J., Arslan, A. A., Bueno-de-Mesquita, H. B., Fuchs, C. S., Gross, M., Helzlsouer, K., Jacobs, E. J., LaCroix, A., Petersen, G., Zheng, W., Allen, N., Ammundadottir, L., Bergmann, M. M., Boffetta, P., Buring, J. E., Canzian, F., Chanock, S. J., Clavel-Chapelon, F., Clipp, S., Freiberg, M. S., Gaziano, J. M., Giovannucci, E. L., Hankinson, S., Hartge, P., Hoover, R. N., Hubbell, F. A., Hunter, D. J., Hutchinson, A., Jacobs, K., Kooperberg, C., Kraft, P., Manjer, J., Navarro, C., Peeters, P. H. M., Shu, X., Stevens, V., Thomas, G., Tjønneland, A., Tobias, G. S., Trichopoulos, D., Tumino, R., Vineis, P., Virtamo, J., Wallace, R., Wolpin, B. M., Yu, K., Zeleniuch-Jacquotte, A. and Stolzenberg-Solomon, R. Z. (2010) Alcohol intake, and pancreatic cancer: a pooled analysis from the pancreatic cancer cohort consortium (PanScan), *Cancer Causes Control*, 21(8), pp.1213-1225.

Mie, G. (1908) Beiträge zur Optik trüber Medien, speziell kolloidaler Metallösungen, *Annalen der Physik*, 330(3), pp.377-445.

Mikuni, K., Nakanishi, K., Hara, K., Hara, K., Iwatani, W., Amano, T., Nakamura, K., Tsuchiya, Y., Okumoto, H. and Mandai, T. (2008) In Vivo Antitumor Activity of Novel Water-Soluble Taxoids, *Biological and Pharmaceutical Bulletin*, 2008, 31(6), pp.1155-1158.

Mock, J. J., Barbic, M., Smith, D. R., Schultz, D. A. and Schultz, S. (2002) Shape effects in plasmon resonance of individual colloidal silver nanoparticles, *Journal of Chemical Physics*, 116(15), pp.6755-6759.

Moore, M. J., Goldstein, D., Hamm, J., Figer, A., Hecht, J. R., Gallinger, S., Au, H. J., Murawa, P., Walde, D., Wolff, R. A., Campos, D., Lim, R., Ding, K., Clark, G., Voskoglou-Nomikos, T., Ptasynski, M. and Parulekar, W. (2007) Erlotinib Plus Gemcitabine Compared

With Gemcitabine Alone in Patients With Advanced Pancreatic Cancer: A Phase III Trial of the National Cancer Institute of Canada Clinical Trials Group, *Journal of Clinical Oncology*, 25, pp.1960-1966.

Morones, J. R., Elechiguerra, J. L., Camacho, A., Holt, K., Kouri, J. B., Ramírez, J. T. and Yacaman, M. J. (2005) The bactericidal effect of silver nanoparticles, *Nanotechnology*, 16(10), pp.2345-2353.

Mu, Q., Lin, G., Patton, V. K., Wang, K., Press O. W. and Zhang M. (2016) Gemcitabine and chlorotoxin conjugated iron oxide nanoparticle for glioblastoma therapy, *Journal of Materials Chemistry B*, 4(1), pp.32-36.

Na, H. B., Song, I. C. and Hyeon, T. (2009) Inorganic nanoparticles for MRI contrast agents, *Advanced Materials*, 21(21), pp.2133-2148.

Nagesh, P. K. B., Johnson, N. R., Boya, V. K. N., Chowdhury, P., Othman, S. F., Khalilzad-Sharghi, V., Hafeez, B. B., Ganju, A., Khan, S., Behrman, S. W., Zafar, N., Chauhan, S. C., Jaggi M. and Yallapu, M. M. (2016) PMSA targeted docetaxel-loaded superparamagnetic iron oxide nanoparticles for prostate cancer, *Colloids and Surfaces B Biointerfaces*, 144, pp.8-20.

Neoptolemos, J. P., Palmer, D. H., Ghaneh, P., Psarelli, E. E., Valle, J. W., Halloran, C. M., Faluyi, O., O'Reilly, D. A., Cunningham, D., Wadsley, J., Darby, S., Meyer, T., Gillmore, R., Anthoney, A., Lind, P., Glimelius, B., Falk, S., Izbicki, J. R., Middleton, G. W., Cummins, S., Ross, P. J., Wasan, H., McDonald, A., Crosby, T., Ma, Y. T., Patel, K., Sherriff, D., Soomal, R., Borg, D., Sothi, S., Hammel, P., Hackert, T., Jackson, R. and Büchler, M. W. (2017) Comparison of adjuvant gemcitabine and capecitabine with gemcitabine monotherapy in patients with resected pancreatic cancer (ESPAC-4): a multicentre, open-label, randomised, phase 3 trial, *Lancet*, 389, pp.1011-1024.

Neoptolemos, J. P., Stocken, D. D., Friess, H., Bassi, C., Dunn, J. A., Hickey, H., Beger, H., Fernandez-Cruz, L., Dervenis, C., Lacaine, F., Falconi, M., Pederzoli, P., Pap, A., Spooner, D., Kerr, D. J. and Büchler, M. W. (2004) A randomized trial of chemoradiotherapy and chemotherapy after resection of pancreatic cancer, *The New England Journal of Medicine*, 350(12), pp.1200-1210.

Nistal, G., Caminero, A., Herrán, A. R., Arias, L., Vivas, S., de Morales, J. M., Calleja, S., de Miera, L. E., Arroyo, P. and Casqueiro, J. (2012) Differences of small intestinal bacteria populations in adults and children with/without celiac disease: effect of age, gluten diet, and disease, *Inflammatory Bowel Diseases*, 18(4), pp.649-656.

Nguyen, D. X. and Massagué, J. (2007) Genetic determinants of cancer metastasis, *Nature Reviews Genetics*, 8, pp.341-352.

NHS England Specialised Services Clinical Reference Group for Chemotherapy (2018) Clinical Commissioning Policy: Gemcitabine and capecitabine following surgery for pancreatic cancer (all ages), [online] Available at: https://www.england.nhs.uk/commissioning/wp-content/uploads/sites/12/2018/12/Gemcitabine-and-capecitabine-following-surgery-for-pancreatic-cancer.pdf Last accessed: 30/07/2019.

Nikaido, H. (1976) Outer membrane of Salmonella typhimurium transmembrane diffusion of some hydrophobic substances, *Biochimica et Biophysica Acta*, 433(1), pp.118-132.

Office for National Statistics (2019) Cancer survival in England - Office for National Statistics, [online] Available at: https://www.ons.gov.uk/peoplepopulationandcommunity/healthandsocialcare/conditionsanddiseases/bulletins/cancersurvivalinengland/nationalestimatesforpatientsfollowedupto2017#toc Last accessed 30/07/2019.

Olariu, C. I., Yiu, H. H. P., Bouffier, L., Nadjadi, T., Costello, E., Williams, S. R., Halloran, C. M. and Rosseinsky, M. J. (2011) Multifunctional Fe3O4 nanoparticles for targeted bi-modal imaging of pancreatic cancer, *Journal of Materials Chemistry*, 21(34), pp.12650-12659.

Oluwasanmi, A., Malekigorji, M., Jones, S., Curtis, A. and Hoskins, C. (2016) Potential of hybrid iron-oxide-gold nanoparticles as thermal triggers for pancreatic cancer therapy, *RSC Advances*., 6(97), pp.95044-95054.

Otari, S. V., Patil, R. M., Waghmare, S. R., Ghosh, S. J. and Pawar, S. H. (2013) A novel microbial synthesis of catalytically active Ag–alginate biohydrogel and its antimicrobial activity, *Dalton Trans*, 42(27), pp.9966-9975.

Ou, G., Hedberg, M., Hörstedt, P., Baranov, V., Forsberg, G., Drobni, M., Sandström, O., Wai, S. N., Johansson, I., Hammarström, M. L., Hernell, O. and Hammarström, S. (2009) Proximal small intestinal microbiota and identification of rod-shaped bacteria associated with childhood celiac disease, *American Journal of Gastroenterology*, 104(12), pp.3058-3067.

Padinjarathil, H., Joseph, M. M., Unnikrishnan, B. S., Preethi, G. U., Shiji, R., Archana, M. G., Maya, S., Syama, H. P. and Sreelekha, T. T. (2018) Galactomannan endowed biogenic silver nanoparticles exposed enhanced cancer cytotoxicity with excellent biocompatibility, *International Journal of Biological Macromolecules*, 118(Part A), pp.1174-1182.

Papp, I., Sieben, C., Ludwig, K., Roskamp, M., Böttcher, C., Schlecht, S., Herrmann, A. and Haag, R. (2010) Inhibition of Influenza Virus Infection by Multivalent Sialic-Acid-Functionalized Gold Nanoparticles, *Small*, 6(24), pp.2900-2906

Peixoto, R. C. A., Miranda-Vilela, A. L., de Souza Filho, J., Carneiro, M. L. B., Oliveira, R. G. S., de Silva, M. O., de Souza A. R. and Báo, S. N. (2015) Antitumor effect of free rhodium (II) citrate and rhodium (II) citrate-loaded maghemite nanoparticles on mice bearing breast cancer: a systemic toxicity assay, *Tumor Biology*, 36(5), pp.3325-3336.

Permuth-Wey J. and Egan K. M. (2009) Family history is a significant risk factor for pancreatic cancer: results from a systematic review and meta-analysis, *Familial Cancer*, 8(2), pp.109–117

Petica, A., Gavriliu, S., Lungu, M., Buruntea N. and Panzaru, C. (2008) Colloidal silver solutions with antimicrobial properties, *Materials Science and Engineering B*, 152(1-3), pp.22-27.

Petri-Fink, A., Chastellain, M., Juillerat-Jeanneret, L., Ferrari A. and Hofmann H. (2005) Development of functionalized superparamagnetic iron oxide nanoparticles or interaction with human cancer cells, *Biomaterials*, 26(15), pp.2685-2694.

Picozzi, S. C. M., Casellato, S., Rossini, M., Paola, G., Tejada, M., Costa, E. and Carmignani, L. (2014) Extended-spectrum beta-lactamase-positive Escherichia coli causing complicated upper urinary tract infection: Urologist should act in time, *Urology Annals*, 6(2), pp.107-112.

Picozzi, S., Ricci, C., Gaeta, M., Macchi, A., Dinang, E., Paola, G., Tejada, M., Costa, E., Bozzini, G., Casellato, S. and Carmignani, L. (2013) Do we really know the prevalence of multi-drug resistant Escherichia coli in the territorial and nosocomial population?, *Urology Annals*, 5(1), pp.25-29.

Popescu, R. C., Andronescu, E., Vasile, B. S., Truşcă, R., Boldeiu, A., Mogoantă, L., Mogoșanu, G. D., Temelie, M., Radu, M., Grumezescu, A. M. and Savu, D. (2017) Fabrication and cytotoxicity of gemcitabine-functionalized magnetite nanoparticles, Molecules, 2017, 22(7), pp.1080(1-22).

Pumbwe, L. and Piddock, L. J. (2000) Two efflux systems expressed simultaneously in multidrug-resistant Pseudomonas aeruginosa, *Antimicrobial Agents and Chemotherapy*, 44(10), pp.2861-2964.

Rahib, L., Smith, B. D., Aizenberg, R., Rosenzweig, A.B., Fleshman, J. M. and Matrisian. L. M. (2014) Projecting cancer incidence and deaths to 2030: the unexpected burden of thyroid, liver, and pancreas cancers in the United States, *Cancer Research*, 74(11), pp.2913-2921.

Rao, Y. F., Chan, W., Liang, X. G., Huang, Y. Z., Miao, J., Liu, L., Lou, Y., Zhang, X. G., Wang, B., Tang, R. K., Chen, Z. and Lu, X. Y. (2015) Epirubicin-loaded Superparamagnetic Iron-oxide nanoparticles for transdermal delivery: cancer therapy by circumventing the skin barrier, *Small*, 11(2), pp.239-247.

Reni, M., Bonetto, E., Cordio, S., Passoni, P., Milandri, C., Cereda, S., Spreafico, A., Galli, L., Bordonaro, R., Staudacher, C., Di Carlo, V. and Johnson, C. D. (2006) Quality of life assessment in advanced pancreatic adenocarcinoma: results from a phase III randomized trial, *Pancreatology*, 6(5), pp.454-463.

Reni, M., Cordio, S., Milandri, C., Passoni, P., Bonetto, E., Oliani, C., Luppi, G., Nicoletti, R.., Galli, L., Bordonaro, R., Passardi, A., Zerbi, A., Balzano, G., Aldrighetti, L., Staudacher, C., Villa, E. and Di Carlo, V. (2005) Gemcitabine versus cisplatin, epirubicin, fluorouracil, and gemcitabine in advanced pancreatic cancer: a randomised controlled multicentre phase III trial, *Lancet Oncology*, 6(6), pp.369-376.

Reni, M., Zanon, S., Balzano, G., Passoni, P., Pircher, C., Chiaravalli, M., Fugazza, C., Ceraulo, D., Nicoletti, R., Arcidiacono, P. G., Macchini, M., Peretti, U., Castoldi, R., Doglioni, C., Falconi, M., Partelli, S. and Gianni, L. (2018) A randomised phase 2 trial of nab-paclitaxel plus gemcitabine with or without capecitabine and cisplatin in locally advanced or borderline resectable pancreatic adenocarcinoma, *European Journal of Cancer*, 102, pp.95-102.

Ruiz de Alegría, C., Rodríguez-Baño, J., Cano, M. E., Hernández-Bello, J. R., Calvo, J., Román, E., Díaz, M. A., Pascual, A. and Martínez-Martínez, L. (2011) Klebsiella pneumoniae

Strains Producing Extended-Spectrum β-Lactamases in Spain: Microbiological and Clinical Features, *Journal of Clinical Microbiology*, 49(3), pp.1134-1136.

Sanderson, R. D. and Yang, Y. (2008) Syndecan-1: A dynamic regulator of the myeloma microenvironment, *Clinical and Experimental Metastasis*, 25(2), pp.149-159.

Sarojamma V. and Ramakrishna V. (2011) Prevalence of ESBL-Producing *Klebsiella pneumoniae* Isolates in Tertiary Care Hospital, *ISRN Microbiology*, 2011, pp.318348(1-5).

Saung, M. T. and Zheng, L. (2017) Current Standards of Chemotherapy for Pancreatic Cancer, *Clinical Therapeutics*, 39(11), pp.2125-2134.

Schultheis, B., Reuter, D., Ebert, M. P., Siveke, J., Kerkhoff, A., Berdel, W. E., Hofheinz, R., Behringer, D. M., Schmidt, W. E., Goker, E., De Dosso, S., Kneba, M., Yalcin, S., Overkamp, F., Schlegel, F., Dommach, M., Rohrberg, R., Steinmetz, T., Bulitta M. and Strumberg, D. (2017) Gemcitabine combined with the monoclonal antibody nimotuzumab is an active first-line regimen in KRAS wildtype patients with locally advanced or metastatic pancreatic cancer: a multicenter, randomized phase IIb study, *Annals of Oncology*, 28(10), pp.2429–2435.

Shahverdi, A. R., Fakhimi, A., Shahverdi, H. R. and Minaian, S. (2007) Synthesis and effect of silver nanoparticles on the antibacterial activity of different antibiotics against Staphylococcus aureus and Escherichia coli, *Nanomedicine: NBM*, 3(2), pp.168-171.

Shankar, S., Wang, L. F. and Rhim, J. W. (2016) Preparations and characterization of alginate/silver composite films: Effect of types of silver particles, *Carbohydrate Polymers*, 146, pp.208-216.

Shrivastava, S., Bera, T., Roy, A., Singh, G., Ramachandrarao, P. and Dash, D. (2007) Characterization of enhanced antibacterial effects of novel silver nanoparticles, *Nanotechnology*, 18(22), pp.225103(1-9).

Siegel, R., Miller, K. and Jemal, A. (2018) Cancer statistics, 2018, *CA: A Cancer Journal for Clinicians*, 68(1), pp.7-30.

Sierra, J. R., Corso, S., Caione, L., Cepero, V., Conrotto, P., Cignetti, A., Piacibello, W., Kumanogoh, A., Kikutani, H., Comoglio, P. M., Tamagnone, L. and Giordano, S. (2008) Tumor angiogenesis and progression are enhanced by Sema4D produced by tumor-associated macrophages, *Journal of Experimental Medicine*, 205(7), pp.1673-1685.

Sondi, I. and Salopek-Sondi, B. (2004) Silver nanoparticles as antimicrobial agent: a case study on E. coli as a model for Gram-negative bacteria, *Journal of Colloid and Interface Science*, 275(1), pp.177-182.

Sriram, M. I., Kanth, S. B., Kaishwaralal, K. and Gurunathan, S. (2010) Antitumor activity of silver nanoparticles in Dalton's lymphoma ascites tumor model, *International Journal of Nanomedicine*, 5, pp.753-762.

St Jean, A. T., Zhang, M. and Forbes, N. S. (2008) Bacterial therapies: completing the cancer treatment toolbox, *Current Opinions Biotechnol*ogy, 19(5), pp.511-517.

Starup-Linde, J., Karlstad, Ø., Eriksen, S., Vestergaard, P., Bronsveld, H. K., de Vries, F., Andersen, M., Auvinen, A., Haukka, J., Hjellvik, V., Bazelier, M. T., de Boer, A., Furu, K. and de Bruin, M. L. (2013) CARING (CAncer Risk and INsulin analoGues): The Association of Diabetes Mellitus and Cancer Risk with Focus on Possible Determinants - A Systematic Review and a Meta-Analysis, *Current Drug Safety*, 8(5), pp.296–332.

Stathis, A. and Moore, M. J. (2010) Advanced pancreatic carcinoma: current treatment and future challenges, *Nature Reviews Clinical Oncology*, **7**(3), pp.163-172.

Straussman, R., Morikawa, T., Shee, K., Barzily-Rokni, M., Qian, Z. R., Du, J., Davis, A., Mongare, M. M., Gould, J., Frederick, D. T., Cooper, Z. A., Chapman, P. B., Solit, D. B., Ribas, A., Lo, R. S., Flaherty, K. T., Ogino, S., Wargo, J. A. and Golub, T. R. (2012) Tumour

micro-environment elicits innate resistance to RAF inhibitors through HGF secretion, *Nature*, 487, pp.500–504.

Strumberg, D., Schultheis, B., Scheulen, M. E., Hilger, R. A., Krauss, J., Marschner, N., Lordick, F., Bach, F., Reuter, D., Edler, L. and Mross, K. (2012) Phase II study of nimotuzumab, a humanized monoclonal anti-epidermal growth factor receptor (EGFR) antibody, in patients with locally advanced or metastatic pancreatic cancer, *Investigational New Drugs*, 30(3), pp.1138–1143.

Su, D., Jiao, S. C., Wang, L. J., Shi, W. W., Long, Y. Y., Li, J. and Bai, L. (2014) Efficacy of nimotuzumab plus gemcitabine usage as first-line treatment in patients with advanced pancreatic cancer, *Tumour Biology*, 35(3), pp.2313–2318.

Sun, H. Y., Lin, S. W., Ko, T. P., Pan, J. F., Liu, C. L., Lin, C. N., Wang, A. H. and Lin, C. H. (2007) Structure and mechanism of Helicobacter pylori fucosyltransferase. A basis for lipopolysaccharide variation and inhibitor design, *Journal of Biological Chemistry*, 282(13), pp.9973-9982.

Tanaka, Y., Matsu, K. and Yuzuriha, S. (2011) Objective assessment of skin rejuvenation using near-infrared 1064-nm neodymium: YAG laser in Asians, *Clinical, Cosmetic and Investigational Dermatology*, 4, pp.123–130.

Tannock, I. F., Lee, C. M., Tunggal, J. K., Cowan, D. S. M., and Egorin, M. J. (2002) Limited Penetration of Anticancer Drugs through Tumor Tissue: A Potential Cause of Resistance of Solid Tumors to Chemotherapy, *Clinical Cancer Research*, 8(3), pp.878-884.

Tassa, C., Duffner, J. L., Lewis, T. A., Weissleder, R., Schreiber, S. L., Koehler, A. N. and Shaw, S. Y. (2010) Binding Affinity and Kinetic Analysis of Targeted Small Molecule-Modified Nanoparticles, *Bioconjugate Chemistry*, 2010, 21(1), pp.14-19.

Topalian, S. L., Hodi, F. S., Brahmer, J. R., Gettinger, S. N., Smith, D. C., McDermott, D. F., Powderly, J. D., Carvajal, R. D., Sosman, J. A., Atkins, M. B., Leming, P. D., Spigel, D. R., Antonia, S. J., Horn, L., Drake, C. G., Pardoll, D. M., Chen, L., Sharfman, W. H., Anders, R. A., Taube, J. M., McMiller, T. L., Xu, H., Korman, A. J., Jure-Kunkel, M., Agrawal, S., McDonald, D., Kollia, G. D., Gupta, A., Wigginton, J. M. and Sznol, M. (2012) Safety, Activity, and Immune Correlates of Anti–PD-1 Antibody in Cancer, *The New England Journal of Medicine*, 366(26), pp.2443–2454.

Trabulo, S., Aires, A., Aicher, A., Heeschen, C. and Cortajarena, A. L. (2017) Multifunctionalised iron oxide nanoparticles for selective targeting of pancreatic cancer cells, *Biochimica et Biophysica Acta General Subjects*, 1861(6), pp.1597-1605.

Tramacere, I., Scotti, L., Jenab, M., Bagnardi, V., Bellocco, R., Rota, M., Corrao, G., Bravi, F., Boffetta, P. and La Vecchia, C. (2010) Alcohol drinking and pancreatic cancer risk: a meta-analysis of the dose-risk relation, *International Journal of Cancer*, 126(6), pp.1474-1486.

Van Rompay, A. R., Johansson, M. and Karlsson, A. (1999) Phosphorylation of Deoxycytidine Analog Monophosphates by UMP-CMP Kinase: Molecular Characterization of the Human Enzyme, *Molecular Pharmacology*, 56(3), pp. 562-569.

von Hoff, D. D., Ervin, T., Arena, F. P., Chiorean, E. G., Infante, J., Moore, M., Seay, T., Tjulandin, S. A., Hidalgo, M., Goldstein, D., Van Cutsem, E., Wei, X., Iglesias, J. and Renschler, M. F. (2013) Increased survival in pancreatic cancer with nab-paclitaxel plus gemcitabine, *The New England Journal of Medicine*, 369(18), pp.1691-1703.

Vu, X. H., Duong, T. T. T., Pham, T. T. H., Trinh, D. K., Nguyen, X. H. and Dang, V. S. (2018) Synthesis and study of silver nanoparticles for antibacterial activity against Escherichia coli and Staphylococcus aureus, *Advances in Natural Sciences Nanoscience and Nanotechnology*, 9, pp.025019(1-7).

Wang-Gillam, A., Li, C. P., Bodoky, G., Dean, A., Shan, Y. S., Jameson, G., Macarulla, T., Lee, K. H., Cunningham, D., Blanc, J. F., Hubner, R. A., Chiu, C. F., Schwartsmann, G., Siveke, J. T., Braiteh, F., Moyo, V., Belanger, B., Dhindsa, N., Bayever, E., von Hoff, D. D. and Chen, L. T. (2016) Nanoliposomal irinotecan with fluorouracil and folinic acid in metastatic pancreatic cancer after previous gemcitabine-based therapy (NAPOLI-1): a global, randomised, open-label, phase 3 trial, *Lancet*, 387(10018), pp.545-557.

Whitesides, G. M. (2006) The origins and the future of microfluidics, *Nature*, 442, pp.368-373.

Witkiewicz, A. K., McMillan, E. A., Balaji, U., Baek, G., Lin, W. C., Mansour, J., Mollaee, M., Wagner, K. U., Koduru, P., Yopp, A., Choti, M. A., Yeo, C. J., McCue, P., White, M. A. and Knudsen, E. S. (2015) Whole-exome sequencing of pancreatic cancer defines genetic diversity and therapeutic targets, *Nature Communications*, 6, pp.6744(1-11).

Wu, J., Jiao, Y., Dal Molin, M., Maitra, A., de Wilde, R. F., Wood, L. D., Eshleman, J. R., Goggins, M. G., Wolfgang, C. L., Canto, M. I., Schulick, R. D., Edil, B. H., Choti, M. A., Adsay, V., Klimstra, D. S., Offerhaus, G. J., Klein, A. P., Kopelovich, L., Carter, H., Karchin, R., Allen, P. J., Schmidt, C. M., Naito, Y., Diaz Jr, L. A., Kinzler, K. W., Papadopoulos, N., Hruban, R. H. and Vogelstein. B. (2011) Whole-exome sequencing of neoplastic cysts of the pancreas reveals recurrent mutations in components of ubiquitin-dependent pathways, *Proceedings of the National Academy of Sciences of the United States of America*, 108(52), pp.21188-21193.

Wu, M., Zhang, D., Zeng, Y., Wu, L., Liu, X. and Liu, J. (2015) Nanocluster of superparamagnetic iron oxide nanoparticles coated with poly(dopamine) for magnetic field-targeting, highly sensitive MRI and photothermal cancer therapy, *Nanotechnology*., 26(11), pp.115102(1-13)

Xia, Y. and Halas, N. J. (2005) Shape-controlled synthesis and surface plasmonic properties of metallic nanostructures, *MRS Bulletin*, 30(5), pp.338-348.

Xiu, Z. M., Zhang, Q. B., Puppala, H. L., Colvin, V. L. and Alvarez, P. J. J. (2012) Negligible Particle-Specific Antibacterial Activity of Silver Nanoparticles, *Nano Letters*, 12(8), pp.4271-4275.

Xu, Z., Vonlaufen, A., Phillips, P. A., Fiala-Beer, E., Zhang, X., Yang, L., Biankin, A. V., Goldstein, D., Pirola, R. C., Wilson, J. S. and Apte, M. V. (2010) Role of pancreatic stellate cells in pancreatic cancer metastasis, *The American Journal of Pathology*, 177(5), pp.2585-2596.

Yachida, S., Jones, S., Bozic, I., Antal, T., Leary, R., Fu, B., Kamiyama, M., Hruban, R. H., Eshleman, J. R., Nowak, M. A., Velculescu, V. E., Kinzler, K. W., Vogelstein B. and Iacobuzio-Donahue C. A. (2010) Distant metastasis occurs late during the genetic evolution of pancreatic cancer, *Nature*, 467, pp.1114-1119.

Yan, X., He, B., Liu, L., Qu, G., Shi, J., Hu, L. and Jiang, G. (2018) Antibacterial mechanism of silver nanoparticles in Pseudomonas aeruginosa: proteomics approach, *Metallomics*, 10(4), pp.557-564.

Ying, H., Dey, P., Yao, W., Kimmelman, A. C., Draetta, G. F., Maitra, A. and DePinho, R. A. (2016) Genetics and biology of pancreatic ductal adenocarcinoma, *Genes and development*, 30(4), pp.355-385.

Yoshida, M., Takimoto, R., Murase, K., Sato, Y., Hirakawa, M., Tamura, F., Sato, T., Iyama, S., Osuga, T., Miyanishi, K., Takada, K., Hayashi, T., Kobune, M. and Kato, J. (2012) Targeting Anticancer Drug Delivery to Pancreatic Cancer Cells Using a Fucose-Bound Nanoparticle Approach, *PLoS One*, 7(7), pp.e39545(1-12).

Yu, M. K., Kim, D., Lee, I. H., So, J. S., Jeong, Y. Y. and Jon, S. (2011) Image-guided prostate cancer therapy using aptamer-functionalised thermally cross-linked superparamagnetic iron oxide nanoparticles, *Small*, 7(15), pp.2241-2249.

Yuan, Y. G., Peng, Q. L. and Gurunathan, S. (2017) Silver nanoparticles enhance the apoptotic potential of gemcitabine in human ovarian cancer cells: combination therapy for effective cancer treatment, *International Journal of Nanomedicine*, 2017(12), pp.6487-6502.

Zanganeh, S., Hutter, G., Spitler, R., Lenkov, O., Mahnoudi, M., Shaw, A., Pajarinen, J. S., Nekadnik, H., Goodman, S., Moseley, M., Coussens, L. M. and Daldrup-Link, H. E. (2016) Iron oxide nanoparticles inhibit tumour growth by inducing pro-inflammatory macrophage polarization in tumour tissues, *Nature Nanotechnology*, 11, pp.986-994.

Zhang, X. and Xiao, C. (2018) Biofabrication of silver nanoparticles and their combined effect with low intensity ultrasound for treatment of lung cancer, *Journal of Photochemistry and Photobiology B*, 181, pp.122-126.

Zielinska, E., Zauszkiewicz-Pawlak, A., Wojcik, M. and Inkielewicz-Stepniak, I. (2018) Silver nanoparticles of different sizes induce a mixed type of programmed cell death in human pancreatic ductal adenocarcinoma, *Oncotarget*, 9(4), pp.4675-4697.

Zou, L., Zhong, R., Shen, N., Chen, W., Zhu, B., Ke, J., Lu, X., Zhang, T., Lou, J., Wang, Z., Liu, L., Qi, L. and Miao, X. (2014) Non-linear dose–response relationship between cigarette smoking and pancreatic cancer risk: Evidence from a meta-analysis of 42 observational studies, *European Journal of Cancer*, 50(1), pp.193-203.

Zu, C. and Wang, J. (2014) Tumor-colonizing bacteria: a potential tumor targeting therapy, *Critical Reviews in Microbiology*, 40, pp.225-235.